Studies on Optical Sensing of Charged Analytes and DNA Interaction/Photocleavage Activities

A Thesis

Submitted for the Degree of

DOCTOR OF PHILOSOPHY

By

Tamal Ghosh

School of Chemistry
University of Hyderabad
Hyderabad 500 046
India

January 2006

To

My Family

Statement

I hereby declare that the matter embodied in the thesis entitled "**Studies on Optical Sensing of Charged Analytes and DNA Interaction/Photocleavage Activities**" is the result of investigations carried out by me in the School of Chemistry, University of Hyderabad, Hyderabad, India under the supervision of Prof. Anunay Samanta and Late Prof. Bhaskar G. Maiya.

In keeping with the general practice of reporting scientific observations, due acknowledgements have been made wherever the work described is based on the findings of other investigators.

Tamal Ghosh

SCHOOL OF CHEMISTRY
UNIVERSITY OF HYDERABAD
HYDERABAD 500 046, INDIA

Phone: +91-40-23011594 (O)
+91-40-23010715 (R)
Fax: +91-40-23012460
Email: assc@uohyd.ernet.in
anunay_s@yahoo.com

Anunay Samanta, F. A. Sc.
Professor

30th January 2006

Certificate

Certified that the work embodied in this thesis entitled "**Studies on Optical Sensing of Charged Analytes and DNA Interaction/Photocleavage Activities**" has been carried out by **Mr. Tamal Ghosh** under my supervision and that the same has not been submitted elsewhere for any degree.

Anunay Samanta
(Thesis Supervisor)

Dean
School of Chemistry
University of Hyderabad

Acknowledgements

It is with immense regards and profound admiration I wish to articulate my deep sense of gratitude to Late Prof. Bhaskar G. Maiya, under whose guidance I joined as a Ph. D. student. I owe it to him for introducing me to this field of research and teaching me many principles and techniques.

I would like to express my sincere thanks and gratitude to my present guide Prof. Anunay Samanta for important discussions and suggestions about the thesis as well as the papers. Without his kind cooperation and generous help, it was impossible to finish this research work.

I would like to thank Prof. M. Periasamy, Dean, School of Chemistry, former Deans and all the faculty members of School of Chemistry especially Prof. E. D. Jemmis, Prof. T. P. Radhakrishnan, Prof. K. C. Kumara Swamy, Prof. M. Durga Prasad, Prof. M. J. Swamy, Prof. S. Pal, Dr. S. Mahapatra, Dr. A. K. Bhuyan and Dr. S. K. Das for their help during the course of my study.

I would like to thank Prof. C. K. Mitra, Department of Biochemistry, School of Life Sciences for his kind help and constant encouragement.

I would like to admit the kind help of Prof. M. W. Wong (National University of Singapore), by carrying out the computation studies on molecules of chapter 5.

I would like to thank Dr. Amitava Das and his student Dr. Atindra D. Shukla (Central Salt and Marine Chemicals Research Institute, Bhavnagar) for synthesizing and providing the molecules of chapter 3 and 7.

I thank my lab seniors Dr. L. Giribabu, Dr. C. V. Sastri, Dr. A. Ashok Kumar, Dr. D. Raghunath Reddy, Dr. P. Prashanth Kumar, Dr. M. Mariappan, Dr. Satyen Saha, Dr. Rana Karmakar, Dr. N. B. Sankaran, Dr. Sandip Banthia and my present labmates Premaladha, Prasun, Moloy, Aniruddha, Bhaswati, Narahari and Prathap for the helpful discussions and above all, for creating a pleasant atmosphere in the laboratory. I would like to convey my thanks to Sunirban and Manab for solving X-ray crystallographic structures and helping me to learn it.

I would like to thank DST, New Delhi for the National Single Crystal X-ray Diffractometer Facility and Universities with Potential for Excellence (UPE) programme

of UGC, New Delhi at school of chemistry. Financial assistance from CSIR, New Delhi is gratefully acknowledged. Central Drug Research Institute, Lucknow for the FAB-mass spectral data and Central Salt and Marine Chemicals Research Institute, Bhavnagar for analytical data are highly acknowledged.

I would like to thank Mr. Satyanarayana and Mr. Bhaskar Rao for recording NMR, LC-mass, analytical data; Mrs. Vijayalakshmi and Mrs. Ayesa Parwez for IR; Mr. Raghavaiah for mounting crystals in diffractometer. I also thank Mr. Shetty, Mr. Vijay Bhaskar, Mr. Vara Prasad and other non-teaching staff of school of chemistry for their help.

I would like to thank Rahul, Dinabandhu, Binay, Abhik, Archan, Subhas, Biswarup, Saikat, Satabdi, Prashant, Abhijit, Susmita, Utpal, Bipul, Tanmoy, Anindita, Suparna who made my stay in the campus a memorable one.

I would like to take this opportunity to express my deep regards to my parents. I would like to thank my all relatives, uncles, aunties and cousin brother and sisters for their constant support. Finally, I thank my wife Soma for her patience and consistent encouragement.

Contents

CHAPTER 1

Introduction

Molecular recognition is one of the most important events of chemistry, biology and material sciences. Information about this event is conveniently transmitted in the form of light signals, emitted by purpose-built molecular devices.[1-6] Such types of molecular devices also have potential for information processing since their output signal can be switched between two distinguishable states by environmental stimuli.[7-13] These devices serve several branches of sciences such as microscopy,[14-16] analytical chemistry,[17,18] clinical and medical science[19,20] etc. with very different needs and methods.

Chemosensors are molecules capable of binding selectively and reversibly the analyte of interest (molecule, cation, anion) with subsequent change in one or more properties of the system, such as absorption or fluorescence spectra, redox potentials.[10,21] The two different processes occurring during analyte detection, i.e. molecular recognition and signal transduction, can be visualized[6] as made of three different components: a receptor, which is responsible for selective analyte binding, a signaling unit, whose properties should changes upon complexation and, eventually, a spacer that can tune the electronic interaction between the two former moieties. The binding interactions between receptor and analyte can be of different kinds: hydrogen-bond or π-interactions for molecule, coordinative interactions for cation, hydrogen-bond or coordinative or electrostatic interactions for anion.[22] The recognition process is generally fast and characterized by moderate energy gain.

1.1 Cation Sensing

Detection of cation is of great interest to chemist, biologist, biochemists and environmentalists. Sodium, potassium, magnesium and calcium are involved in biological processes such as transmission of nerve impulses, muscle contraction, regulation of cell activity etc. Moreover, various metal ions belong to metalloenzymes. Transition metal ions represent an environmental concern when present in uncontrolled amounts, but at the same time, some of them such as, iron, zinc, copper, and cobalt are present as essential elements in biological systems. In medicine, it is important to control the lithium level in serum of patients under treatment for manic depression, and potassium in the case of high blood pressure. The toxicity of aluminium has long been recognized and there is a controversy on its possible implication in Alzheimer's disease. In chemical oceanography, it has been demonstrated that some nutrients required for survival of microorganisms in sea water contain zinc, iron and manganese as enzyme cofactors. Finally, it is well known that mercury, lead and cadmium are toxic for organisms, and early detection in the environment is desirable.

Among the numerous analytical methods that are available for detection of cations, flame photometry, atomic absorption spectrometry, ion sensitive electrodes, electron microprobe analysis, neutron activation analysis, etc., are expensive, often require samples of large size and do not allow continuous monitoring. In contrast, the methods based on colorimetric and fluorescent detection[10,12,21,22] offer distinct advantages in terms of sensitivity, selectivity and response time. Moreover, remote sensing is possible by using optical fibres with a molecular sensor immobilized at the tip.[17] Therefore, considerable efforts are being made to develop selective colorimetric and fluorescent sensors for cation detection.

Although, the receptor moiety of the chemosensor is responsible for the overall selectivity of the molecule, the signaling unit is the utmost important part as it converts the recognition event information into an optical signal expressed as the changes in the photophysical characteristics of the chromophore/fluorophore. These changes are due to the perturbation (by the bound cation) of photoinduced processes such as electron transfer, charge transfer, energy transfer, excimer or exciplex formation or disappearance, etc. Most well-known and well-studied fluorescent chemosensors for cation sensing involve photoinduced electron transfer (PET) or photoinduced charge transfer (PCT) processes.

1.1.1 Fluorescent PCT (photoinduced charge transfer) cation sensors

When a fluorophore contains an electron-donating group conjugated to an electron-withdrawing group, it undergoes intramolecular charge transfer from the donor to the acceptor upon excitation by light. The consequent change in dipole moment results in a Stokes shift that depends on the microenvironment of the fluorophore. Polarity probes have been designed on this basis.[11] It can thus be anticipated that cations in close interaction with the donor or the acceptor moiety will change the photophysical properties of the fluorophore by modulating the efficiency of the intramolecular charge transfer process in the system.[10,12]

When the group playing the role of an electron-donor interacts with a cation, the electron-donating character of this group is diminished and a blue-shift of the absorption spectrum is expected. Conversely, a cation interacting with the acceptor group enhances the electron-withdrawing character of this group; the absorption spectrum is thus red-shifted. The fluorescence spectra are in principle shifted in the same direction as those of the absorption spectra.

In addition to these shifts, changes in quantum yields and lifetimes are often observed. The influence of binding of cation with the donor or acceptor group of a PCT sensor on absorption or fluorescence spectrum can be visualized and understood by fig. 1.1. All these photophysical effects are obviously dependent on the charge and size of the cation, and selectivity of these effects are expected.[23]

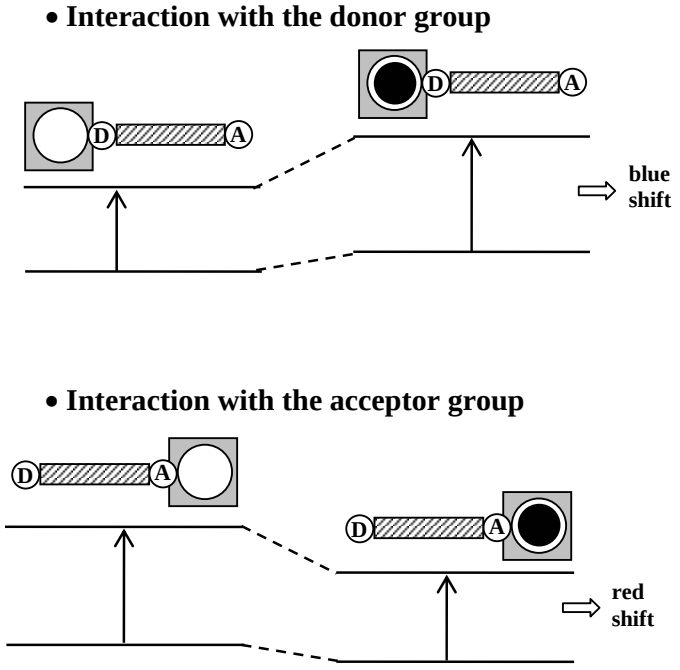

Fig. 1.1 Spectral changes of PCT sensors resulting from interaction of a cation with an electron-donating or electron-withdrawing group.

The photophysical changes upon cation binding can also be described in terms of charge dipole interaction.[24] Considering only the case where the dipole moment in the excited state is larger than that in the ground state, the excited state is more strongly destabilized than the ground state when the

cation interacts with the donor group, and a blue-shift of the absorption and emission spectra is expected. Conversely, when the cation interacts with the acceptor group, the excited state is more stabilized by the cation than the ground state, and this leads to a red-shift of the absorption and emission spectra (Fig. 1.1).

1.1.2 Some examples

Some fluorescent PCT cation sensors, along with a few others relevant to the present work such as phenylazo-dye based chemosensors and chemosensors where pyrene is connected to 2,2′-bipyridyl or [2,2′:6′,2′′]-terpyridyl by unsaturated linkage are discussed in the following section.

Bourson and Valeur have shown that upon complexation with alkaline earth metal ions, **1** (Fig. 1.2) exhibits drastic hypsochromic shift of the absorption spectrum and the fluorescence is quenched, whereas the emission spectrum is only slightly blue-shifted and the fluorescence lifetime is almost unchanged.[25] These effects, which strongly depend on the charge density of the cation, is interpreted in terms of cation-steered reduction of the efficiency of transfer from a nonemissive locally excited state to an emissive relaxed intramolecular charge transfer state (RICT).

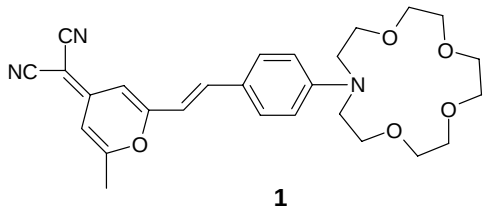

1

Fig. 1.2

Bourson et. al. have also reported the photophysical properties of fluoroionophores composed of the laser dye coumarin 153 linked to monoaza-12-crown-4 (**2**), monoaza- 15-crown-5 (**3**), and diaza-18-crown-6 (**4**) (Fig. 1.3).[26] The photohpysical changes upon complexation with alkali and alkaline earth metal ions can be described in terms of enhancement in the intramolecular charge transfer in the coumarin dye owing to direct interaction between bound cation and carbonyl group of the coumarin. The magnitude of the photophysical changes is controlled by the charge density of the bound cation. In the case of **4**, an interesting specific increase of the fluorescence quantum yield upon binding of potassium and barium ions is observed. The high stability constants of the complexes arise from the participation of the carbonyl group of the coumarin into the complexes and from the deconjugation of the nitrogen atom of the aza-crown ether from the π-electron system.

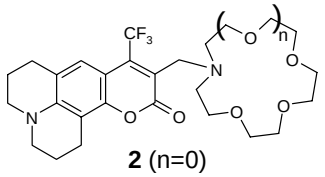

2 (n=0)
3 (n=1)

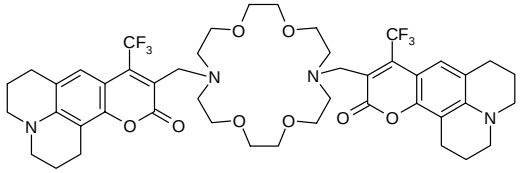

4

Fig. 1.3

Yang et. al. reported a cyclometalated platinum(II) bipyridyl acetylide complex (**5**) containing a monoazacrown moiety in the acetylide ligand acting as metal ion receptor (Fig. 1.4), which can signal Mg^{2+} specifically by change

in fluorescence.[27] Descalzo et. al. have reported a Hg^{2+} selective colorimetric and fluorescent chemosensor based on phenoxazin-3-one scaffold with a dithia-dioxa-monoaza crown unit at the 7-position (**6**) (Fig. 1.4), which senses Hg^{2+} in the ppb range in water.[28] The characteristic charge transfer band above 500 nm in absorption spectrum of **6** shows a drastic hypsochromic shift on

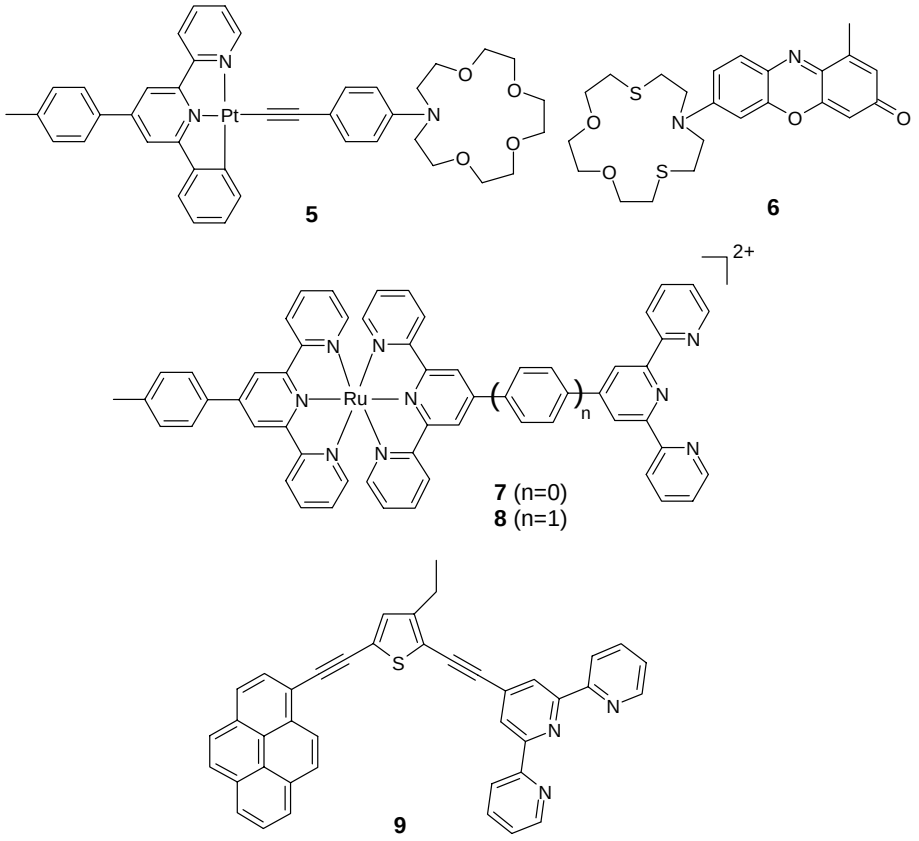

Fig. 1.4

addition of Hg^{2+} ion, both in polar solvent (CH_3CN) and water. Barigelletti et. al. studied functionalized Ru(II)-bisterpyridine complexes (**7**) and (**8**) as a rod-like systems for signaling of Zn(II) (Fig. 1.4).[29] Benniston et. al. reported a fluorescent chemosensor that comprises a pyrene moiety tethered to a

[2,2′:6′,2′′]-terpyridyl ligand *via* a diethynylated thiophene linker (**9**) (Fig. 1.4) for Zn^{2+} ion.[30] Addition of Zn^{2+} to a solution of **9** causes a red shift of the lowest energy absorption band with subsequent loss of some of the fine structure.

Leroy-Lhez et. al. described the synthesis and photophysical properties of a series of pyrene containing π-conjugated 2,2′-bipyridyl ligands (**10**, **11**, **12**, **13**) (Fig. 1.5).[31,32] Harriman et. al. reported a dyad (**14**) where pyrene and 2,2′-

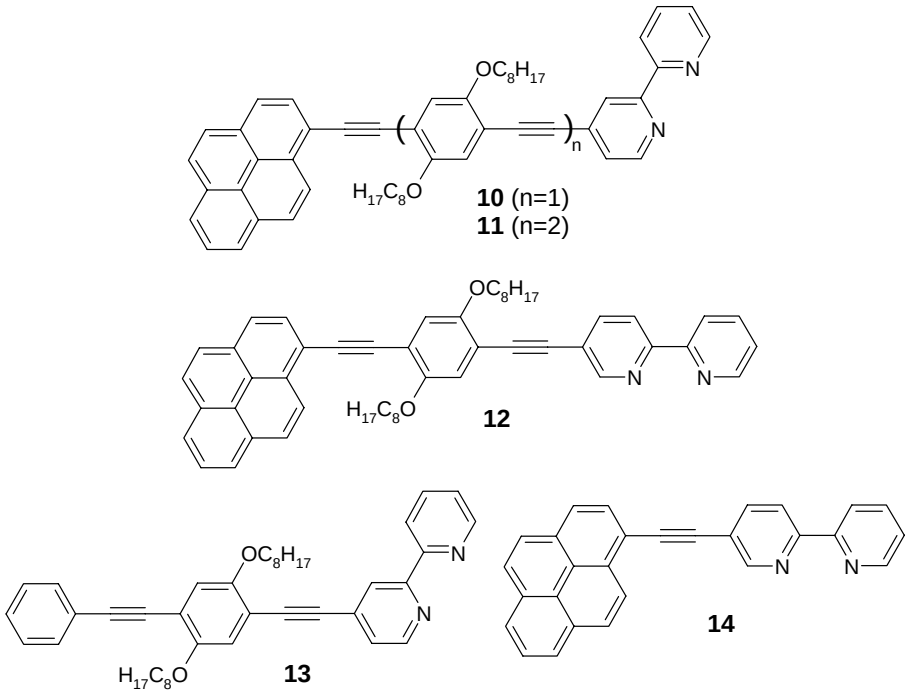

Fig. 1.5

bipyridine are connected by a single ethynylene group (Fig. 1.5).[33] Coordination of Zn(II) or H^+ to the vacant 2,2′-bipyridine of **14** enhances the ICT state formation and opens up a new route for deactivation of the pyrene-like excited singlet state.

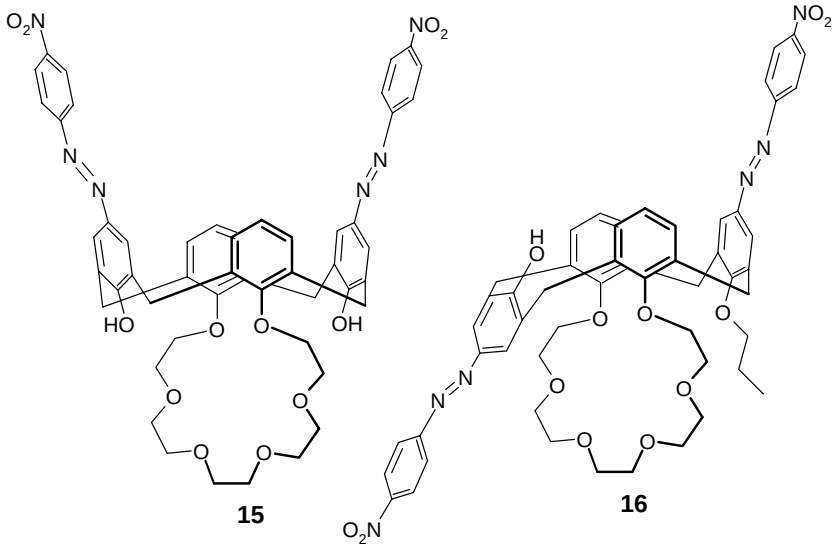

Fig. 1.6

Kim et. al. reported Calixcrown-6 compounds carrying a pair of phenylazo moieties on the upper rim and two OH groups (**15**) or one OH and one OR group (**16**) on the lower rim in both the cone and partial cone conformations (Fig. 1.6).[34] Addition of Ca^{2+} into the solution of host **15** leads

to a marked bathochromic shift (150 nm) of the absorption spectrum of **15**. On the other hand, a hypsochromic shift of 20 nm for **16** on binding with Ca^{2+} was observed. Kim and co-workers reported a series of 1,3-alternate chromogenic azo-coupled calix[4]biscrowns (Fig. 1.6) in which the crown size varied with crown-5 and crown-6 (**17**, **18**, **19**).[35] Metal ions were entrapped only by the upper crown loop, causing the hypsochromic shift in the absorption spectrum of **17** and **18**. Calix[4]bis(crown-5)(crown-6) **17** showed K^+ ion selectivity while Cs^+ ion selectivity was observed for **18**, caused by a size complementarity between hosts and guest ions. However, bathochromic shift of the absorption spectrum of **19** was observed upon metal ions addition, in which the NO_2 groups are replaced by NH_2 group, indicating that the metal ions are encapsulated in the lower crown ring because of strengthened π-cation interaction by introduction of the electron-donating NH_2 unit, regardless of the steric hindrance between two azo-phenyl groups adjacent to the crown ring.

Gunnlaugsson and co-workers reported a number of azo-dye based chemosensors where monoazacrown/diazacrown ether or phenyliminodiacetate acts as receptors for alkali metal ions[36-38] or transition metal ions,[39] respectively. The azo-dye based chemosensor appended with monoazacrown ether receptor (**20**) (Fig. 1.7)[36,37] displays a large change in its absorption spectrum upon addition of Na^+ and shows high selectivity for Na^+ over other alkali and alkaline-earth metal cations. Two azo-dye based colorimetric chemosensors containing diazacrown ether as receptor (**21** and **22**) were designed for the detection of intracellular concentrations of Na^+ and K^+, respectively by the same group (Fig. 1.7).[38] Both displayed good selectivity and sensitivity for the relevant group I cations in the physiological conditions.

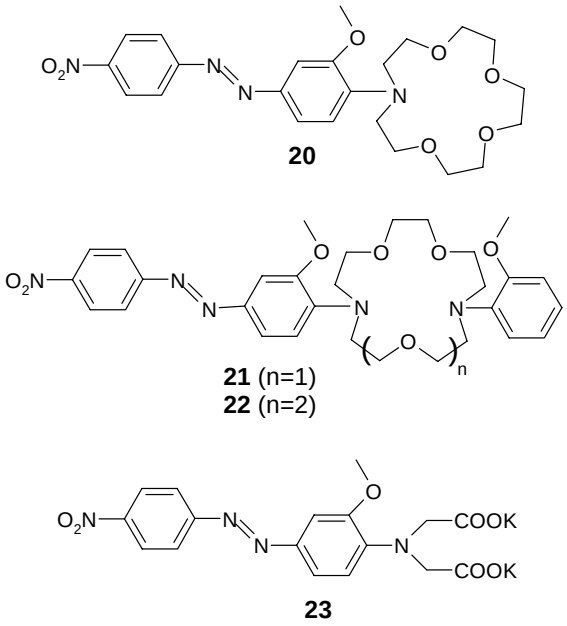

Fig. 1.7

Colorimetric azobenzene based chemosensor (**23**) (Fig. 1.7) was also designed by Gunnlaugsson and co-workers for detection of transition metal ions such as Cu(II) under physiological pH conditions.[39] The use of *o*-methoxy functionality gives rise to an extra chelation site and high selectivity and sensitivity of this sensor for Cu(II) under physiological pH conditions. The Cu(II) recognition by **23** gives rise to large changes in the absorption spectra with subsequent change in color form red to yellow which is reversible upon addition of EDTA.

1.2 Anion Sensing

Anions play an important role in various industrial processes, energy transduction and enzymatic activity in organisms, clinical treatment of various

disease states etc.[40-44] Anions are ubiquitous throughout biological systems. They carry genetic information (DNA is a polyanion) and the majority of the enzyme substrates and co-factors are anionic. A well known example is carboxypeptidase A,[45] an enzyme that coordinates to the C-terminal carboxylate group of polypeptides by the formation of an arginine-aspartate salt bridge, and catalyzes the hydrolysis of this residue. Anions also play roles in the area of medicine and catalysis, whilst pollutant anions have been linked to eutrophication of rivers (from the overuse of phosphate containing fertilizers)[46] and carcinogenesis (metabolites of nitrate).[47] The production of pertechnetate during the reprocessing of nuclear fuel (and its subsequent discharge into the seas and oceans) is also a matter of environmental concern.

The design of anion sensors is particularly challenging and a newly emerging field. Indeed, it is only recently that the coordination chemistry of anions is being developed in comparison to that of cations. Anions are larger than isoelectronic cations and therefore, have a lower charge to radius ratio. This means that electrostatic binding interactions are less effective than they would be for the smaller cation. Additionally anions may be sensitive to pH values (becoming protonated at low pH), thus sensors must function within the pH window of their target anion. Anionic species have a wide range of geometries and therefore a higher degree of design may be required to make receptors complementary to their anionic guest.

Another crucial role in controlling anion binding strength and selectivity is played by solvent effects. Electrostatic interactions generally dominate in anion solvation, and hydroxylic solvents in particular can form strong hydrogen-bonds with anions. Hence, a potential anion sensor must effectively compete with the solvent environment in which the anion recognition event takes place. The biological anion sensor systems are optimized to operate in a

very specific range of environments where the source of selectivity for biological anion is the difference of free energy lost on dehydrating the anion and that gained by the interaction of the anion with the binding site.[43] Hydrophobicity can also influence the selectivity of an anion sensor. The Hofmeister series,[48] which was first established through studies on the effects of salts on the solubility of proteins, orders anions by their hydrophobicity.

A useful way of categorizing anion sensors is to consider the types of noncovalent interaction used to complex the anionic guest. These include electrostatic interactions, hydrogen-bonding, hydrophobicity, coordination to a metal ion or other Lewis acids, and combinations of these interactions working together. There are many examples of each type of these interactions and all of them are well surveyed in a number of literatures.[43,49-54] The recognition of anion leads to change in optical signals (absorption or fluorescence) or change in redox potentials or change in NMR spectrum of the sensor. In some cases, structure of the supramolecule made by guest-host interaction is determined by single crystal X-ray crystallography which gives a clear picture of degree of binding between the sensor and anion at the molecular level.

1.2.1 Some examples

Many molecules have been synthesized that are known for anion sensing by electrostatic interactions,[55-57] hydrophobicity,[58,59] coordination to a metal ion or other Lewis acids,[60-64] and combinations of these interactions.[65,66] Some of the examples where the anion sensing event takes place by hydrogen-bonding interaction are discussed in the following section.

One of the most easily and widely used approach to detect anion is by employing colorimetric sensor, where the hydrogen-bonding interaction between sensor molecule and anion is communicated by subsequent noticeable

change in color of the solution. Sessler and co-workers used some easily available molecules such as 4-nitro-1,2-phenylenediamine, alizarin, naphthol AS, 9(10H)-acridone etc., which were termed as 'off-the-shelf' colorimetric anion sensors.[67] These molecules showed non-selective visible color change in presence of anions such as F^-, Cl^-, Br^-, $H_2PO_4^-$, HSO_4^-, CH_3COO^-, $C_6H_5COO^-$ etc. in organic medium.

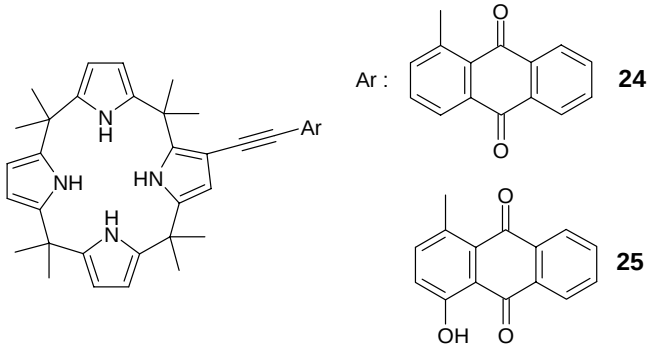

Fig. 1.8

However, selective sensing of anions was achieved by Sessler and co-workers by utilizing functionalized calix[4]pyrrole or dipyrrolylquinoxaline (DPQ) class of compounds. Anthraquinones linked to calix[4]pyrrole skeleton by C–C triple bond (Fig. 1.8) behave as colorimetric anion sensors (**24** and **25**).[68] **24** shows a dramatic color change from yellow to red on addition of F^- in CH_2Cl_2 whereas for Cl^- or $H_2PO_4^-$ the color changes from yellow to reddish-orange and requires greater concentration of anions to effect a commensurate change. On the other hand, exposure to Br^-, I^- and HSO_4^- ions, which do not bind to calix[4]pyrrole appreciably, no noticeable change in color of **24** could be detected. The other calix[4]pyrrole derivative **25** changes color from red to blue or purple upon addition of anions (F^-, Cl^- or $H_2PO_4^-$),

again the effect being most dramatic and pronounced in the case of fluoride ion.

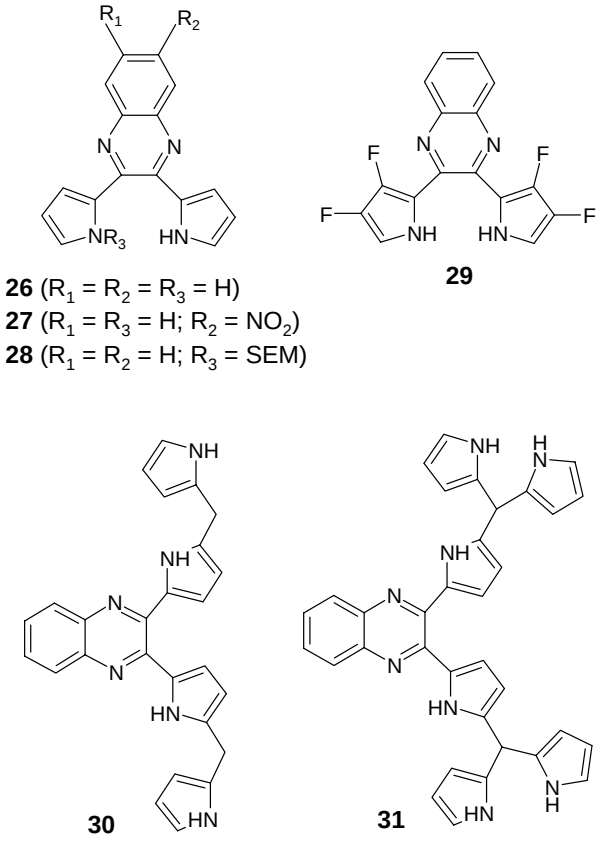

26 ($R_1 = R_2 = R_3 = H$)
27 ($R_1 = R_3 = H$; $R_2 = NO_2$)
28 ($R_1 = R_2 = H$; $R_3 = SEM$)

29

30

31

Fig. 1.9

The same group has synthesized a number of dipyrrolylquinoxaline (DPQ) group containing anion sensors, as shown in fig. 1.9. Out of the three compounds **26**, **27**, **28**, the nitro derivative of DPQ **27** acts as colorimetric sensor for F^- in CH_2Cl_2 or DMSO solution with color change from yellow to purple.[69] No change in color is observed for Cl^- or $H_2PO_4^-$ under similar condition. The other two compounds, **26** and **28** do not bind with F^-, Cl^- or

$H_2PO_4^-$ and show no color change. The greater affinity of **27** relative to **26** is expected considering that the greater electron-deficiency of the mono-nitro derivative should lead to an increase in its hydrogen-bond donating character. Addition of trace amount of water, however, restores the original color indicating that the complexation between sensor and anion is reversible. The monotrimethylsilylethoxymethyl (SEM)-protected species **28** does not bind with even F^-, smallest among the anions used in the study, due to lack of full complement of NH hydrogen-bonding donor functionality. Anzenbacher et. al. reported the anion binding ability of **29** where the β-pyrrolic positions were replaced by electron-withdrawing fluorine substituent (Fig. 1.9).[70] The substitution at β-pyrrolic positions by electron-withdrawing fluorine increases the hydrogen-bond donating character of **29** and it undergoes a selective yellow to orange color change in the presence of both F^- and $H_2PO_4^-$ ions, but not for Cl^- or Br^- ions, in CH_2Cl_2 medium. Sessler et. al. also reported two anion sensors (**30** and **31**) based on quinoxaline derivatives bearing dipyrromethane or tripyrromethane (Fig. 1.9).[71] The binding constants of **30** with F^-, $H_2PO_4^-$ and Cl^- are of the order of 10^4, 10^3 and 10^2 M^{-1} in CH_2Cl_2 medium, that for **31** are of the order of $>10^6$, 10^5 and 10^3 M^{-1}, respectively under the similar condition. The stronger binding of Cl^- and $H_2PO_4^-$ ions with **30** and **31** compared to that with **26** is ascribed to size effects and is thought to reflect the fact that larger anion is better able to fit into the pyrrolic 'claws' and are 'chelated' with **30** and **31**.

Sessler and co-workers investigated the anion binding property of Ru(II) (**32**) or Co(III) (**33**) complexes where DPQ moiety is fused with phenanthroline ligand of the metal complexes (Fig. 1.10).[72] The rationale for making **32** and **33** was that they would contain electron-withdrawing moieties

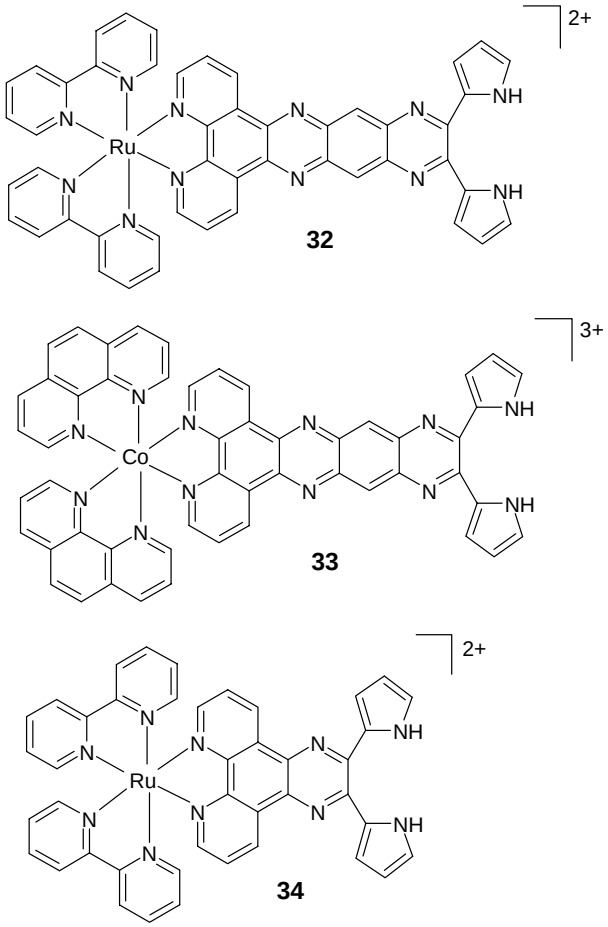

Fig. 1.10

(metal centers) that would render the pyrrole NH protons more acidic, thereby promoting the key anion-to-DPQ interactions, just as in **27** or **29**. In the case of complexes **32** and **33**, these electron-withdrawing effects were expected to relay efficiently through the quinoxaline backbone and lead to enhanced anion binding affinities. Both **32** and **33** bind with F^-; binding constants are of the order of 10^4 M^{-1} in DMSO and color of **33** changes from red-pink to pale

purple. The Co(III) complex **33** shows a sharp reduction peak for Co^{III}/Co^{II} couple in differential pulse voltammetry in DMSO. Addition of F^- leads to complete disappearance of the Co^{III}/Co^{II} reduction signal because the complex formed between **33** and F^- is very strong and as a consequence, redox inactive.

Anzenbacher and co-workers reported another Ru(II) complex for anion sensing (**34**) where the ligand contains DPQ moiety in its architecture (Fig. 1.10).[73] Complex **34** possesses the strongest binding affinity for F^- and CN^-. Also, the binding constants for all the anions enhanced in comparison to that of **26** because Ru(II) center makes DPQ moiety electron-deficient, thereby rendering the pyrrole NH of **34** more available for hydrogen-bonding to the anions. Complex **34** also acts as fluorescence lifetime-based sensor for anions.

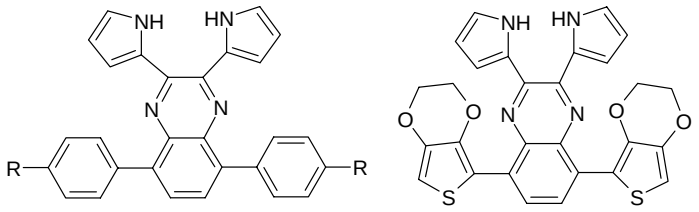

35 (R = H)
36 (R = OMe)
37 (R = NMe_2)

38

Fig. 1.11

Aldakov and Anzenbacher explored the anion sensing behavior of DPQ derivatives (**35**, **36**, **37**, **38**) connected with extended chromophores (Fig. 1.11) by fluorescence quenching.[74] On addition of F^- or $HP_2O_7^{3-}$ (pyrophosphate) ions, the colors of **35**-**38** change from yellow to red and fluorescence is quenched completely in CH_2Cl_2 medium, but no such changes are observed for Cl^- and $H_2PO_4^-$ ions. The binding constants calculated from

fluorescence quenching data indicate that pyrophosphate binds strongly with **35**-**38** than fluoride ion.

Urea or thiourea receptors connected to fluorophores or chromophores have been used for anion sensors. Cho et. al. studied anion binding properties of a urea based anion sensor (**39**) containing naphthalene fluorophore (Fig. 1.12).[75] The anion sensor **39** shows almost 40-fold selective binding of F^- compared to Cl^- in CH_3CN/DMSO (9:1, v/v). On addition of F^-, a new emission peak at 445 nm is observed; on the other hand, only changes in intensity of the original band are observed in presence of Cl^-, Br^- or I^-. Although, the selectivity for F^- over Cl^- is not that high, the appearance of a new peak in the presence of F^- provides a great advantage for detecting F^- ion. Jose et. al. reported colorimetric sensors selective for fluoride ion based on anthraquinone as chromogenic signaling subunit and urea (**40**) or thiourea (**41**) as receptor moieties (Fig. 1.12).[76] Well-defined color changes from yellow to red (**40**) or purple (**41**) were observed upon addition of F^- ion in CH_3CN/DMSO solution of the sensors.

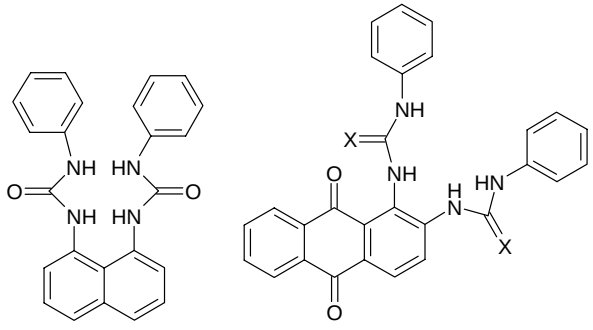

Fig. 1.12

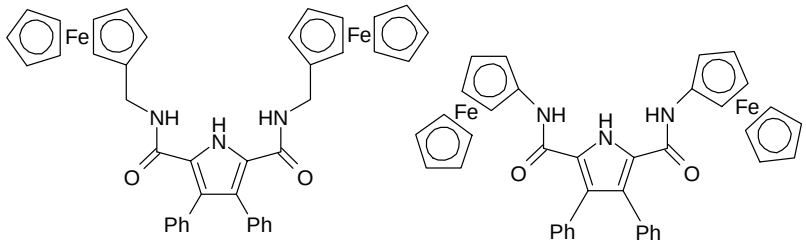

42 **43**

Fig. 1.13

Denuault et. al. investigated anion binding properties of two amido-pyrrole cleft anion sensors (**42** and **43**) bearing two ferrocene reporter groups by electrochemistry and ^{1}H NMR titration technique (Fig. 1.13).[77] The sensors contain either a non-conjugated or conjugated link between the anion-binding amido-pyrrole unit and the ferrocene reporter groups. The binding constants of **42** and **43** with different anions were determined by ^{1}H NMR titration which shows that **43** has a higher affinity for anions than **42**. In cyclic voltammetry experiments, anions (F^-, Cl^-, HSO_4^- and $C_6H_5COO^-$) were found to shift the wave negatively with respect to that without anions for both **42** and **43**. However, Br^- does not affect the electrochemistry of either **42** or **43**.

1.3 Ion-Pair Recognition

Ion-pair recognition, the simultaneous complexation of cationic and anionic guest species by multisite receptors, is a newly emerging and topical field of coordination chemistry. These heteroditopic ligands can be designed to exhibit novel co-operative and allosteric behavior, whereby the binding of one charged guest can influence, through electrostatic and conformational effects, the subsequent coordination of the pairing ions.[78-82] Such systems have potential as new selective extraction and transportation reagents for ion-pair

species of environmental importance and for zwitterion recognition. Recognition event of ion-pair by multisite receptors is studied mainly by ^{1}H NMR spectroscopy and sometimes by absorption or fluorescence spectroscopy. Also, sometimes single crystal of ion-pair bound receptor is grown from solution and its structure is solved by X-ray crystallography.

1.3.1 Some examples

Smith and co-workers synthesized two bicyclic receptors (**44** and **45**) and evaluated their ability to bind alkali halide salts and polar neutral molecules in organic solvents (Fig. 1.14).[83] The receptor design is relatively straightforward in the sense that it is a combination of a dibenzo-18-crown-6 and a bridging 1,3-phenyldicarboxamide. In the presence of 1 mole equivalent of metal cation, chloride affinities of **44** are enhanced in the order: K^+ (9-fold) > Na^+ (8-fold) >> Cs^+ (no enhancement).

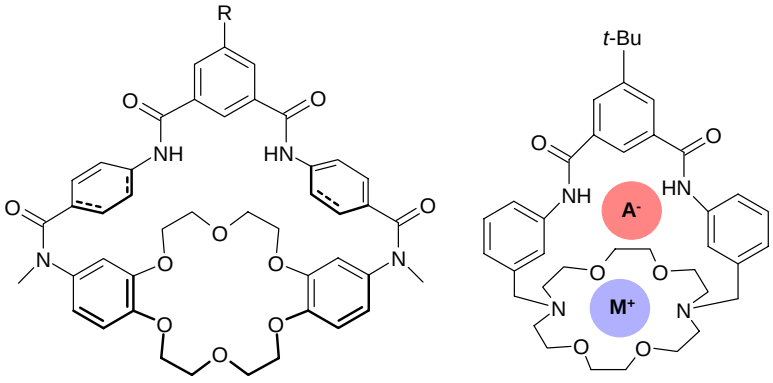

44 (R = H)
45 (R = *t*-Bu)

46

Fig. 1.14

Smith and co-workers reported another macrobicyclic receptor (**46**) as a salt binding analogue of **44** or **45**, but with a smaller distance between anion

and cation binding sites (Fig. 1.14).[84,85] Receptor **46** binds alkali halides as their contact ion-pairs. This result is in contrast to the case of receptor **44** that binds MCl as a solvent separated ion-pair. The structures of the receptor complexed with KAcO, $LiNO_3$, $NaNO_3$, KNO_3 and $NaNO_2$ have been characterized in solution by NMR spectroscopy and in the solid state by X-ray crystallography. The sodium and potassium salts are bound to the receptor as contact ion-pairs, with the metal cation located in the receptor's crown ether ring and the trigonal oxyanion hydrogen-bonded to the receptor NH residues.

Tobey and Anslyn reported the receptors containing a Cu(II) binding site with appended ammonium groups (**47**) and guanidinium groups (**48**), along with thermodynamics analyses of anion binding (Fig. 1.15).[86] Both receptors **47** and **48** show high affinities (10^4 M^{-1}) and selectivities for phosphate over other anions in 98:2 water:methanol at biological pH. The binding of the host-guest pairs is proposed to proceed through ion-pairing interactions between the charged functional groups on both the host and the guest. The affinities and selectivities for oxyanions were determined using absorption titration techniques. Additionally, thermodynamic investigations

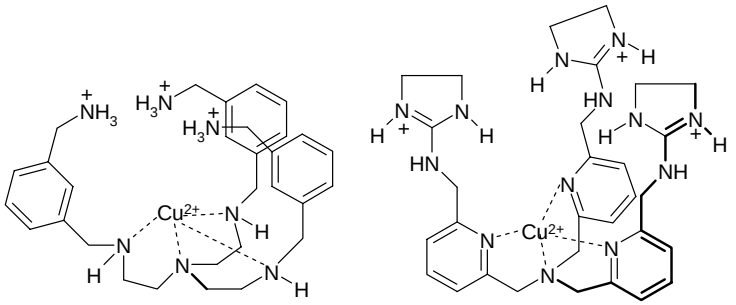

Fig. 1.15

indicate that the **47**:phosphate complex is primarily entropy driven, while the **48**:phosphate complex displays both favorable enthalpy and entropy changes.

Plieger et. al. reported Ni(II) and Cu(II) complexes containing macrocyclic ligand (**49**) in which the metal cation and the sulfate anion are bound in separated sites in a zwitterionic form of the ligand (Fig.1.16).[87] Formation of metal sulfate complexes in the zwitterionic forms of the macrocyclic ligand **49** occurs in pH regions which allow loading and stripping under convenient operating conditions. X-Ray structures of the Cu(II) and Ni(II) sulfate complexes of the *tert*-butyl substituted ligand suggest that the

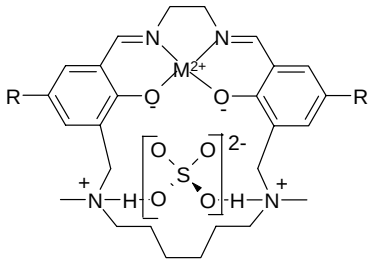

49 (R = *t*-Bu or *n*-C_9H_{19})

Fig. 1.16

de-tuning of M^{2+}-binding results from a distortion from planarity of the "salen" $N_2O_2^{2-}$ donor set imposed by the incorporation of the hexamethylene strap in the ligand. It also reveals that the sulfate is bound as a hydrate in a 2:2:2:2, ligand–M^{2+}–SO_4^{2-}–H_2O, assembly. The formation of assemblies with water-bridged dimers opens up the possibility of transporting the very hydrophilic SO_4^{2-} and HSO_4^- ions as dimers.

Smith et. al. investigated the ability of a pendant donor macrocyclic ligand ((*S*)-thphpc12) in $[Cd((S)\text{-thphpc12})]^{2+}$ complex (**50**) to act as a metal ion-dependent receptor for aromatic anions in solution and in the solid state

(Fig. 1.17).[88] [Cd((*S*)-thphpc12)]$^{2+}$ adopts a stable conical conformation with a large hydrophobic cavity, which has been shown to contain, via complementary multiple hydrogen-bonding, *p*-nitrophenolate, aromatic carboxylates, *p*-toluenesulfonate, certain aromatic amino acid anions, phenoxyacetate, and acetate.

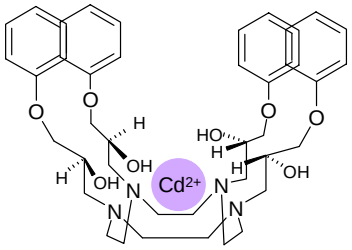

50

Fig. 1.17

Zhou et. al. demonstrated the selective binding of HSO_4^- (or $H_2PO_4^-$) over other anions to the metal-ligand complex $[Mg(L)]^{2+}$ (or $[Ca(L)]^{2+}$) (**51**) by using absorption and fluorescence spectroscopy (Fig. 1.18).[89] The studied complex exhibits the remarkable color change from yellow to rose-red upon introducing HSO_4^- (or $H_2PO_4^-$) in acetonitrile. Same anions cause quenching of fluorescence of **51**. Theoretical computation and ^{1}H NMR spectrum

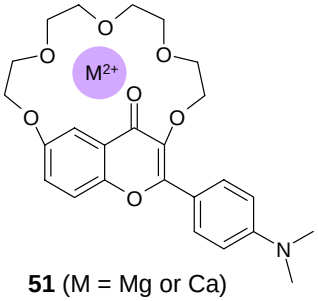

51 (M = Mg or Ca)

Fig. 1.18

indicated that the central-metal assisted hydrogen-bonding between anion and carbonyl group of flavone moiety are possibly the major contributor to the observed change in the absorption and the fluorescence quenching.

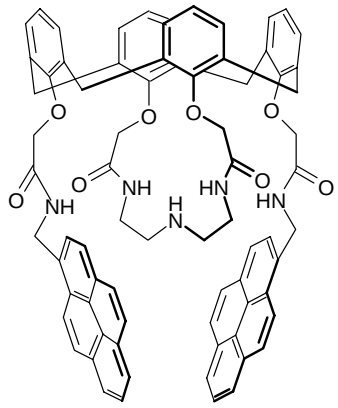

52

Fig. 1.19

Lee et. al. recently reported a new fluorogenic cone calix[4]triazacrown-5 (**52**) bearing two pyrene amide groups (Fig. 1.19) that can detect both Pb^{2+} and F^{-} selectively.[90]

1.4 DNA interaction and photocleavage by metal complexes

In recent years, small molecules are being employed in studies with DNA, with the views to design and develop synthetic restriction enzymes, new anti-tumor drugs, and DNA foot printing agents. A more complete understanding of how to target DNA sites with specificity will lead not only to novel chemotherapeutics but also to a greatly expanded ability for chemists to probe DNA and to develop highly sensitive diagnostic agents. For applications that require specificity of the cleavage such as in the development of drugs or

structural probes, the reagents should have high binding affinity for the site of interest and cleave with high specificity.

Among the reagents studied over the past decades are numerous synthesized molecules that can be activated photochemically. One most attractive characteristic of photocleavage agents is the fact that all components of a system to be studied can be mixed together without initiating the chemical reaction until the sample is irradiated. The most important feature of photoinduced cleavage is the fact that light can be a very selective cofactor in a chemical reaction. Provided the chromophore of the photocleavage agent is sensitive to light at wavelength longer than 300 nm, nucleic acid and most proteins will be transperant, thereby allowing selective excitation of the photocleavage agent. This is critical in limiting the number of side reactions in the system as well as in analyzing the reaction mechanisms.

The DNA photocleavage agents developed so far may be classified as those that are based on derivatives of organic molecules and those that are based on metal complexes. Especially, transition metal complexes are being used at the forefront of many of these efforts. Stable, inert and water-soluble complexes containing spectroscopically active metal centers are extremely valuable as probes of various biological systems. As both spectroscopic tags and functional model for the active centers of proteins, metal complexes have helped to elucidate the mechanism by which metalloproteins function. More recently, such metal complexes have been applied to probe both structural and functional aspects of nucleic acid chemistry.

1.4.1 Structure of DNA

DNA is composed of a series of polymerized nucleotides, joined by phosphodiester bonds between the 5' and 3' carbons of deoxyribose units. A

double helix is formed between the two strands, running in opposite directions.[91] The nucleotide bases form hydrogen-bonds to maintain the structure, with two bonds between adenine and thymine bases (A=T) and three between cytosine and guanine (C≡G) residues. These bases are in the center of the double helix, with the deoxyribose and phosphate groups outside.

The most common form of the DNA double helix is referred to as B-DNA. The B-DNA helix contains two grooves; the major groove and the minor groove. The major groove is wider and deeper. There is a greater opportunity for the molecules to interact in the major groove due to its larger size. In addition, there is a potential for hydrogen-bonding with the base pairs in these grooves, as there is access to both sides of DNA. A-DNA is a helical form that is generated when the duplex is dehydrated. This helix is wider and shorter than B-DNA, and has a narrower major groove and almost no minor groove. A third DNA species is the Z-DNA - a form which consists of a left handed helix (A- and B-DNA are right handed). Z-DNA has only a single groove, and this form is present in oligonucleotides with alternating pyrimidine and purine bases. Most physiological DNA is present in the B-form.

The drugs (DNA binding species/'ligands') can interact with DNA, primarily, in the following ways (Fig. 1.20): (i) Surface binding by inter-ionic interactions with the positively charged species; (ii) Intercalation of the polycyclic aromatic rings in between the base stacks; (iii) Specific recognition in major and minor grooves *via* hydrophobic and hydrogen-bonding interactions.

Among the three basic components of DNA *viz.* sugars, phosphate and heterocyclic bases, the sugar and phosphate provide centers for non-specific hydrophobic and electrostatic interactions, respectively. The heterocyclic

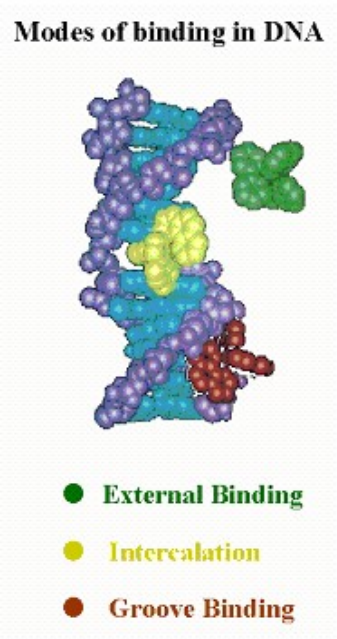

Fig. 1.20

bases are responsible for the specific hydrogen-bonding interactions in the major and minor grooves. Many molecules use combination of the above modes to generate high sequence specificity in DNA binding.

If the ligand has an extended aromatic portion, it can position itself between the base pairs in a sandwich like complex. This phenomenon, called intercalation,[92-94] was first described by Lerman to explain the binding of aminoacridines to DNA.[95] Intercalation is generally brought out by π-π interaction between the molecule and the aromatic heterocyclic bases of DNA. Intercalation increases the separation of adjacent base pairs and the resulting helix distortions are compensated by adjustments in the sugar phosphate backbone, generally by an unwinding of the duplex. Ethidium bromide (EtBr) is the classical example of a DNA intercalator.[93,94]

1.4.2 Methods to study drug-DNA interactions

The drug-DNA interactions can be conveniently monitored by the spectroscopic, electrochemical and other physical methods and also by various biochemical methods.[96-105] The techniques which are relevant to the present work on metal complex-DNA interactions are briefly discussed here.

Absorption and fluorescence titrations are the methods of choice to monitor the metal complex-DNA interactions. The hypochromism and bathochromic shift in the absorption maxima, appearance of isosbestic point(s)

in the absorption spectra and fluorescence enhancement of the metal complex in the presence of DNA are all characteristic features of DNA-metal complex interactions. The different modes of interaction of Δ and Λ isomers of a given metal complex with DNA can be studied not only by the above techniques but also by the circular dichroism (CD) spectroscopy. The CD spectroscopy is also useful in monitoring the conformational changes occurring in DNA upon binding with the metal complexes. DNA exhibits chiral properties, and its ellipticity generally changes upon binding with the metal complex. The transition between single and double stranded DNA can also be monitored effectively by this method.

Study of emission lifetime of the metal complex in the presence of DNA has the potential to provide comprehensible details of binding. An increase in the emission lifetime of the drug is generally observed in its DNA-bound state. Competitive binding studies using EtBr can be done for evaluating the DNA binding by nonfluorescent complexes. On the other hand, better understanding of the mode of binding, *viz.* intercalation/surface binding can be achieved by monitoring the lifetime quenching of the DNA-bound metal complex in the presence of various external quenchers.

Thermal denaturation method is based on the stabilization of DNA in the presence of the drug. Thermal melting of DNA is conversion of the double stranded DNA into the single strand at elevated temperatures. This conversion results in the increase in the absorbance of DNA, which can be conveniently monitored at 260 nm. The mode of binding of the drug to DNA can be interpreted based on the thermal melting data.

Intercalation of a ligand of metal complex to DNA is known to cause a significant increase in the viscosity of DNA solution due to an increase in the separation of the base pairs at the intercalation site and hence, an increase in

the overall DNA molecular length. In contrast, a ligand that binds in the DNA grooves causes either a less pronounced change (positive or negative) or no change in the viscosity of a DNA solution. A partial, non-classical intercalation could bend (or kink) the DNA helix and reduce its effective length and, hence, its viscosity.

Electrophoresis is the standard method used to separate, identify or purify DNA fragments. The technique is simple, rapid to perform and capable of resolving fragments of DNA that cannot be separated by other procedures. In general, electrophoretic separation is carried out on agarose gel for DNA samples. Separation in agarose gel is assisted by resistance to the movement caused by the gel matrix. Closed circular (Form I), nicked circular (Form II) and linear (Form III) DNA of the same molecular weight migrate through agarose gels at different rates.[104,105] Form I of DNA (super coiled) is seen to have maximum mobility due to its shape while form II of DNA (open circular)

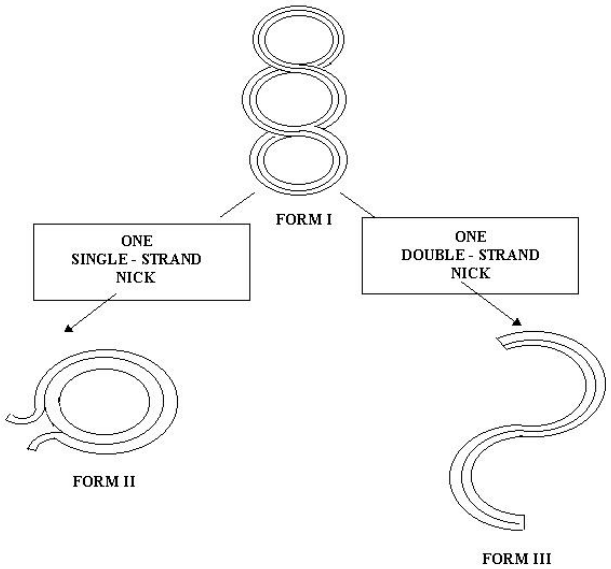

Fig. 1.21

has the least mobility. The mobility of form III (linear) is in between that of the other two forms (Fig. 1.21). In the present study absorption, fluorescence, thermal denaturation and agarose gel electrophoretic techniques have been employed to monitor the metal complex-DNA interactions and photocleavage.

1.4.3 DNA interaction with metal complexes

First major breakthrough in the use of transition metal complexes in bioinorganic/biomedicinal chemistry came from the discovery of "cisplatin" in 1969 by Rosenberg and co-workers.[106] Keck and Lippard have established that square planar platinum(II) complexes containing an aromatic heterocyclic ligand could bind to DNA by intercalation.[107] Ever since, much effort has been devoted to investigate the interactions of platinum(II) complexes with DNA in order to develop more potent "cisplatin" analogues with improved pharmacological properties.[108]

The possible advantages in using transition metal ions other than platinum(II) may involve (i) availability of additional coordination sites, (ii) changes in oxidation state, (iii) alterations in ligand affinity and substitution kinetics and (iv) photodynamic approaches to therapy.[109-111] In this regard, the use of 1,10-phenanathroline (phen)[112] and 2,2′-bipyridine (bpy)[113] ligands has been found to be of immense utility in designing efficient nucleases. The phen-copper(II) complex, $[Cu(phen)_2]^+$, is the first synthetic coordination complex demonstrated to have an efficient nuclease activity.[114,115] Encouraged by this discovery, detailed chemical and biochemical studies were undertaken to understand the properties of various square planar copper(II) complexes.[116,117] This metallointercalation was later extended to three dimension using octahedral complexes. The application of octahedral metallointercalators has permitted the targeting of specific DNA sites by

matching the shape, symmetry and functionalities of the metal complex to that of the DNA target. Moreover, taking advantage of the photophysical and redox properties of metallointercalators, sensitive spectroscopic and reactive probes of DNA have been developed.[109,118-128]

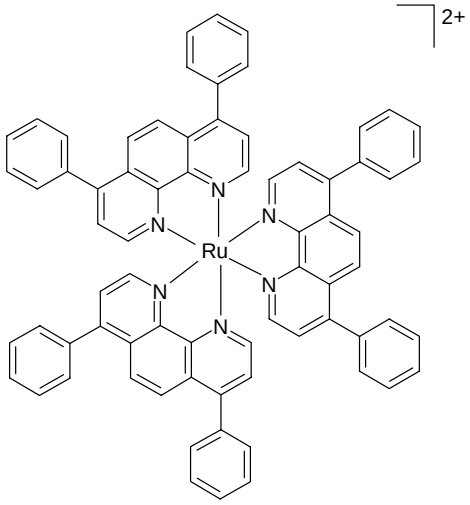

Fig. 1.22

Barton and co-workers have pioneered the application of polypyridyl transition metal complexes as tools to probe recognition of double helical DNA using coordination complexes, matching their shapes, symmetries, and functionalities to sites along the strand.[129-131] Studies with these simple complexes provided a basis for conceptualizing how octahedral complexes might interact noncovalently with DNA and for exploring how the properties of metal complexes, most notably their photophysical and redox characteristics, might be utilized in developing novel probes for DNA. Early experiments indicated a preference for the right handed Δ-isomer to intercalate into the right handed DNA.[132] The enantiometric discrimination in binding was seen for ruthenium(II) complex of 4,7-diphenylphenanthroline,

$[Ru(DIP)_3]^{2+}$ (Fig. 1.22). While Δ-$[Ru(DIP)_3]^{2+}$ was seen to preferentially bind to B form of DNA, Λ-$[Ru(DIP)_3]^{2+}$, the left handed isomer, did not bind intercalatively to the right handed helix. Quite different results were obtained with Z-DNA; both Δ- and Λ-$[Ru(DIP)_3]^{2+}$ bind essentially with equal binding strengths.[131] While the binding interactions of these Δ and Λ-isomers are still being debated, the enantiomeric preferences were seen quite consistently in many such complexes.[133-135]

Increasing the surface area for intercalative stacking by a complex leads to a substantial increase in intercalative binding affinity. As a result, metallointercalators that contain an extended aromatic heterocyclic ligand can provide immensely powerful tools to probe nucleic acids.[124,136-138] In an elegant experiment, Barton and co-workers have shown that $[Ru(bpy)_2(dppz)]^{2+}$ (dppz = dipyrido[3,2-*a*:2',3'-*c*]phenazine) works as a "molecular light switch" for DNA.[139] $[Ru(bpy)_2(dppz)]^{2+}$ is non-luminescent in aqueous buffered solution but, the luminescence increases to ~10^4 times in the presence of CT DNA or Z form of DNA to which the complex binds avidly (K_b = > 10^6 M^{-1}). Hartshorn and Barton have synthesized a series of mixed-ligand ruthenium(II) complexes with modified dppz as a ligand.[140] All these new complexes were found to be luminescent to some degree in aqueous solution in the absence of DNA. However, for a few complexes 20-300 times emission enhancement was observed upon binding with DNA. The molecular light switch effects seen for $[Ru(bpy)_2(dppz)]^{2+}$ and $[Ru(phen)_2(dppz)]^{2+}$ upon intercalation to DNA has been attributed to the protection of phenazine nitrogen atoms from interaction with water whereas, in the free complex, the excited state is quenched by water. Examples of such ruthenium(II) complexes

bearing planar ligands and behaving as molecular light switches are provided in fig. 1.23.

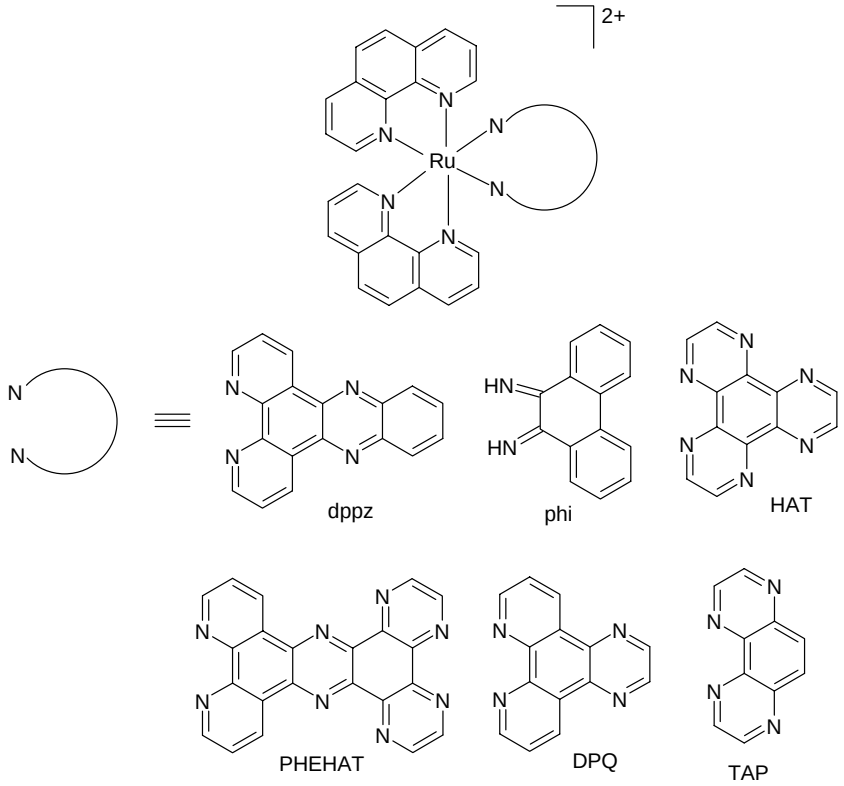

Fig. 1.23

More recently, it has been shown that further derivatization of dppz with suitable electron withdrawing groups not only accentuates DNA binding and photocleavage efficiencies of the ensuing complexes but also facilitates the study of other interesting associated functional aspects.[141-143] For example, $[Ru(phen)_2(qdppz)]^{2+}$ (qdppz = naptho[2,3-*a*]dipyrido[3,2-*h*:2',3'-*f*]phenazine-5,18-dione) endowed with a novel, quinone fused dipyridophenazine ligand, is not only an avid binder of DNA but also an efficient photocleavage agent of the plasmid DNA. The corresponding reduced species, $[Ru(phen)_2(hqdppz)]^{2+}$,

also binds and photocleaves DNA, albeit with less efficiency.[141,142] It has also been demonstrated that the redox couple $[Ru(phen)_2(qdppz)]^{2+}$/ $[Ru(phen)_2(hqdppz)]^{2+}$ represents an "electro-photo switch". A series of ruthenium(II) complexes containing another modified dipyridophenazine ligand, viz: 6,7-dicyanodipyrido quinoxaline (dicnq) was reported to bind to DNA with moderate strengths.[141,143] $[Ru(phen)_2(dicnq)]^{2+}$ has been shown to be an efficient "molecular light switch" for DNA.[141] Thus, these results testify to importance of the architectural intricacies and electronic structures of the new dppz-based ligands in dictating the useful photochemical/electrochemical functions of their complexes.

Most of the ruthenium(II) complexes contain only planar aromatic ligands and investigations of polypyridyl ruthenium(II) complexes with non planar ligands as DNA binding reagents have been relatively few.[118,130,144-147] A few such latter type of complexes are known to exhibit interesting properties upon binding to DNA as discussed below.

Strekas and co-workers have designed two ruthenium(II) complexes with 'out of plane' ligands; $[Ru(bpy)_2(qpy)]^{2+}$ (qpy = quaterpyridyl) and $[Ru(bpy)_2(dpp)]^{2+}$ (dpp = 2,3-di-2-pyridylpyrazine) are two illustrative examples.[146,147] While the former complex can intercalate DNA, the latter cannot. Ji and co-workers have reported a series of imidazole fused phen ligands wherein the imidazole ring is out of the plane from the phen moiety (Fig. 1.24) and also biphenyl derivatives of phen/dppz, all of which exhibit the effect of ligand planarity on the DNA binding strength of the complexes.[118,120,148-151] The DNA binding affinity for $[Ru(bpy)_2(PIP)]^{2+}$ is higher than that of $[Ru(bpy)_2(IP)]^{2+}$, and this has been attributed to the extended conjugation provided by the phenyl ring in PIP (Fig. 1.24).[151] DNA binding affinities of the corresponding modified PIP ligands

($[Ru(bpy)_2(HPIP)]^{2+}$, $[Ru(bpy)_2(CIP)]^{2+}$ and $[Ru(bpy)_2(NIP)]^{2+}$) are quite varied.[149,150] In the case of $[Ru(bpy)_2(HPIP)]^{2+}$, the *ortho*- phenolic group of HPIP would be nearly coplanar with the imidazole ring due to the formation of an intramolecular hydrogen-bond with the nitrogen atom of the imidazole ring, leading to some additional affinity.[149] On the other hand, intramolecular hydrogen-bond is nonexistent for $[Ru(bpy)_2(CIP)]^{2+}$ and $[Ru(bpy)_2(NIP)]^{2+}$ and hence, phenyl group is out of plane leading to lower DNA binding affinity in each case.[149]

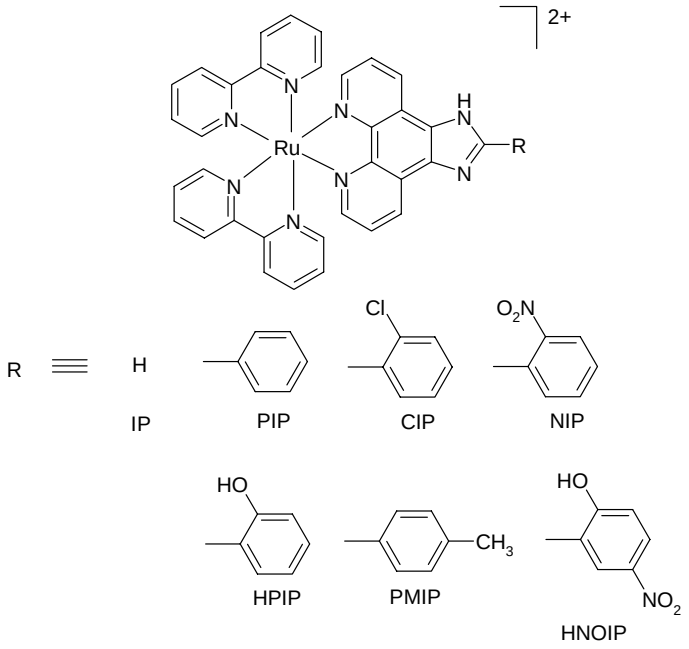

Fig. 1.24

Quinones and its reduced species such as semiquinone radicals represent a class of toxicological intermediates which can create a variety of hazardous effects in vivo, including acute cytotoxicity, immunotoxicity, and carcinogenesis.[152-155] Quinones are Michael acceptors, and cellular damage can occur through alkylation of crucial cellular proteins and/or DNA.

Alternatively, quinones are highly redox active molecules which can redox cycle with their semiquinone radicals, leading to formation of reactive oxygen species (ROS), including superoxide, hydrogen peroxide, and ultimately the hydroxyl radical. Production of ROS can cause severe oxidative stress within cells through the formation of oxidized cellular macromolecules, including lipids, proteins, and DNA. Formation of oxidatively damaged bases such as 8-oxodeoxyguanosine has been associated with ageing and carcinogenesis.

1.5 Motivation of the present work

Optical properties of small molecules, where 2,2′-bipyridyl or 2,2′:6′,2′′-terpyridine are connected with pyrene via a conjugated linker such as 2,5-diethynylated thiophene,[30] 1,4-diethynylated-2,5-dioctyloxyphenylene[31,32] or ethynylene,[33] have been studied elaborately with transition metal ions. Although, there are many reports where pyrene is connected with 2,2′-bipyridyl via ethynylene linkage, the photophysical properties and influence of metal ions on the dyads, where anthracene or pyrene are linked to 2,2′-bipyridyl via ethylene linker, have not been studied so far. Therefore, we intended to study the photophysical behavior of two dyads where 2,2′-bipyridyl is connected with anthracene (**mpae**) or pyrene (**mppe**) by ethylene linker (Fig. 1.25). Emission spectra of both **mpae** and **mppe** comprise dual bands which are attributed to emission from the π, π^* excited singlet state and the intramolecular charge transfer (ICT) state. Formation of new low energy absorption band has been observed for **mppe** in presence of transition (Mn^{2+}, Co^{2+}, Ni^{2+}, Cu^{2+}) and post-transition (Zn^{2+}, Cd^{2+}, Pb^{2+}) metal ions whereas, no such new absorption band at low energy has been formed for **mpae** on addition of these metal ions. **mppe** exhibits fluorescent

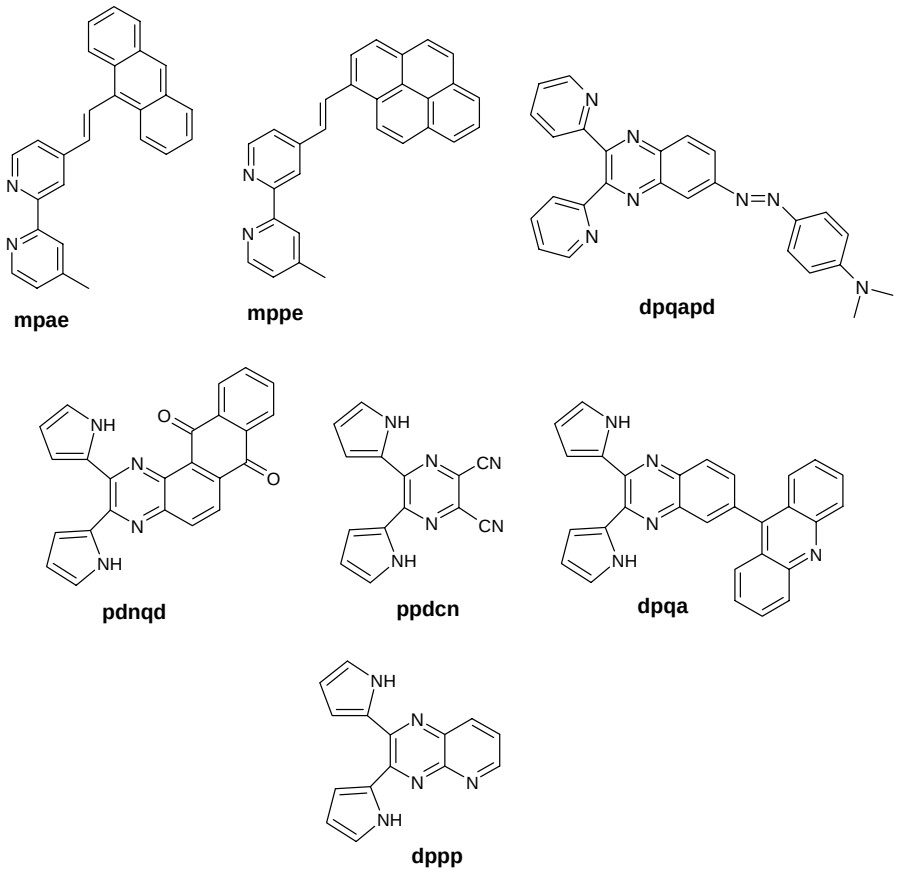

Fig. 1.25

OFF/ON signaling behavior in presence of post-transition metal ions Zn^{2+}, Cd^{2+} and Pb^{2+}, leading to the generation of a new broad, red-shifted emission band.

The cation sensing property of azo-dye derivatives by colorimetric method have been exploited only in few cases[36-39] and just one report is available where transition metal ion, *viz.* Cu^{2+} is detected by color change using an azo-dye derivative.[39] The azo-dye derivatives are easy to prepare and color change of such molecules with metal ion input are drastic. This is why

we intended to synthesize and study the transition metal ion binding property of the azo-dye derivative **dpqapd** (Fig. 1.25) where dimethylamine acts as electron-donor and dipyridylquinoxaline as electron-acceptor moieties. The sensing of transition metal ions (Co^{2+}, Ni^{2+}, Cu^{2+}, Zn^{2+} and Cd^{2+}) by **dpqapd** in CH_3CN is demonstrated by change in color from yellow to pink or light-pink or colorless.

Recently, functionalized calix[4]pyrrole[68] or dipyrrolylquinoxaline (DPQ)[69-74] class of compounds have been employed extensively for selective colorimetric sensing of anions. The latter class of sensors has the dual advantage of possessing a built-in chromophore and being readily accessible in two steps from commercially available materials. In addition, introduction of electron withdrawing groups at the pyrrole or quinoxaline subunits of the DPQ moiety is known to result in enhanced binding of the anion with the receptor.[69-73] Hence, we were interested to synthesize two DPQ derivatives **pdnqd** and **dpqa**, and one dipyrrolylpyrazine (DPP) derivative **ppdcn** (Fig. 1.25) which show dramatic, binding-induced color changes in the presence of F^-. As both quinone and cyano substituents are redox active, F^- binding event of **pdnqd** and **ppdcn** was monitored by the electrochemical methods as well.

Simultaneous sensing of both cations and anions has been achieved by integrating cationic and anionic guest binding sites in a single molecule.[78-90] We have recently embarked upon designing systems that can sense both anions and transition metal ions. In order to accomplish this goal, we have exploited fluoride ion signaling potential of the DPP derivatives and transition metal ion binding ability of the pyridine moiety. Amalgamating these approaches we have developed **dppp**, wherein a pyridine ring has been fused with the pyrazine frame (Fig. 1.25). This new DPP derivative binds the metal ions much more strongly compared to the previously reported DPP derivative,

ppdcn which lack the additional fused pyridine ring. The sensing of F^- and metal ions (Co^{2+}, Ni^{2+}, Cu^{2+}, Zn^{2+} and Cd^{2+}) by **dppp** in acetonitrile is observable by change in color from yellowish-green to red in the case of former and to brown or light-brown in the latter cases.

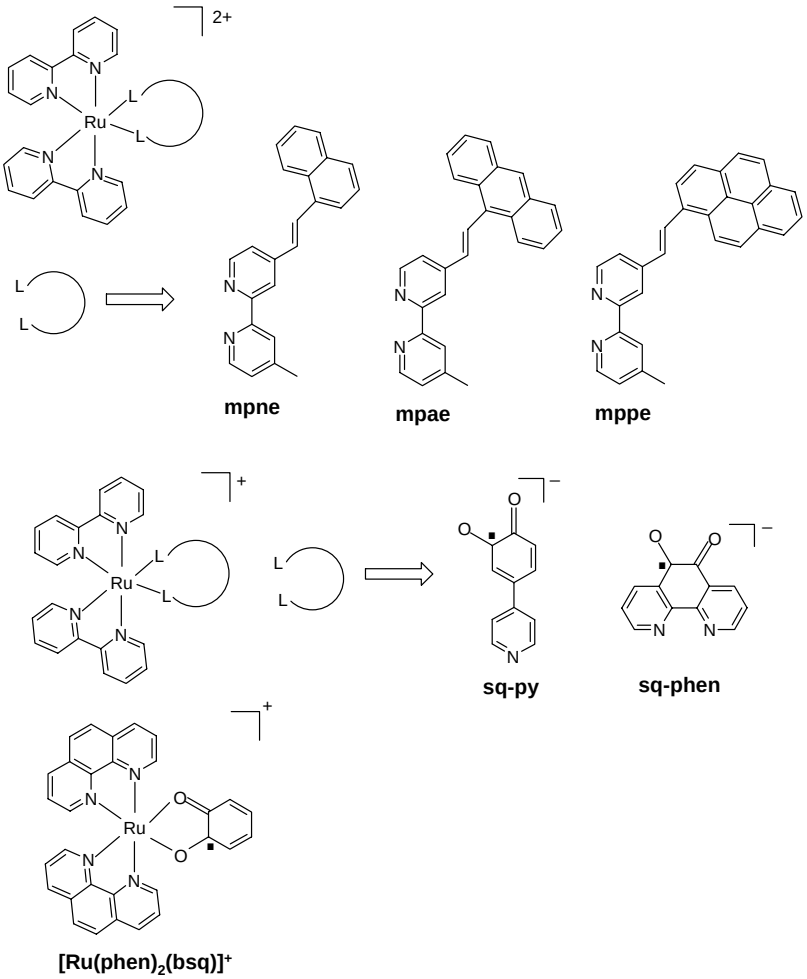

Fig. 1.26

Ruthenium(II) polypyridyl complexes are being employed in studies with DNA, with a view to design and develop synthetic restriction enzymes, new drugs, and DNA foot printing agents in recent years.[109-128] These complexes have been found to be particularly useful for the above-mentioned purposes because of their potential to bind DNA *via* multitude of interactions and to cleave the duplex by virtue of their intrinsic chemical, electrochemical and photochemical reactivity. Presently, a great deal of attention is centered around DNA interactions of ruthenium(II) complexes containing modified **bpy**/**phen** ligands (**bpy** = 2,2′-bipyridyl and **phen** = 1,10-phenanthroline), where the modification of the **bpy**/**phen** is done in such a way that it augments the intercalative interaction of the complexes.[112,113,117-124,126] Earlier studies show that **[Ru(bpy)$_2$(sq)]$^+$** -based (**sq** is semiquinone) complexes act as a mild oxidant towards organic substrate.[156-159] Detrimental roles of intermediate semiquinone radicals forming oxidized cellular macromolecules including lipids, proteins and DNA inside cells are well known[152-155] and thus **[Ru(bpy)$_2$(sq)]$^+$** -based complexes are expected to behave as an non-innocent molecule towards DNA. With these in our mind, we have investigated DNA binding and photocleavage/redox properties of six new ruthenium(II) complexes that incorporate modified **bpy**/**phen** or semiquinone ligands (Fig. 1.26). Both **[Ru(bpy)$_2$(mpne)]$^{2+}$** and **[Ru(bpy)$_2$(mpae)]$^{2+}$** are moderate-to-strong binders of calf thymus (CT) DNA. However, supercoiled pBR 322 DNA photocleavage activities of these two complexes follow the order: **[Ru(bpy)$_2$(mpne)]$^{2+}$** > **[Ru(bpy)$_2$(mpae)]$^{2+}$**, under the identical conditions of drug and light dose. The other ruthenium(II) complexes containing the semiquinone-based ligands are found to oxidize the sugar unit of DNA.

1.6 Layout of the thesis

The thesis has been divided into eight chapters. The first chapter provides the discussions on recent literatures related to cation sensing, anion sensing, ion-pair sensing, DNA binding and photocleavage by metal complexes, and motivation of the present investigation. A general description of the synthesis of various compounds as well as various techniques and methodologies used in the research work are presented in the second chapter. The third chapter describes photophysical properties and metal ion sensing behavior of two anthracene/pyrene-(2,2′-bipyridine) dyads, **mpae** and **mppe**. Colorimetric sensing of transition metal ions by dipyridylquinoxalinazo compound **dpqapd** has been provided in fourth chapter. The fifth chapter has been devoted to colorimetric sensing of F^- by three dipyrrolyl derivatives **pdnqd**, **ppdcn** and **dpqa**. The sixth chapter elaborates the colorimetric sensing of both F^- and transition metal ions by dipyrrolylpyrazine derivative **dppp**. DNA binding and photocleavage/redox properties of six new ruthenium(II) complexes that incorporate modified 2,2′-bipyridyl/1,10-phenanthroline or semiquinone ligands are presented in the seventh chapter. The last chapter summarizes the findings of the present investigation.

1.7 References

1) Lehn, J.-M. *Angew. Chem., Int. Ed. Engl.* **1990**, *29*, 1304.
2) Lehn, J.-M. *Supramolecular Chemistry;* VCH: Weinheim, 1995.
3) Balzani, V.; Scandola, F. *Supramolecular Photochemistry*; Ellis-Horwood: Chichester, 1991.

4) Balzani, V.; Credi, A.; Scandola, F. In *Transition Metals in Supramolecular Chemistry*; Fabbrizzi, L., Poggi, A., Eds.; Kluwer: Dordrecht, 1994.

5) Bryan, A. J.; de Silva, A. P.; de Silva, S. A.; Rupasinghe, R. A. D. D.; Sandanayake, K. R. A. S. *Biosensors* **1989**, *4*, 169.

6) Bissell, R. A.; de Silva, A. P.; Gunaratne, H. Q. N.; Lynch, P. L. M.; Maguire, G.E. M.; Sandanayake, K. R. A. S. *Chem. Soc. Rev*. **1992**, *21*, 187.

7) *Biochemical Fluorescence*: *Concepts*; Chen, R. F., Edelhoch, H., Eds.; Dekker: New York, 1976; Vols. 1 and 2.

8) *Fluorescent Probes*; Beddard, G. S., West, M. A., Eds.; Academic: London, 1981.

9) Fernandez-Gutierrez, A.; Munoz de la Pena, A. In *Molecular Luminescence Spectroscopy. Methods and Applications*; Schulman, S. G., Ed.; Wiley, New York, 1985; Part 1, p 371.

10) *Fluorescent Chemosensors of Ion and Molecule Recognition*. Czarnik, A. W., Ed.; ACS Symp. Ser. 538; American Chemical Society: Washington DC, 1993.

11) Valeur B. In *Molecular Luminescence Spectroscopy*; Schulman, S. G.; Ed.; Wiley, New York, 1993; Part 3, p 25.

12) Probe Design and Chemical Sensing. *Topics in Fluorescence Spectroscopy*; Lakowicz, J. R.; Ed.; Plenum, New York, 1994; Vol. 4.

13) *Biophysical and Biochemical Aspects of Fluorescence Spectroscopy*; Dewey, T. G., Ed.; Plenum: New York, 1991.

14) Sharp, S. L.; Warmack, R. J.; Goudonnet, J. P.; Lee, I.; Ferrell, T. L. *Acc. Chem. Res.* **1993,** *26*, 377.

15) Lewis, A.; Lieberman, K. *Anal. Chem*. **1991,** *63*, 625A.

16) Xie, X. S. *Acc. Chem. Res*. **1996**, *29*, 598.

17) *Fibre Optic Chemical Sensors and Biosensors*; Wolfbeis, O. S., Ed.; CRC Press: Boca Raton, 1991; Vols. 1 and 2.

18) *Biosensors with Fiberoptics*; Wise, D. L., Wingard, L. B., Eds.; Humana Press, Clifton, 1991.

19) Tsien, R. Y., *Chem. Eng. News*, **1994**, July 18, 34.

20) Dixon, A. J.; Benham, G. S. *Int. Lab*. **1988** (4), 38.

21) de Silva, A. P.; Gunaratne, H. Q. N.; Gunnlaugsson, T.; Huxley, A. J. M.; McCoy, C. P.; Rademacher, J. T.; Rice, T.E. *Chem. Rev.* **1997**, *97*, 1515.

22) Fabbrizzi, L.; Poggi, A. *Chem. Soc. Rev*. **1995**, 197.

23) Valeur, B.; Leray, I. *Coord. Chem. Rev.* **2000**, *205*, 3.

24) Lohr, H.-G.; Vogtle, F. *Acc. Chem. Res*. **1985**, *18*, 65.

25) Bourson, J.; Valeur, B. *J. Phys. Chem*. **1989**, *93*, 3871.

26) Bourson, J.; Pouget, J.; Valeur, B. *J. Phys. Chem.* **1993**, *97*, 4552.

27) Yang, Q.-Z.; Wu, L.-Z.; Zhang, H.; Chen, B.; Wu, Z.-X.; Zhang, L.-P.; Tung, C.-H. *Inorg. Chem.* **2004**, *43*, 5195.

28) Descalzo, A. B.; Martınez-Manez, R.; Radeglia, R.; Rurack, K.; Soto, J. *J. Am. Chem. Soc.* **2003**, *125*, 3418.

29) Barigelletti, F.; Flamigni, L.; Calogero, G.; Hammarstrom, L.; Sauvage, J.-P.; Collin, J.-P. *Chem. Commun.* **1998**, 2333.

30) Benniston, A. C.; Harriman, A.; Lawrie, D. J.; Mayeux, A.; Rafferty, K.; Russell, O. D. *Dalton Trans.* **2003**, 4762.

31) Leroy-Lhez, S.; Parker, A.; Lapouyade, P.; Belin, C.; Ducasse, L.; Oberle, J.; Fages, F. *Photochem. Photobiol. Sci.* **2004**, *3*, 949.

32) Leroy, S.; Soujanya, T.; Fages, F. *Tetrahedron Lett.* **2001**, *42*, 1665.

33) Harriman, A.; Hissler, M.; Ziessel, R. *Phys. Chem. Chem. Phys.* **1999**, *1*, 4203.

34) Kim, J. Y.; Kim, G.; Kim, C. R.; Lee, S. H.; Lee, J. H.; Kim, J. S. *J. Org. Chem.* **2003**, *68*, 1933.

35) Lee, S. H.; Kim, J. Y.; Ko, J.; Lee, J. Y.; Kim, J. S. *J. Org. Chem.* **2004**, *69*, 2902.

36) Gunnlaugsson, T.; Nieuwenhuyzen, M.; Richard, L.; Thoss, V. *Tetrahedron Lett.* **2001**, *42*, 4725.

37) Gunnlaugsson, T.; Nieuwenhuyzen, M.; Richard, L.; Thoss, V. *J. Chem. Soc., Perkin Trans. 2* **2002**, 141.

38) Gunnlaugsson, T.; Leonard, J. P. *J. Chem. Soc., Perkin Trans. 2* **2002**, 1980.

39) Gunnlaugsson, T.; Leonard, J. P.; Murray, N. S. *Org. Lett.* **2004**, *6*, 1557.

40) Stryer, L. *Biochemistry*; 4th Ed.; W. H. Freeman & Co.: New York, 1995.

41) *Riegel's Handbook of Industrial Chemistry*, 9th Ed.; Kent, J. A., Ed.; Van Nostrad Reinhold-Interantional Thomson Publishing: New York, 1992.

42) *Ullmann's Encyclopedia of Industrial Chemistry*, 6th Ed.; Bailey, J. E., Bohnet, M., Brinker, C. J., Cornils, B., Evans, T., Greim, H., Hegedus, L. L., Heitbaum, J., Keim, W., Kleemann, A., Kreysa, G., Loliger, J., McGuire, J. L., Mitsutani, A., Plass, L., Stephanopoulos, G., Werner, D., Woditsch, P., Yoda, N., Eds.; 1999 Electronic Release; Wiley VCH: New York, 1999.

43) *Supramolecular Chemistry of Anions*; Bianchi, A., Bowman-James, K., Garcia-Espana, E., Eds.; Wiley-VCH: New York, 1997.

44) *Comprehensive Supramolecular Chemistry*; Atwood, J. L., Davies, J. E., MacNicol, D. D., Vogtle, F., Reinhoudt, D. N., Lehn, J. M., Eds.; Pergamon-Elsevier Science: Oxford, 1996.

45) Christianson, D. W.; Lipscomb, W. N. *Acc. Chem. Res.* **1989**, *22*, 62.

46) Moss, B. *Chem. Ind.* **1996**, 407.

47) Glidewell, C. *Chem. Br.* **1990**, *26*, 137.

48) Hofmeister, F. *Arch. Exp. Pathol. Pharmakol.* **1888**, *24*, 247.

49) Schmidtchen, F. P.; Berger, M. *Chem. Rev.* **1997**, *97*, 1609.

50) Gale, P. A. *Coord. Chem. Rev.* **2000**, *199*, 181.

51) Gale, P. A. *Phil. Trans. R. Soc. Lond. A.* **2000**, *358*, 431.

52) Beer, P. D.; Gale, P. A. *Angew. Chem. Int. Ed.* **2001**, *40*, 486.

53) *Special Issue on 'Synthetic Anion Receptor Chemistry', Coord. Chem. Rev.* **2003**, *240*.

54) Martinez-Manez, R.; Sancenon, F. *Chem. Rev.* **2003**, *103*, 4419.

55) Camiolo, S.; Gale, P. A.; Ogden, M. I.; Skelton, B. W.; White, A. H. *J. Chem. Soc., Perkin Trans. 2* **2001**, 1294.

56) Abouderbala, L. O.; Belcher, W. J.; Boutelle, M. G.; Cragg, P. J.; Dhaliwal, J.; Fabre, M.; Steed, J. W.; Turner, D. R.; Wallace, K. J. *Chem. Commun.* **2002**, 358.

57) Bazzicalupi, C.; Bencini, A.; Bianchi, A.; Cecchi, M.; Escuder, B.; Fusi, V.; Garcia-Espana, E., Giorgi, C.; Luis, S. V.; Maccagni, G.; Marcelino, V.; Paoletti, P.; Valtancoli, B. *J. Am. Chem. Soc.* **1999**, *121*, 6807.

58) Inoue, Y.; Hakushi, T.; Liu, Y.; Tong, L.-H.; Shen, B.-J.; Jin, D.-S. *J. Am. Chem. Soc.* **1993**, *115*, 475.

59) Steed, J. W.; Juneja, R. K.; Atwood, J. L. *Angew. Chem. Int. Ed. Engl.* **1994**, *33*, 2456.

60) Newcomb, M.; Horner, J. H.; Blanda, M. T.; Squattrito, P. J. *J. Am. Chem. Soc.* **1989**, *111*, 6294.

61) Yamaguchi, S.; Akiyama, S.; Tamao, K. *J. Am. Chem. Soc.* **2000**, *122*, 6793.

62) Yamaguchi, S.; Akiyama, S.; Tamao, K. *J. Am. Chem. Soc.* **2001**, *123*, 11372.

63) Ogawa, K.; Aoyaki, S.; Takeuchi, Y. *J. Chem. Soc., Perkin Trans. 2* **1993**, 2389.

64) Yang. X.; Knobler, C. B.; Hawthorne, M. F. *Angew. Chem. Int. Ed. Engl.* **1991**, *30*, 1507.

65) Echavarren, A.; Galan, A.; de Mendoza, J.; Salmeron, A.; Lehn, J.-M. *J. Am. Chem. Soc.* **1989**, *111*, 4994.

66) Sessler, J. L.; Cyr, M. J.; Lynch, V.; McGhee, E.; Ibers, J. A. *J. Am. Chem. Soc.* **1990**, *112*, 2810.

67) Miyaji, H.; Sessler, J. L. *Angew. Chem. Int. Ed. Engl.* **2001**, *40*, 154.

68) Miyaji, H.; Sato, W.; Sessler, J. L. *Angew. Chem. Int. Ed. Engl.* **2000**, *39*, 1777.

69) Black, C. B.; Andrioletti, B.; Try, A. C.; Ruiperez, C.; Sessler, J. L. *J. Am. Chem. Soc.* **1999**, *121*, 10438.

70) Anzenbacher, P., Jr.; Try, A. C.; Miyaji, H.; Jursikova, K.; Lynch, V. M.; Marquez, M.; Sessler, J. L. *J. Am. Chem. Soc.* **2000**, *122*, 10268.

71) Sessler, J. L.; Maeda, H.; Mizuno, T.; Lynch, V. M.; Furuta, H. *Chem. Commun.* **2002**, 862.

72) Mizuno, T.; Wei, W.-H.; Eller, L. R.; Sessler, J. L. *J. Am. Chem. Soc.* **2002**, *124*, 1134.

73) Anzenbacher, P., Jr.; Tyson, D. S.; Jursikova, K.; Castellano, F. N. *J. Am. Chem. Soc.* **2002**, *124*, 6232.

74) Aldakov, D.; Anzenbacher, P., Jr. *Chem. Commun.* **2003**, 1394.

75) Cho, E. J.; Moon, J. W.; Ko, S. W.; Lee, J. Y.; Kim, S. K.; Yoon, J.; Nam, K. C. *J. Am. Chem. Soc.* **2003**, *125*, 12376.

76) Jose, D. A.; Kumar, D. K.; Ganguly, B.; Das, A. *Org. Lett.* **2004**, *6*, 3445.

77) Denuault, G.; Gale, P. A.; Hursthouse, M. B.; Light, M. E.; Warriner, C. N. *New J. Chem.* **2002**, 811.

78) Shukla, R.; Kida, T.; Smith, B. D. *Org. Lett.* **2000**, *2*, 3099.

79) Kubik, S.; Goddard, R. *J. Org. Chem.* **1999**, *64*, 9475.

80) Beer, P. D.; Hopkins, P. K.; Mckinney, J. D. *J. Chem. Soc., Chem. Commun.* **1999**, 1253.

81) Beer, P. D.; Cooper, J. B. *J. Chem. Soc., Chem. Commun.* **1998**, 129.

82) Tozawa, T.; Misawa, Y.; Tokita, S.; Kubo, Y. *Tetrahedron Lett.* **2000**, *41*, 5219.

83) Deetz, M. J.; Shang, M.; Smith, B. D. *J. Am. Chem. Soc.* **2000**, *122*, 6201.

84) Mahoney, J. M.; Beatty, A. M.; Smith, B. D. *J. Am. Chem. Soc.* **2001**, *123*, 5847.

85) Mahoney, J. M.; Stucker, K. A.; Jiang, H.; Carmichael, I.; Brinkmann, N. R.; Beatty, A. M.; Noll, B. C.; Smith, B. D. *J. Am. Chem. Soc.* **2005**, *127*, 2922.

86) Tobey, S. L.; Anslyn, E. V. *J. Am. Chem. Soc.* **2003**, *125*, 14807.

87) Plieger, P. G.; Tasker, P. A.; Galbraith, S. G. *Dalton Trans.* **2004**, 313.

88) Smith, C. B.; Stephens, A. K. W.; Wallwork, K. S.; Lincoln, S. F.; Taylor, M. R.; Wainwright, K. P. *Inorg. Chem.* **2002**, *41*, 1093.

89) Zhou, L.-L.; Sun, H.; Li, H.-P.; Wang, H.; Zhang, X.-H.; Wu, S.-K.; Lee, S.-T. *Org. Lett.* **2004**, *6*, 1071.

90) Lee, J. Y.; Kim, S. K.; Jung, J. H.; Kim, J. S. *J. Org. Chem.* **2005**, *70*, 1463.

91) Watson, J. D.; Crick, F. H. *Nature* **1953,** *171*, 737.

92) Neidle, S.; Abraham, Z. *CRC Crit. Rev. Biochem*. **1984,** *17*, 73.

93) Wang, J. C. *J. Mol. Biol.* **1974**, *89*, 783.

94) Wang, A. H-J. *Current Opinion in Structrural Biology* **1992,** *2*, 361.

95) Lerman, L. S. *J. Mol. Biol*. **1961**, *3*, 18.

96) *Practical Biochemistry*; Wilson, K., Walker, J., Eds.; Cambridge University Press: Cambridge, 2000.

97) *Nucleic Acid – Metal Ion Interactions*; Spiro, T. G., Ed.; John Wiley & Sons: New York, 1980.

98) Sambrook, J.; Russell, D. W. *Molecular Cloning A Laboratory Manual;* 3rd Ed. Cold Spring Harbor Laboratory Press: New York, 2001.

99) Long, E. C.; Barton, J. K. *Acc. Chem. Res.* **1990,** *23*, 271.

100) Kelly, J. M.; Tossi, A. B.; McConnell, D. J.; OhUigin, C. *Nucl. Acid. Res*. **1985**, *13*, 6017.

101) Marmur, J.; Doty, P. *J. Mol. Biol*. **1962**, *5*, 109.

102) Cohen, G.; Eisenberg, H. *Biopolymers* **1969,** *8*, 45.

103) Thorne, H. V. *J. Mol. Biol*. **1967**, *24*, 203.

104) Wang, J. *J. Mol. Biol*. **1974**, *89*, 783.

105) Waring, M. J. *J. Mol. Biol*. **1970**, *54*, 247.

106) Rosenberg, B.; van Camp, L.; Trosko, J. E. *Nature* **1969**, *222*, 385.

107) Keck, M. V.; Lippard, S. J. *J. Am. Chem. Soc.* **1992,** *114*, 3386.

108) Jamieson, E. R.; Lippard, S. J. *Chem. Rev.* **1999**, *99*, 2467.

109) Clarke, M, J.; Zhu, F.; Frasca, D. R. *Chem. Rev.* **1999**, *99*, 2511.

110) Ali, H.; van Lier, J. E. *Chem. Rev.* **1999**, *99*, 2379.

111) Clarke, M. J.; Stubbs, M. *Metal Ions in Biological Systems;* Sigel, A., Sigel, H., Eds.; Marcel Dekker: New York 1996, *32*, 727.

112) Sammes, P. G.; Yahioglu, G. *Chem. Soc. Rev*. **1994**, 327.

113) Kaes, C.; Katz, A.; Hosseini, M. W. *Chem. Rev.* **2000**, *100*, 3553.

114) Sigman, D. S.; Graham, D. R.; D'Aurora, V.; Stern, A. M. *J. Biol. Chem*. **1979,** *254*, 12269.

115) Sigman, D. S. *Acc. Chem. Res*. **1986**, *19*, 180.

116) Sigman, D. S.; Bruice, T. W.; Mazumder, A.; Sutton, C. L. *Acc. Chem. Res*. **1993**, *26*, 98.

117) McMillin, D. R.; McNett, K. M. *Chem. Rev.* **1998**, *98*, 1201.

118) Xiong, Y.; Ji, L-N. *Coord. Chem. Rev*. **1999**, *185-186*, 711.

119) Clarke, M, J. *Coord. Chem. Rev*. **2002**, *232*, 69.

120) Ji, L-N.; Zou, X-H.; Liu, J-G. *Coord. Chem. Rev*. **2001**, *216-217*, 513.

121) Ortmans, I.; Moucheron, C.; Mesmaeker, A. K. *Coord. Chem. Rev*. **1998**, *168*, 233.

122) Yam, V. W-W.; Lo, K. K-W. *Coord. Chem. Rev*. **1998**, *184*, 157.

123) Muller, J. G.; Kayser, L. A.; Paikoff, S. J.; Duarte, V.; Tang, N.; Perez, R. J.; Rokita, S. E.; Burrows, C. J. *Coord. Chem. Rev*. **1999**, *185-186*, 761.

124) Erkkila, K. E.; Odom, D. T.; Barton, J. K. *Chem. Rev*. **1999**, *99*, 2777.

125) Mesmaeker, A. K.; Lecomte, J-P.; Kelly, J-M. *Topics in Current Chem*. **1996,** *177*, 25.

126) Burrows, C. J.; Rokita, S. E. *Acc. Chem. Res.* **1994**, *27*, 295.

127) Johnston, D. H.; Welch, T. W.; Thorp, H. H. *Metal Ions in Biological Systems;* Sigel, A., Sigel, H., Eds.; Marcel Dekker: New York, 1996, *33*, 297.

128) Norden, B.; Lincoln, P.; Akerman, B.; Tuite, E. *DNA Interactions with Substitution-Inert Transition Metal Ion Complexes*; Sigel, A., Sigel, H., Eds.; Marcel Dekker: New York, 1996, *33*, 177.

129) Barton, J. K.; Danishefsky, A. T.; Goldberg, J. M. *J. Am. Chem. Soc.* **1984**, *106*, 2172.

130) Barton, J. K.; Raphael, A. L. *Proc. Natl. Acad. Sci. U. S. A.* **1985**, *82*, 6460.

131) Kumar, C. V.; Barton, J. K.; Turro, N. J. *J. Am. Chem. Soc.* **1985**, *107*, 5518.

132) Barton, J. K. *Science* **1986**, *233*, 727.

133) Satyanarayana, S.; Dabrowiak, J. C.; Chaires, J. B. *Biochemistry* **1992**, *31*, 9319.

134) Satyanarayana, S.; Dabrowiak, J. C.; Chaires, J. B. *Biochemistry* **1993**, *32*, 2573.

135) Eriksson, M.; Leijon, M.; Hiort, C.; Norden, B.; Graslund, A. *Biochemistry* **1994**, *33*, 5031.

136) Pyle A. M.; Barton, J. K. *Progress in Inorganic Chemistry: Bioinorganic Chemistry*; Lippard, S. J., Ed.; John Wiley & Sons: New York, 1990, *38*, 413.

137) Kelly, S. O.; Barton, J. K. *Metal Ions in Biological Systems;* Sigel, A., Sigel, H., Eds. Marcel Dekker: New York, 1999**,** *39*, 211.

138) Mesmaeker, A. K.; Lecomte, J-P.; Kelly, J-M. *Topics in Current Chem*. **1996,** *177*, 25.

139) Friedman, A. E.; Kumar, C. V.; Turro, N. J.; Barton, J. K. *Nucleic Acid. Res*. **1991**, *19*, 2595.

140) Hartshorn, R. M.; Barton, J. K. *J. Am. Chem. Soc*. **1992**, *114*, 5919.

141) Arounaguiri, S.; Maiya, B. G. *Inorg. Chem.* **1999**, *38*, 842.

142) Ambroise, A.; Maiya, B. G. *Inorg. Chem.* **2000**, *39*, 4256.

143) Ambroise, A.; Maiya, B. G. *Inorg. Chem.* **2000**, *39*, 4264.

144) Pyle, A. M.; Rehman, J. P.; Meshoyrer, R.; Kumar, C. V.; Turro, N. J.; Barton, J. K. *J. Am. Chem. Soc*. **1989**, *111*, 3051.

145) Barton, J. K.; Raphael, A. L. *J. Am. Chem. Soc*. **1984**, *106*, 2466.

146) Morgan, R. J.; Chatterjee, S.; Baker, A. D.; Strekas, T. C. *Inorg. Chem.* **1991**, *30*, 2687.

147) Tysoe, S. A.; Morgan, R. J.; Baker, A. D.; Strekas, T. C. *J. Phys. Chem*. **1993**, *97*, 1707.

148) Zhen, Q-Z.; Ye, B-H.; Zhang, Q-L.; Liu, J-G.; Li, H.; Ji, L-N.; Wang, L. *J. Inorg. Biochem*. **1999**, *76*, 47.

149) Liu, J-G.; Ye, B-H.; Li, H.; Zhen, Q-H.; Ji, L-N.; Fu, Y-H. *J. Inorg. Biochem*. **1999**, *76*, 265.

150) Xiong, Y.; He, X-F.; Zou, X-Z.; Wu, J-H.; Chen, X-M.; Ji, L-N.; Li, R-H.; Zhou, J-Y.; Yu, K-B. *J. Chem. Soc*., *Dalton Trans*. **1999**, 19.

151) Wu, J-Z.; Ye, B-H.; Wang, L.; Ji, L-N.; Zhou, J-Y.; Li, R-H.; Zhou, Z-Y. *J. Chem. Soc*., *Dalton Trans*. **1997**, 1395.

152) Flowers, L.; Ohnishi, S. T.; Penning, T. M. *Biochemistry* **1997**, *36*, 8640.

153) Bolton, J. L.; Trush, M. A.; Penning, T. M.; Dryhurst, G.; Monks, T. J. *Chem. Res. Toxicol.* **2000**, *13*, 135.

154) Schelvis, J. P. M.; Ramsey, M.; Sokolova, O.; Tavares, C.; Cecala, C.; Connell, K.; Wagner, S.; Gindt, Y. M. *J. Phys. Chem. B* **2003**, *107*, 12352.

155) Yang, C. H.; Chen, W. F.; Jong, M. C.; Jong, B. J.; Chang, J. C.; Waring, M. J.; Ma, L.; Sheh, L. *J. Am. Chem. Soc.* **2004**, *126*, 8104.

156) Ghosh, D.; Shukla, A. D.; Banerjee, R.; Das, A. *J. Chem. Soc. Dalton Trans.* **2002**, 1220 (and references therein).

157) Shukla, A. D.; Das, A. *Polyhedron* **2000**, *19*, 2605.

158) Shukla, A. D.; Ganguly, B.; Dave, P. C.; Samanta, A.; Das, A. *Chem. Commun.* **2002**, 2648.

159) Jose, A. D.; Shukla, A. D.; Krishnakumar, D.; Ganguly, B.; Das, A.; Ramakrishna, G.; Ghosh, H. N. *Inorg. Chem.* **2005**, *44*, 2414.

CHAPTER 2

Materials, Methods and Instrumentation

2.1 Introduction

In this chapter, different synthesized or commercially procured precursor materials employed at different stages of the investigation are listed and the procedures for purification of different solvents are described. The method of preparation of the buffers of different pH values used for biochemical techniques are also described in this chapter. Methodologies for absorption titration, fluorescence titration, time-resolved fluorescence spectroscopy, IR spectroscopy, NMR spectroscopy, X-ray crystallography, thermal denaturation, gel electrophoresis and estimation of binding constants are also presented.

2.2 Materials

2,2′-pyridil, 2,2′-bipyridine, N,N-dimethylaniline, anthracene, 4,5-dihydroxy-1,3-benzenedisulphonic acid disodium salt monohydrate, 1,2-diaminoanthraquinone, 2,3-diaminopyridine and acridine were obtained from Aldrich Chemical Co. (USA). 1,2-Diaminobenzene and 4-nitro-1,2-diaminobenzene were purchased from Acros (Belgium) and recrystallised from water. Pyridine, 1,2-diaminomaleonitrile, sodium borohydride, palladium on charcoal (Pd/C, 10%), 1,4-diazabicyclo[2.2.2]octane (DABCO) and mannitol were purchased from E. Merck (India) or Merck (Germany). $BF_3.Et_2O$ and pyrene were obtained from Lancaster (UK). Pyrrole was obtained from Sisco Research Laboratories (India) and distilled under reduced pressure over CaH_2 prior to use.[1] Oxalyl chloride was procured from

Spectrochem (India). The hydrated metal perchlorates used for metal ion titrations were acquired from either Aldrich Chemical Co. (USA) or Acros (Belgium) or were synthesized from their corresponding carbonate salts. All anions, in the form of tetrabutylammonium salts, were purchased from Aldrich Chemical Co. (USA), stored in a dessicator under vacuum containing self-indicating silica and used for anion titration or as supporting electrolyte in electrochemical experiments without any further purification.

Aluminium oxide (basic and neutral) and silica gel (60-200 mesh size) for column chromatography were obtained from Acme Synthetic Chemicals (India). The drying agents employed at various stages of purification procedures *viz*: anhydrous sodium sulphate, calcium chloride, calcium hydride, magnesium turnings and magnesium sulphate and the acids such as hydrochloric acid, sulphuric acid, nitric acid and acetic acid were all of Analytical Reagent grade, obtained from either B.D.H. (India) or Ranbaxy (India). All the spectroscopy grade solvents were procured from Ranbaxy (India). All other common chemicals were purchased from locally available sources. The nitrogen gas utilized in this study was obtained from India Oxygen Limited (India). It was further purified by passage through Fieser's solution (20% KOH solution containing 2% sodium anthraquinone-2-sulphonate and 15% sodium dithionite) before use.[2]

Supercoiled DNA pBR 322 (cesium chloride purified) was obtained from Bangalore Genei (India). Agarose (low melt, 65^{o}C, Molecular Biology grade for DNA gels) was purchased from Bio-Rad Laboratories Inc. (USA). Highly polymerized calf thymus DNA (CT DNA), ethidium bromide (EtBr) and bromophenol blue were procured from Sigma (USA). These biochemicals were used as received. Tris(hydroxylmethyl)aminomethane (Tris), sucrose, sodium chloride, ethylenediaminetetraacetic acid disodium salt (EDTA-Na_2),

disodium hydrogen phosphate (Na_2HPO_4) and sodium dihydrogen phosphate (NaH_2PO_4) were of Molecular Biology grade, obtained from Sisco Research Laboratories (India).

2.3 Preparation of starting materials

The following precursor molecules required for the synthesis of new sensors investigated in this study were prepared by adopting the published procedures.

1,2-Di(1*H*-2-pyrrolyl)-1,2-ethanedione[3,4]

Oxalyl chloride (6.4 g, 0.05 mol) and dichloromethane (25 mL) were placed together under an argon atmosphere and stirred. Upon cooling to -78^{o}C in an acetone/CO_2 bath, dry pyridine (10 g, 0.12 mol) was added resulting in the formation of a yellow precipitate. To this cooled suspension was added a solution of freshly distilled pyrrole (6.7 g, 0.1 mol) in dichloromethane (25 mL) by use of a canula. The reaction mixture turned from yellow to brown immediately. The reaction was allowed to stir at -60^{o}C for an additional 15 minutes, after which hydrochloric acid (5 M, 100 mL) was added to quench the reaction. The biphasic system was then separated off and the organic phase was collected. The aqueous phase extracted with dichloromethane (3 x 30 mL), and the combined organic phase were washed with water (100 mL), dried over sodium sulphate, filtered and evaporated to dryness. This afforded a green precipitate which was purified by silica gel column chromatography (eluent: dichloromethane) to obtain the required product as yellow powder (Yield = 1.51 g, 16%). Anal. Calcd. For $C_{10}H_8N_2O_2$: C, 63.83; H, 4.25; N, 14.89. Found: C, 64.05; H, 4.20; N, 14.63. ^{1}H NMR (200 MHz, DMSO-d_6, TMS) δ,

ppm: 6.24-6.26 (2H, m), 6.90-6.93 (2H, m), 7.33-7.36 (2H, m), 12.22 (2H, br s). UV-Visible (CH_2Cl_2) λ_{max}, nm (ε, M^{-1} cm^{-1}): 340 (15750).

9-(3,4-diaminophenyl)acridine[5]

Acridine was dissolved in C_2H_5OH and anhydrous HCl gas was passed through the solution for 5 min. The solution was concentrated and the hydrochloride salt was precipitated by the addition of ether and then dried. A mixture of the acridine hydrochloride salt (0.57 g, 2.60 mmol) thus obtained, sulphur (0.25 g, 7.80 mmol) and 1,2-diaminobenzene (0.57 g, 5.30 mmol) was heated to 130^{o}C with vigorous stirring. The mixture turned black and formed a tar with the evolution of H_2S. Heating was continued for 1 h. The melt was cooled and washed with ether. The black solid was extracted with 10% HCl and the acidified solution was neutralized with aqueous ammonia. A brown solid was precipitated which was dried and recrystallized by using xylene to get the desired product (Yield = 0.42 g, 56%). Anal. Calcd. For $C_{19}H_{15}N_3$: C, 80.00; H, 5.26; N, 14.74. Found: C, 79.68; H, 5.33; N, 14.95. ^{1}H NMR (200 MHz, DMSO-d_6, TMS) δ, ppm: 4.78 (4H, s), 6.51 (1H, dd, *J* = 7.6 Hz, 2.1 Hz), 6.65 (1H, d, *J* = 2.1 Hz), 6.78 (1H, d, *J* = 7.6 Hz), 7.47-7.53 (2H, m), 7.80 (1H, dd, *J* = 6.4 Hz, 1.2 Hz), 7.82 (1H, dd, *J* = 6.4 Hz, 1.2 Hz), 7.89 (2H, d, *J* = 8.5 Hz), 8.16 (2H, d, *J* = 8.5 Hz).

2.4 Purification of solvents

The solvents used at various stages of the study were purified using the general procedures available in the literature.[1,2] The purified solvents were optically transparent in the spectral region of interest.

Toluene, 1,4-dioxan and tetrahydrofuran. The solvent was heated under reflux over metallic sodium for 3-4 h and added benzophenone. The resultant dark blue solution was further refluxed for 1 h and distilled under dry conditions.

Acetonitrile. Acetonitrile was stirred with calcium hydride for 5-6 h and then distilled under dry conditions.

Methanol. Methanol, kept over CaH_2 for overnight, was taken (50-75 mL) in a round-bottom flask and clean, dry magnesium turnings (5 g) and iodine (0.5 g) were added to it. The solution was warmed until all the magnesium was converted into magnesium methoxide. About 1 L of methanol was added to it, refluxed for 4-5 h and distilled.

Ethanol. Ethanol was refluxed with stirring over anhydrous calcium oxide for 6 h. The solution was left at room temperature overnight. This was then distilled and further dried over magnesium and iodine and collected under dry atmosphere.

N, N-dimethylformamide. The solvent was stirred with calcium hydride for 5-6 h, distilled under vacuum at 75^{o}C and stored over molecular sieves.

2.5 Instrumentation

All the compounds synthesized during this study were characterized by elemental analysis, mass (FAB or LC), infrared (IR), absorption, steady-state fluorescence, time-resolved fluorescence, nuclear magnetic resonance (NMR), electron paramagnetic resonance (EPR) spectroscopy, and electrochemical (cyclic and differential-pulse voltammetry) methods. The solid state structures were determined by X-ray crystallography whenever we were able to grow X-ray quality single crystals. These methods are briefly described below.

Elemental analyses were carried out on a Thermo Finnigan Flash EA 1112 series CHNS analyzer. Acetanilide was used as a reference standard. FAB mass spectra were recorded on a JEOL SX 102/DA-6000 mass spectrometer/data system. The accelerating voltage was 10 kV and the spectra were recorded using m-nitrobenzyl alcohol (NBA) as the matrix. LC mass spectra were recorded on a Shimadzu LCMS-2010A mass spectrometer. The infrared spectra were recorded on a Jasco FT-IR 5300 spectrophotometer. The spectra of the solid samples were recorded by dispersing the samples as KBr pellets. The ^{1}H or ^{13}C NMR spectra were recorded on either Bruker NR-200 AF-FT or Bruker AVANCE 400 NMR spectrometer using $CDCl_3$, CD_3CN, CD_3OD or $(CD_3)_2SO$ as the solvent. Tetramethylsilane (TMS) was the internal standard employed while recording these spectra. The electron paramagnetic resonance (EPR) spectra were recorded for the Ru(II)-semiquinone complexes at room temperature and 77K on a Bruker ESP-300 spectrometer. Diphenylpicrylhydrazide (DPPH) was used as the g-marker. Cyclic (CV) and differential-pulse (DPV) voltametric experiments were carried out on a CH instruments model CHI 620A electrochemical analyzer (working and auxiliary electrodes: Pt; reference electrode: Ag). Fc^{+}/Fc (Fc = ferrocene) couple was used to calibrate the redox potential values.

UV-visible spectra were recorded with either a Shimadzu UV-3101PC or Varion Cary 100 Bio spectrophotometer. A matched pair of quartz cuvettes (path length = 1 cm) were employed. Steady-state fluorescence spectra were recorded in a four-walled, all-transparent, quartz cell (path length = 1 cm) using either FluoroMax-3 (Jobin Yvon-Spex) or FluoroLog-3 (Jobin Yvon-Spex) spectrofluorimeter for solutions having low optical densities at the wavelengths of excitation. Detection of emission was done at the right angle

to the incident beam. The excitation and emission slit widths employed were typically, 3/3 nm.

The fluorescence lifetime (τ) of the samples were measured on a single photon counting spectrofluorimeter (IBH-5000)[6] using laser diodes (IBH; $\lambda_{exc.}$(FWHM): 281 nm (1.072 ns), 374 nm (65 ps)) as the excitation source and an MCP photomultiplier (rise time of 60 ps) as the detector. The decay times were estimated from the measured fluorescence decays and the lamp profile, using a nonlinear least-squares iterative fitting procedure,[7] by IBH-DAS (version 6) decay analysis software. The goodness of the fit was evaluated from the χ^2 values and the plot of the residuals. For recording the lamp profile, a scatterer (dilute solution of Ludox in water) was placed in place of the sample.

Single crystal X-ray data was collected on a Bruker-Nonius SMART APEX CCD single crystal diffractometer at 298K, equipped with a graphite monochromator and a Mo Kα fine-focus sealed tube (λ = 0.71073 Å) operated at 2.0 kW. The SMART software was used for data acquisition.[8] The detector frames were integrated by use of the program SAINT-PLUS[9] and the intensities corrected for absorption by Gaussian integration using the program SADABS.[10] The structure solution was carried out using direct methods. Full-matrix least squares refinement on F^2 (including all data) was performed using the program SHELXTL.[11] PLATON package was used for molecular graphics.[12] All non-hydrogen atoms were refined with anisotropic thermal parameters. Hydrogen atoms attached to pyrrole nitrogen were picked from difference Fourier maps. All other hydrogen atoms were fixed in their ideal geometric positions.

2.6 Sample preparation for spectral measurements

The solution of sensors of the concentration of 5 x 10^{-6} - 2 x 10^{-5} M were used for absorption titration. For fluorescence titration, the optical densities at the wavelength of excitation were maintained less than 0.2. Hydrated metal perchlorate salts and tetrabutylammonium salts of anions were dissolved in a given solvent and used for cation and anion titrations, respectively. The concentration of these standard stock solutions were adjusted such that not more than 200 μL were added (using a micro-litre pipette) to a 3 mL solution of sensor molecule during the titration in a quartz cuvette.

2.7 Measurement of the fluorescence quantum yield

Fluorescence quantum yields (ϕ_f) were estimated by integrating the area under the fluorescence curves and by using the formula:[13]

$$\phi_{sample} = \frac{I_{sample} \times OD_{standard} \times \eta^2_{sample}}{I_{standard} \times OD_{sample} \times \eta^2_{standard}} \times \phi_{standard} \qquad (2.1)$$

where ϕ is the quantum yield, I is the integrated intensity, OD is optical density, and η is refractive index of the solvent(s) used. The subscript 'sample' or 'standard' refers to the fluorophore of unknown quantum yield or fluorophore of known quantum yield, respectively. The fluorescence quantum yields of different compounds or complexes have been calculated using 1,6-diphenyl-1,3,5-hexatriene (ϕ_f = 0.80 in cyclohexane)[14], 5,10,15,20-tetraphenylporphyrin (ϕ_f = 0.13 in CH_2Cl_2)[15] or $[Ru(bpy)_3]^{2+}$ (ϕ_f = 0.062 in CH_3CN)[16] as the standards. Refractive index corrections have been incorporated while reporting the fluorescence data in different solvents.[17]

2.8 Estimation of fluorescence enhancement

The magnitude of the maximum fluorescence enhancement was calculated from the following equation, using the integrated area of the fluorescence curves.

$$FE = I_F \text{ (max)} / I_F \text{ (zero)} \qquad (2.2)$$

where, FE is the fluorescence enhancement, I_F (max) is the integrated area of the fluorescence curve obtained on adding the maximum required amount of the guest species and I_F (zero) is the corresponding area at zero concentration of the guest. Both I_F (max) and I_F (zero) were measured under identical experimental conditions.

2.9 Estimation of binding constants[18]

2.9.1 Using absorption titration data

The binding affinity of sensors with transition metal ions was investigated from the changes in their absorption spectra on addition of these metal ions.

Complex formation between sensor (*F*) and the metal ion (*M*) can be represented as

$$F + M = C \qquad (2.3)$$

where *C* stands for the complex.

The binding constant (*K*) for 1:1 complexation was evaluated from the absorption data by the following method.

At equilibrium, the binding constant

$$K = \frac{[C]}{([F]_0 - [C])([M]_0 - [C])} \qquad (2.4)$$

where, $[C]$ represents the equilibrium concentration of the complex and $[F]_0$ and $[M]_0$ represent the initial concentration of the sensor and metal ion, respectively.

By substituting the term $\Delta A/\Delta\varepsilon$ for $[C]$ (for a path length of 1 cm) the following equation can be derived,

$$\frac{[F]_0[M]_0}{\Delta A} = ([F]_0 + [M]_0 - \frac{\Delta A}{\Delta\varepsilon})\frac{1}{\Delta\varepsilon} + \frac{1}{K\Delta\varepsilon} \qquad (2.5)$$

where, ΔA is the change in absorbance due to the addition of cation, $\Delta\varepsilon$ is the difference between the molar extinction coefficient of the complex and free sensor.

A plot of $\frac{[F]_0[M]_0}{\Delta A}$ vs. $([F]_0 + [M]_0 - \frac{\Delta A}{\Delta\varepsilon})$ would yield a straight line with slope $1/\Delta\varepsilon$ and intercept $1/K\Delta\varepsilon$. However, knowledge of the unknown quantity $\Delta\varepsilon$ is needed to make this plot.

Consequently, a tentative value of $\Delta\varepsilon$ is determined by using data from two solutions and solving equation 2.5 simultaneously for $\Delta\varepsilon$ and K. Using this value of $\Delta\varepsilon$ a plot is made employing data from a series of solutions, and a new value of $\Delta\varepsilon$ is determined along with a new value of K. This procedure is repeated until a consistent set of values for both $\Delta\varepsilon$ and K have been obtained from two successive plots.

The binding ability of sensors with anions was investigated from the changes in their absorption spectra on addition of these anions.

Complex formation between sensor (F') and the anion (A) can be represented as

$$F' + A = C' \qquad (2.6)$$

where C' stands for the complex.

The binding constant (K) for 1:1 complexation was evaluated from the absorption data by the following non-linear equation.

$$\frac{\Delta A}{b} = \frac{Q_t K \Delta\varepsilon [L]}{1 + K[L]} \qquad (2.7)$$

where, ΔA refers to the change in absorbance from initial value at the required wavelength, b is cuvette path length (in cm), Q_t is total concentration of sensors, $\Delta\varepsilon$ is the change in extinction coefficient between free and bound sensor and $[L]$ is the concentration of titrated anion.

2.9.2 Using fluorescence titration data

Since metal ion-induced changes of the fluorescence spectra are more pronounced than those of the absorption spectra in some cases, the K values were evaluated from the fluorescence data. The method of determination of binding constant (K) by using fluorescence titration data is described below.

The binding constant (K) for 1:1 complexation is given by,

$$K = \frac{[C]}{([F]_0 - [C])([M]_0 - [C])} \qquad (2.8)$$

where, $[C]$ represents the equilibrium concentration of the complex and $[F]_0$ and $[M]_0$ represent the initial concentration of the sensor and metal ion, respectively. Because, the measurements were performed with $[F]_0 >> [M]_0$, $([F]_0 - [C]) \approx [F]_0$. Hence,

$$K = \frac{[C]}{[F]_0([M]_0 - [C])} \qquad (2.9)$$

By rearranging, we obtain

$$\frac{[C]}{[F]_0} = \frac{K[M]_0}{1 + K[F]_0} \qquad (2.10)$$

The total fluorescence yield, ϕ, is

$$\phi = \frac{\phi_F I_F + \phi_C I_C}{I_F + I_C} \tag{2.11}$$

where ϕ_F and ϕ_C represent the fluorescence yield of the sensor and the complex, respectively and I_F and I_C stand for the number of photons absorbed per unit volume per unit time by the sensor and the complex, respectively.

Therefore, we can write

$$\phi = \frac{\phi_F + \phi_C I_C / I_F}{1 + I_C / I_F} \tag{2.12}$$

Also, $I_F/I_C = \varepsilon_F[F]_0/\varepsilon_C[C]$ where ε_F and ε_C are the molar extinction coefficients of the sensor and the complex, respectively at the exciting wavelength.

Hence,

$$\frac{[C]}{[F]_0} = \frac{\varepsilon_F I_C}{\varepsilon_C I_F} \tag{2.13}$$

By combining eqs. 2.10 and 2.13 and using $\varepsilon_F = \varepsilon_C$, we get

$$\frac{I_C}{I_F} = \frac{K[M]_0}{1 + K[F]_0} \tag{2.14}$$

By substituting 2.14 into eq. 2.12, we obtain

$$\phi = \frac{\phi_F + \phi_C K[M]_0/(1 + K[F]_0)}{1 + K[M]_0/(1 + K[F]_0)} \tag{2.15}$$

After rearranging, we get

$$\frac{1}{\phi - \phi_F} = \frac{(1 + K[F]_0)/K(\phi_C - \phi_F)}{[M]_0} + \frac{1}{(\phi_C - \phi_F)} \tag{2.16}$$

Hence, a plot of $(\phi - \phi_F)^{-1}$ against $[M]_0^{-1}$ should yield a straight line whose slope (m) and intercept (c) are given by $m = (1+K[F]_0) / K(\phi_C - \phi_F)$ and $c = 1/(\phi_C - \phi_F)$. Therefore, the binding constant,

$$K = (m/c - [F]_0)^{-1} \quad (2.17)$$

The binding ability of sensors with anions was investigated from the changes in their fluorescence spectra on addition of these anions.

The binding constant (K) for 1:1 complexation is evaluated by the following equation. The dependence of F/F_0 upon anion concentration is described by the non-linear equation,

$$\frac{F}{F_0} = \frac{1 + (k_f / k_s)K[L]}{1 + K[L]} \quad (2.18)$$

where, F_0 refers to the fluorescence intensity due to the sensor in the absence of any anion, F is its intensity upon addition of the given anion, k_f is proportionality constant of the bound sensor, k_s is proportionality constant of the free sensor and [L] is the concentration of titrated anion.

2.10 DNA binding experiments

Calf thymus (CT) DNA was used for binding with the various metal complexes investigated during this work. The stock solution was made by dissolving CT DNA in appropriate buffers and kept overnight at 4^{o}C for complete dissolution. The concentration of CT DNA was measured by using its known extinction coefficient at 260 nm (6600 $M^{-1}cm^{-1}$).[19] The absorbance at 260 nm (A_{260}) and at 280 nm (A_{280}) for CT DNA were measured to check its purity. The ratio A_{260}/A_{280} was found to be ~1.84, indicating that CT DNA was satisfactorily free from protein. Concentration of the DNA is expressed in base pairs (BP) throughout, unless otherwise mentioned. Buffer A (5 mM Tris, pH 7.1, 50 mM NaCl) was used for the absorption and fluorescence titration experiments and buffer B (1 mM phosphate, pH 7.0, 2 mM NaCl) was used for the thermal denaturation experiments. TAE (Tris-acetate-EDTANa_2, pH =

8.0) 1X buffer was used for gel electrophoresis of cleavage and inhibition experiments.

2.10.1 Absorption titration

Absorption titration experiments were performed by maintaining a constant metal complex concentration and varying the DNA concentration. Typical concentration of the metal complex used was 5-15 μM and that of DNA ranged between 0-100 μM. After the addition of DNA to the metal complex, the resulting solution was allowed to equilibrate for 10 min. at 25°C, after which the absorption spectra were recorded. The data were then fit to the following equation to obtain the intrinsic binding constant, K_b.[20]

$$\frac{[DNA]}{\varepsilon_a - \varepsilon_f} = \frac{[DNA]}{\varepsilon_b - \varepsilon_f} + \frac{1}{K_b(\varepsilon_b - \varepsilon_f)} \qquad (2.19)$$

where ε_a, ε_f and ε_b are the apparent, free and bound metal complex extinction coefficients, respectively. A plot of $[DNA]/(\varepsilon_a - \varepsilon_f)$ vs. $[DNA]$ would produce a straight line with slope $1/(\varepsilon_b - \varepsilon_f)$ and intercept $1/K_b(\varepsilon_b - \varepsilon_f)$; K_b is the ratio of slope to intercept.

2.10.2 Fluorescence titration

Fluorescence titration experiments were performed by using a fixed metal complex concentration (7-20 μM) and increments of the stock DNA solutions (0-300 μM) were added to it. After the addition of DNA to the metal complex, the resulting solution was allowed to equilibrate for 10 min. at 25°C in the dark and excited at 460 nm. The data obtained were analyzed by using eq. 2.20.[21]

$$C_F = \frac{C_T(F/F_0 - P)}{(1-P)} \qquad (2.20)$$

where, C_F is the concentration of the free complex, C_T is the concentration of the complex added and F_0 and F are the fluorescence intensities in the absence and in the presence of DNA, respectively. P is ratio of the observed fluorescence quantum yield of the bound complex to the free complex. The value of P was obtained from a plot of F/F_0 vs. 1/[*DNA*] such that the maximum limiting fluorescence yield is given by the y-intercept. The amount of bound complex (C_B) at any concentration was equal to $C_T - C_F$. A plot of r/C_F vs. r where r is equal to C_B/[*DNA*], is constructed according to the modified Scatchard equation given by McGhee and Von Hippel.[22]

$$\frac{r}{C_F} = K_b(1-nr)\left[\frac{1-nr}{1-(n-1)r}\right]^{n-1} \qquad (2.21)$$

where, K_b is the intrinsic binding constant and n is the binding site size in base pairs.

2.10.3 Thermal denaturation

Thermal denaturation experiments were carried out by monitoring the absorption of CT DNA (160 μM, nucleotide pairs, NP) at 260 nm at various temperatures in the absence and presence (2-5 μM) of complexes, using a Shimadzu UV-160A spectrophotometer coupled with a temperature controller (model TCC-240A) or a Julabo-F12 circulator. The melting temperature (T_m, the temperature at which 50% of double stranded DNA becomes single stranded) and the curve width (σ_T, the temperature range in which 10% to 90% of the absorption increase occurred) were calculated as reported.[23,24]

2.11 DNA photocleavage and agarose gel electrophoresis

Electrophoresis through agarose is the standard method used to separate, identify or purify DNA fragments.[25-28] Using this technique, bands containing as little as 1-10 ng of DNA can be detected by direct examination of the agarose gel (stained with EtBr) in the UV light.[28] When an electric field is applied across the gel, DNA, which is negatively charged at neutral pH, migrate towards the anode. The intact supercoiled (Form I) DNA migrates faster than the single nicked (Form II) in the gel. This technique has been employed to identify the product(s) of the DNA photocleavage, which was carried out in this work.

2.11.1 Buffers/Reagents

2.11.1.1 Tris-acetate ethylenediaminetetraacetate (TAE) electrolyte buffer (50 X stock)

Tris base (48.4 g) was dissolved in water (100 mL). EDTA disodium salt (7.44 g) was dissolved in water (50 mL) and the pH was adjusted to 8.0 using NaOH. This pH-adjusted EDTA solution was added to the tris solution followed by the addition of glacial acetic acid (11.42 mL). The volume was made up to 200 ml with H_2O and the resulting buffer was stored at 4^oC.

2.11.1.2 Sample buffer (6X)

A 0.25% bromophenol blue in 40% sucrose-H_2O was used as the sample buffer. This buffer was prepared by first dissolving sucrose (2.0 g) in water (3 mL) and then adding bromophenol blue (12.5 g) to this solution. The volume was made up to 5 mL. The resulting buffer was stored at 4^oC.

2.11.1.3 Ethidium bromide stock solution (10 mg/ml)

A 0.1 g of EtBr was dissolved in water (10 mL) by stirring in dark for several hours. The resulting solution was stored in a brown bottle at the ambient temperature. Working concentration of 0.5 μg/mL was used for staining the gels after electrophoresis.

2.11.2 Gel configuration and gel casting

A horizontal slab gel electrophoresis chamber (3.5 x 7.5 inches or 6.0 x 7.5 inches) made of polystyrene snap lock box obtained from Broviga Inc. (India) was used to carry out the agarose gel electrophoresis. Platinum wire was used as electrodes. A platform composed of four lantern slides glued together in a stack is cemented in the center of the box. A gel plate of 7.0 cm x 10.0 cm in size rests on this platform so that the gel is submerged just beneath the surface of the electrophoresis buffer. The details of gel casting are given below.

A 0.4 g of low melt agarose (Molecular Biology grade) was added to TAE buffer (50 mL). The slurry was then heated on a boiling water bath until the agarose dissolved completely. The solution was cooled to 50^{o}C. Both ends of the gel mold were closed with a clean autoclaved tape and a small quantity of agarose solution was applied with a pipette along the edges of the gel mold so as to seal it completely. Remaining warm agarose solution was poured into the gel mold and immediately the comb was clamped into position near one end of the gel. The teeth of the comb formed the sample wells. Care was taken to see that at least 0.5-1.0 mm of agarose was left between the bottom of the teeth and the base of the gel, so that the sample wells are completely sealed. After 35-40 min. (by which time the gel was completely set), the comb and the autoclaved tape were removed carefully and the gel was mounted in the

electrophoresis chamber. Working buffer (TAE 1X) was poured into the gel until the gel was submerged to a depth of about 1 cm.

2.11.3 Photolysis of pBR 322 DNA and separation of the products

Photolysis experiments were carried out for pre-incubated (1 h) samples of pBR 322 DNA (100 μM nucleotide phosphate) and the appropriate concentration of the drug, placed in a quartz tube of 3 mm internal diameter. Tris-HCl buffer (5 mM Tris, pH 8.0, 50 mM NaCl) was the medium in the case of Ru(II) complexes. The samples were irradiated inside the sample chamber of a JASCO Model FP-777 spectrofluorimeter ($\lambda_{irrd.}$ = 450±2 nm; slit width = 5 nm). The temperature was maintained at 20^{o}C throughout the irradiation process.

After irradiation, 2 μL of sample buffer was added to the quartz tube containing the irradiated sample and the contents were directly loaded onto a 0.8% (w/v) agarose gel. The gel was run with standard TAE buffer pH 8.0 at 40 V for 4 h, after which it was stained with 0.5 μg/mL solution of EtBr for 30 min. The data were documented using UVITEC Gel Documentation system.[29]

In order to identify the actual reactive oxygen species responsible for DNA damage, a number of control experiments were carried out using various types of quenchers (‘inhibitor studies’). Nitrogen gas was used to flush dioxygen; DABCO (20 mM) was used as a $^{1}O_{2}$ quencher. DMSO (200 mM) and mannitol (100 mM) were used as $OH^{\bullet}$ scavengers. 4,5-dihydroxy-1,3-benzenedisulfonic acid disodium salt (Tiron, 2 mM) was used as a superoxide anion radical quencher.

2.12 General considerations

Error estimation of the data, reconstruction of various spectra, calculations of equilibrium constants, various regression analysis *etc*. that appear throughout this dissertation, have been carried out on an IBM compatible PC (Pentium 4) using the available in-house software/Origin 6.0 software package.

Care was taken to avoid the entry of direct, ambient light into the samples in all the spectroscopic and electrochemical experiments. Care was also taken to avoid the direct human contact of DNA and EtBr solutions. All solutions containing EtBr and other hazardous chemicals were decontaminated before disposal. Protective goggles, gloves and safety mask were used to minimize the exposure to obnoxious chemicals/biochemicals, ultraviolet light etc. Unless otherwise specified, all the experiments were carried out at 298±1 K. Standard error limits involved in various measurements are as follows.

^{1}H NMR chemical shift (δ)	$\pm$ 0.01 ppm
^{1}H NMR H–H coupling constant (J)	$\pm$ 1 Hz
λ_{max} (Abs./Fluo.)	$\pm$ 2 nm
ε	$\pm$ 10%
FE and ϕ_f	$\pm$ 10%
τ (> 40 ps)	$\pm$ 5%
$E_{1/2}$	$\pm$ 0.03 V
$\lambda_{exc.}$	$\pm$ 2 nm
K and K_b	$\pm$ 10%
T_m	$\pm$ 1^{o}C
σ_T	$\pm$ 1^o

2.13 References

1. Perrin, D. D.; Armarego, W. L. F.; Perrin, D. R. *Purification of laboratory Chemicals*; Pergamon: Oxford, 1986.
2. *Vogel's Text Book of Practical Organic Chemistry*; (Revised by Furniss, B. S.; Hannaford, A. J.; Smith, P. W. G.; Tatchell, A. R.), 5th Edn.; Longmann (ELBS): Essex (UK.), 1991.
3. Behr, D.; Brandange, S.; Lindstrom, B. *Acta. Chem. Scand.* **1973**, *27*, 2411.
4. Black, C. B.; Andrioletti, B.; Try, A. C.; Ruiperez, C.; Sessler, J. L. *J. Am. Chem. Soc.* **1999**, *121*, 10438.
5. Plater, M. J.; Greig, I.; Helfrich, M. H.; Ralston, S. H. *J. Chem. Soc., Perkin Trans. 1* **2001**, 2553.
6. O'Connor, D. V.; Phillips, D. *Time-Correlated Single Photon Counting*; Academic Press: London, 1984.
7. Bevington, P. R. *Data Reduction and Error Analysis for the Physical Sciences*; McGraw-Hill: New York, 1969.
8. *SMART*; version 5.630; Bruker-Nonius Analytical X-ray Systems Inc.: Madison, WI, USA, 2003.
9. *SAINT-PLUS*; version 6.45; Bruker-Nonius Analytical X-ray Systems Inc.: Madison, WI, USA, 2003.
10. Sheldrick, G. M. *SADABS: Empirical Absorption Correction Program*; University of Göttingen: Göttingen, Germany, 1997.
11. Sheldrick, G. M. *SHELXTL: Structure Determination Programs*; version 5.1; Bruker-Nonius Analytical X-ray Systems Inc.: Madison, WI, USA.
12. Spek, A. L. *PLATON: A Multipurpose Crystallographic Tool*; Utrecht University: Utrecht, The Netherlands, 2002.

13. Austin, E.; Gouterman, M. *Bioinorg. Chem.* **1978,** *9*, 281.
14. Berlman, I. B. *Handbook of Fluorescence Spectra of Aromatic Molecules*, 2nd edition, Academic Press: New York, 1971, p. 322.
15. Quimby, D. J.; Lango, F. R. *J. Am. Chem. Soc.* **1975**, *97*, 5111.
16. Juris, A.; Balzani, V.; Barigelletti, F.; Campagna, S.; Belser, P.; Zelewsky, A. V. *Coord. Chem. Rev.* **1988,** *84*, 85.
17. Lackowicz, J. R. *Principles of Fluorescence Spectroscopy*; Plenum Press: New York, 1983**.**
18. Connors, A. K. *Binding Constants: The Measurement of Molecular Complex Stability*; Wiley-VCH: New York, 1987.
19. Reichmann, M. E.; Rice, S. A.; Thomas, C. A.; Doty, P. *J. Am. Chem. Soc.* **1954,** *76*, 3047.
20. Wolfe, A.; Shimer, G. H.; Meehan, T. *Biochemistry* **1987,** *26*, 6392.
21. Kumar, C. V.; Asuncion, E. H. *J. Am. Chem. Soc.* **1993**, *115*, 8547.
22. McGhee, J. D.; Von Hippel, P. H. *J. Mol. Biol*. **1974**, *86*, 469.
23. Kelly, J. M.; Tossi, A. B.; McConnell, D. J.; OhUigin, C. *Nucl. Acid. Res*. **1985**, *13*, 6017.
24. Marmur, J.; Doty, P. *J. Mol. Biol*. **1962**, *5*, 109.
25. Sambrook, J.; Russell, D. W. *Molecular Cloning: A Laboratory Manual*; 3rd ed. Cold Spring Harbor Laboratory Press: New York, 2001.
26. Fisher, M. P.; Dingman, C. W. *Biochemistry* **1971,** *10*, 895.
27. Ajay, C.; Borst, P. *Biochim. Biophys. Acta* **1972,** *269*, 192.
28. Sugden, P. A. B.; Sambrook, J. *Biochemistry* **1973,** *12*, 3055.
29. *UVITEC Gel Documentation*; UVItec Limited: Cambridge, UK, 2001.

CHAPTER 3

Dual Emission of Anthracene/Pyrene-(2,2′-bipyridine) Dyads and Fluorescence OFF/ON Signaling of Pyrene-(2,2′-bipyridine) Dyad with Post-Transition Metal Ions

3.1 Introduction

Design, synthesis and study of the properties of π-conjugated systems is one of the emerging fields as these organic systems can be used for the development of electronic and photonic organic materials.[1-3] Transition metal ions are found to be very effective in altering electronic and/or optical properties of conjugated polymers as coordination to the metal ions leads to conformational, optical, or electrochemical changes in the conjugated polymers.[4-10] 2,2′-bipyridyl and 2,2′:6′,2′′-terpyridine are used mostly as metal binding site because they have high affinity to a number of transition and main group metal ions and they can be easily inserted in the conjugated polymer backbone. Recently, the effect of metal binding on the optical properties of a number of small molecules has been studied where 2,2′-bipyridyl or 2,2′:6′,2′′-terpyridine are connected with pyrene via a conjugated linker such as ethynylene,[11,12] 2,5-diethynylated thiophene,[13] single C–C bond,[14,15] 1,4-diethynylated 2,5-dioctyloxyphenylene[16,17] or phenylenevinylene.[17]

Although, there are many reports where pyrene is connected with 2,2′-bipyridyl via ethynylene linkage, the photophysical properties and influence of the metal ions on the dyads, where anthracene or pyrene is linked to 2,2′-bipyridyl via ethylene linker, have not been studied so far. Therefore, we intended to study the photophysical behavior of two dyads where 2,2′-bipyridyl is connected with anthracene (**mpae**) or pyrene (**mppe**) by ethylene

linker. Dual emissive nature of **mpae** and **mppe** in different solvents is evidenced from two distinct bands in the steady-state emission spectra and bi-exponential fluorescence decay profiles, which arise due to emission from π, π^* excited singlet state and intramolecular charge transfer (ICT) state. We also demonstrate the formation of a new low energy absorption band for **mppe** in presence of transition (Mn^{2+}, Co^{2+}, Ni^{2+}, Cu^{2+}) and post-transition (Zn^{2+}, Cd^{2+}, Pb^{2+}) metal ions. However, no such new absorption band was formed for **mpae** on addition of these metal ions. **mppe** exhibits fluorescent OFF/ON signaling behavior in presence of post-transition metal ions Zn^{2+}, Cd^{2+} and Pb^{2+}, leading to generation of a broad emission in the 550-580 nm region.

3.2 Experimental section

The two dyads, namely (E)-1-(9-anthryl)-2-[2-(4-methyl-2-pyridyl)-4-pyridyl]-1-ethene (**mpae**) and (E)-1-[2-(4-methyl-2-pyridyl)-4-pyridyl]-2-(1-pyrenyl)-1-ethene (**mppe**), were synthesized by a published procedure.[18] **mpae**: Anal. Calcd. for $C_{27}H_{20}N_2$: C, 87.07; H, 5.41; N, 7.52 %. Found: C, 86.9; H, 5.2; N, 7.4 %. ^{1}H NMR (200 MHz, $CDCl_3$, TMS) δ, ppm: 2.41(3H, s), 7.04 (1H, d, *J* = 16 Hz), 7.12-7.15 (3H, m), 7.48-7.53 (2H, m), 7.82 (1H, m), 8.03-8.04 (1H, m), 8.25-8.27 (3H, m), 8.28-8.35 (2H, m), 8.48-8.50 (2H, m), 8.55 (1H, d, *J* = 5 Hz), 8.70 (1H, d, *J* = 5 Hz). EI-MS: *m/z* 372 (M^+). **mppe**: Anal. Calcd. for $C_{29}H_{20}N_2$: C, 87.85; H, 5.08; N, 7.07 %. Found: C, 87.7; H, 5.1; N, 7.0 %. ^{1}H NMR (200 MHz, $CDCl_3$, TMS) δ, ppm: 2.43 (3H, s), 6.1 (1H, dd, *J* = 5 Hz, 7.8 Hz), 7.10-7.17 (2H, m), 7.97-8.26 (10H, m), 8.36-8.43 (2H, m,), 8.52 (2H, m). EI-MS: *m/z* 396 (M^+).

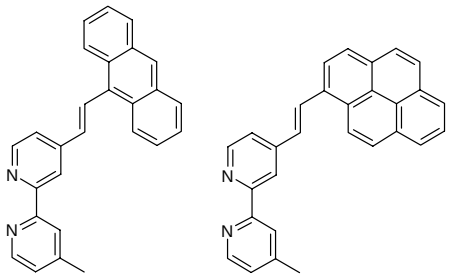

Fig. 3.1. Structures of **mpae** and **mppe**.

3.3 Results and discussion

3.3.1 Absorption spectra

The dyads **mpae** and **mppe**, whose structures are shown in fig. 3.1, contain fluorescent anthracene and pyrene moieties connected to 2,2′-bipyridyl by an ethylene linkage. The absorption spectra of **mpae** and **mppe** along with those of the constituent components i.e. 2,2′-bipyridyl, anthracene and pyrene in CH_3CN are shown in fig. 3.2. The absorption maxima with the corresponding ε values for **mpae** and **mppe** are tabulated in table 3.1. The absorption spectrum of **mpae** contains two intense bands at 250 and 280 nm. In case of **mppe** structured-peaks appear in the 240-345 nm region. The structured progression of **mppe** between 300 and 350 nm is structurally similar to the long wavelength absorption of pyrene except that each structured peak is shifted by 3-8 nm with respect to corresponding pyrene peak.

The most interesting aspect of the absorption spectra of **mpae** and **mppe** is the low energy region (above 380 nm for **mpae** and 365 nm for **mppe**). This band is attributed to charge transfer transition from anthracene/pyrene subunit to 2,2′-bipyridyl subunit through ethylene linkage.

Similar low energy absorption band in pyrene-(2,2′-bipyridine) dyad, where pyrene is connected with 2,2′-bipyridyl by ethynylene linkage, was attributed to pyrene to 2,2′-bipyridyl charge transfer transition.[11,12]

Table 3.1. Absorption and emission spectral data of **mpae** and **mppe** in CH_3CN.

Dyads	$\lambda_{max}^{abs/em}$ (ε, M^{-1} cm^{-1})
mpae	249 (22850), 279 (21250), 387 (1050), 391, 415, 487
mppe	242 (60800), 265 (28600), 276 (44750), 312 (10300), 326 (22600), 342 (33050), 374 (2700), 377, 396, 463

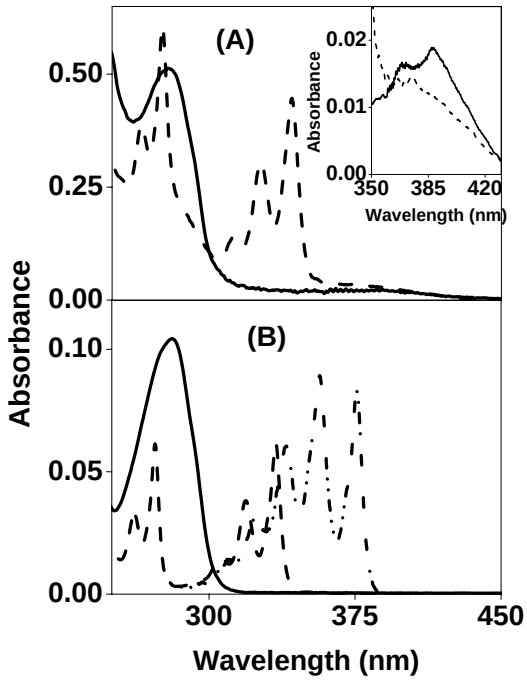

Fig. 3.2. Absorption spectra of (A) **mpae** (——) and **mppe** (– – –); (B) 2,2′-bipyridyl (——), anthracene (— · ·) and pyrene (– – –) in CH_3CN. The low energy region absorption of **mpae** and **mppe** is shown in inset of (A).

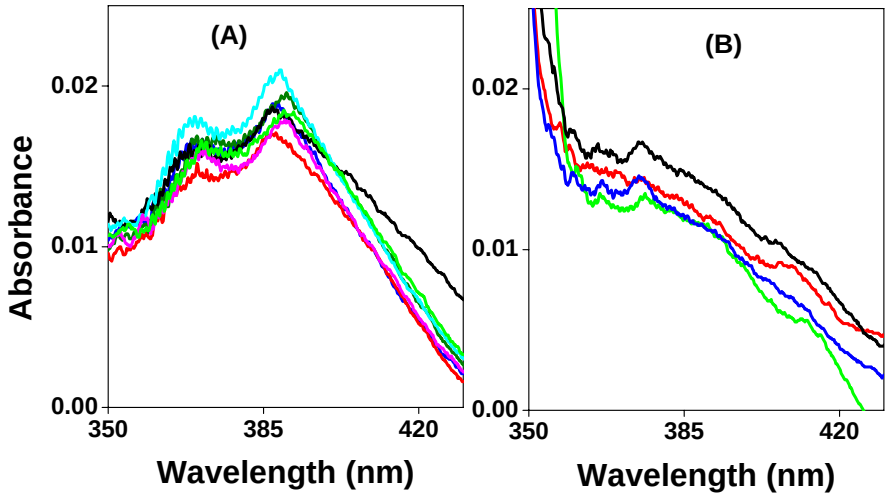

Fig. 3.3. Absorption spectra of (A) **mpae** and (B) **mppe** in different solvents: cyclohexane ( ), toluene ( ), 1,4-dioxane ( ), tetrahydrofuran ( ), acetonitrile ( ), 2-propanol ( ), methanol ( ).

The influence of solvent on the lowest energy absorption band of **mpae** and **mppe** is shown in fig. 3.3. The most noticeable feature of these spectra is the almost invariant absorption maxima with polarity of solvents for both the dyads. The invariant band positions to the polarity of the medium and low molar extinction coefficients (Table 3.1) suggest that the charge transfer contribution is minimal in the ground state.

3.3.2 Emission spectra

The emission spectra of **mpae** and anthracene in CH_3CN are shown in fig. 3.4. **mpae** shows two-component emission: structured, anthracene-like peaks around 385-420 nm are merged with a structureless, broad band around 485 nm. The emission spectra of **mppe** and pyrene in CH_3CN are also shown

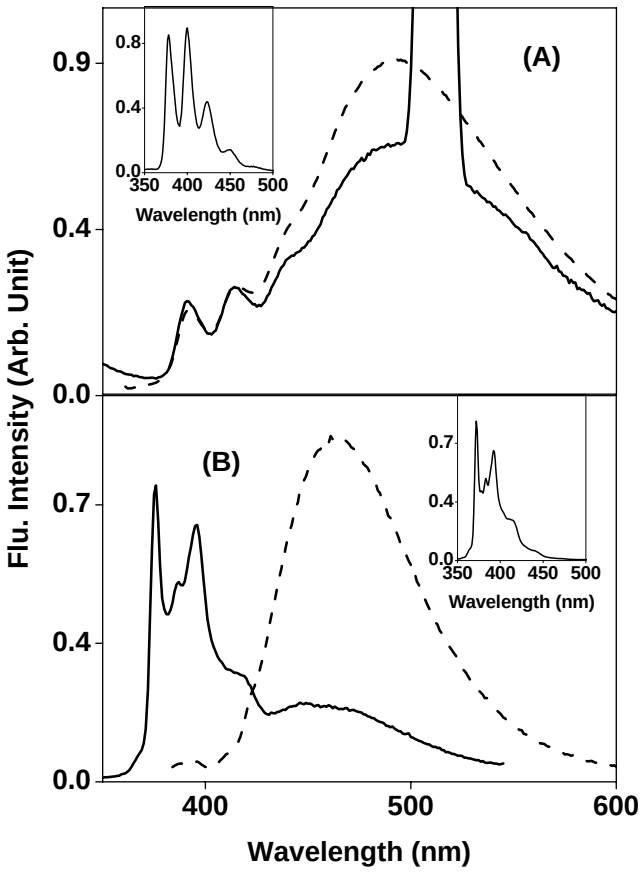

Fig. 3.4. Emission spectra of (A) **mpae** and (B) **mppe** in CH_3CN. The excitation wavelengths of **mpae** are 255 (——), 350 (– – –) nm and that of **mppe** are 275 (——), 375 (– – –) nm. The inset of (A) and (B) shows emission spectrum of anthracene and pyrene, respectively.

in fig. 3.4. The emission of **mppe** also consists of a structureless band around 465 nm, which is well-separated from the structured pyrene-like peaks around 370-400 nm. It is also notable that structured-peaks of **mpae** and **mppe** are red-shifted by 13 nm and 4 nm with respect to that of anthracene and pyrene,

respectively. The structured-peaks are attributed to the emission from the π, π^* excited singlet state of anthracene/pyrene whereas, the structureless broad higher wavelength emission band is ascribed to emission from the excited intramolecular charge transfer state of **mpae** and **mppe**. The latter emission overshadows the former one when **mpae**/**mppe** is excited around the weak charge transfer absorption band.

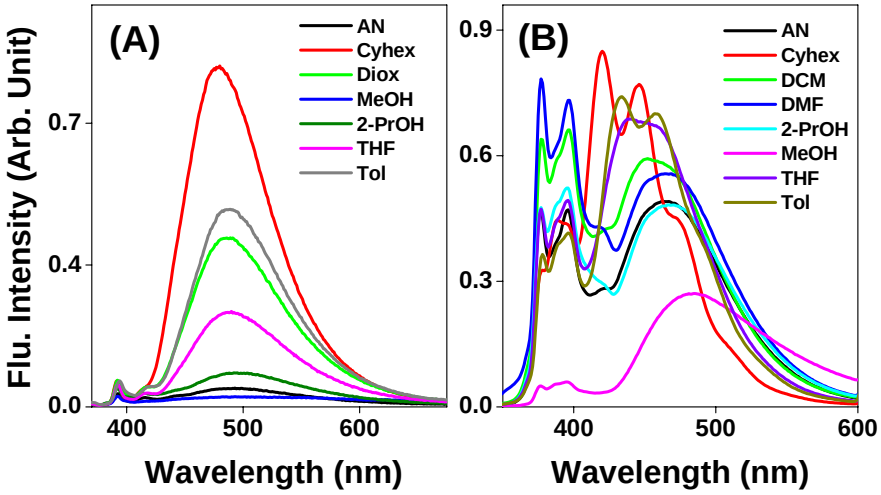

Fig. 3.5. Emission spectra of (A) **mpae** (λ_{exc} = 350 nm) and (B) **mppe** (λ_{exc} = 305 nm) in different solvents: acetonitrile (AN), cyclohexane (Cyhex), dichloromethane (DCM), 1,4-dioxane (Diox), N,N-dimethylformamide (DMF), methanol (MeOH), 2-propanol (2-PrOH), tetrahydrofuran (THF) and toluene (Tol).

The emission spectra of both **mpae** and **mppe** are sensitive to solvent polarity. While the structured-peaks are not influenced by the solvent polarity change, the broad second emission component displays significant red-shift on increase of the solvent polarity, as shown in fig. 3.5. Such behavior, which is

well known for electron donor-acceptor dyads,[19-21] indicates the existence of a fluorescent intramolecular charge transfer (ICT) state together with a anthracene/pyrene-like π, π^* excited singlet state. A more pronounced solvent effect on the emission band compared to the absorption suggests more polar nature of the excited state of **mpae** and **mppe**.

Both structured-peaks and structureless broad emission band are observable in non-polar (cyclohexane), polar (acetonitrile) or hydroxylic (methanol) solvents for **mpae** and **mppe**. However, for the pyrene-(2,2′-bipyridine) dyad, where pyrene is appended with 2,2′-bipyridyl by ethynylene linkage, either the broad structureless fluorescence (in polar solvent, CH_3CN) or structured fluorescence (in non-polar solvent, cyclohexane) is reported.[11,12] The structureless fluorescence is accounted for emission from intramolecular charge transfer (ICT) state. However, this ICT state is destabilized in non-polar solvents such that its energy exceeds that of the pyrene-like π, π^* excited singlet state, leading to only structured fluorescence from the later state.

The fluorescence excitation spectra of **mpae** and **mppe** in CH_3CN are shown in fig. 3.6. The excitation spectra of **mpae** were recorded by monitoring the emission at several wavelengths. When emission is collected at 450 or 490 nm, a broad band around 385 nm is observed and on collection of emission at 395 or 415 nm, structured-peaks are obtained in the region 340-390 nm. This observation clearly points out that the broad emission of **mpae** originates mainly from the excitation of the intramolecular charge transfer state whereas, the structured anthracene-like emission occurs from the π, π^* singlet state of anthracene. The picture is similar for **mppe** for which the emission was monitored at 375, 395 or 465 nm in CH_3CN. A broad band at 375 nm is obtained in the excitation spectrum when emission is collected at

465 nm. On the other hand, when the emission is monitored at 375 or 395 nm, typical pyrene absorption peaks are clearly observed.

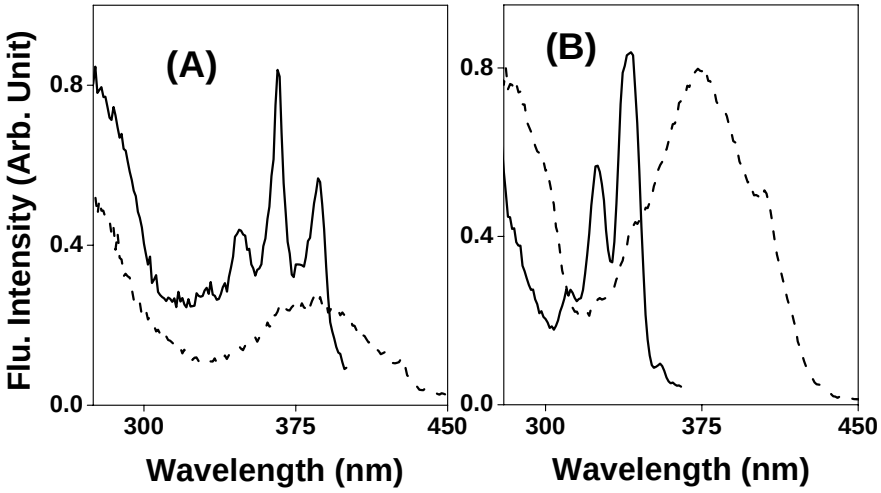

Fig. 3.6. Fluorescence Excitation spectra of (A) **mpae** (λ_{em} = 415 (——) and 490 (– – –) nm) and (B) **mppe** (λ_{em} = 375 (——) and 465 (– – –) nm) in CH_3CN.

3.3.3 Fluorescence decay behavior

Fluorescence decay behavior also provides important information on the nature of excited state of the molecule. The fluorescence quantum yield (ϕ_f) of **mpae** is estimated to be 0.055 in CH_3CN, using 1,6-diphenyl-1,3,5-hexatriene (ϕ_f = 0.80 in cyclohexane)[22] as standard. The compounds **mpae** and **mppe** were excited at 375 nm and 280 nm, respectively in both 1,4-dioxane and CH_3CN and decay profiles were monitored at different wavelengths. Decay profiles were recorded at 415, 480 and 550 nm for **mpae**. Although, a bi-exponential fit to the decay profile of 480 nm and 550 nm was found satisfactory, a tri-exponential fit was necessary for the data collected at

415 nm. The obtained decay parameters are collected in table 3.2. However, it can be seen that among the three components, two components (1.2 ns, 7.2 ns) contribute only 0.2% towards the total emission collected at 415 nm in 1,4-dioxane and hence, unimportant. The lifetime of the major component varies from as short as 4 ps to 1.7 ns. The pattern of the variation of lifetime of **mpae** with the monitoring wavelength is not understood.

Table 3.2. Lifetime data of **mpae** in 1,4-dioxane and acetonitrile (λ_{exc} = 375 nm) recorded at different wavelength.[a]

Solvents	415 nm τ [α] (χ^2)	480 nm τ [α] (χ^2)	550 nm τ [α] (χ^2)
1,4-dioxane	1.2 ns [0.1] 7.2 ns [0.1] ~ 4 ps [99.8] (1.09)	1.8 ns [97.1] 7.3 ns [2.9] (1.15)	1.7 ns [96.4] 4.6 ns [3.6] (1.17)
CH_3CN	1 ns [0.4] 5.8 ns [0.6] ~ 7 ps [99] (1.08)	301 ps [96.1] 4.6 ns [3.9] (1.21)	298 ps [97.6] 3.3 ns [2.4] (1.14)

[a] α is the relative percentage of each component. Lifetimes below 25 ps are not accurate and indicate only the trend.

Decay profiles were monitored at 400 and 475 nm for **mppe** and bi-exponential fit was found satisfactory, yielding one short and one long lifetime component for all of them. The decay parameters are displayed in table 3.3 and one typical decay profile with fitting and residuals is shown in fig. 3.7. The long lifetime component with higher amplitude in the decay profile recorded at low wavelength is associated with emission from the π, π^* singlet state. On the other hand, the short lifetime component, which is the major

component in the decay profile monitored at high wavelength, is coupled with emission from the intramolecular charge transfer state.

Table 3.3. Lifetime data of **mppe** in 1,4-dioxane and acetonitrile (λ_{exc} = 280 nm) recorded at different wavelength.[a]

Solvents	400 nm τ [α] (χ^2)	475 nm τ [α] (χ^2)
1,4-dioxane	6.3 [16], 48.8 [84] (1.01)	2.1 [99.4], 33.5 [0.6] (1.03)
CH_3CN	4.6 [13.2], 18.3 [86.8] (1.04)	1.9 [99.2], 11.9 [0.8] (1.17)

[a] All the lifetimes are in nanosecond (ns) and α is the relative percentage of each component.

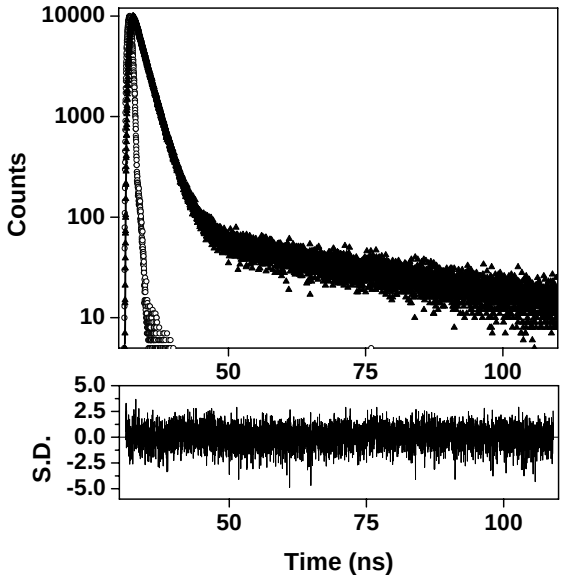

Fig. 3.7. Fluorescence decay profile of **mppe** in 1,4-dioxane. λ_{exc} = 280 nm, λ_{em} = 475 nm. The best fit to the data points (▲) is indicated by the solid line and lamp profile is represented by hollow circles.

3.3.4 Metal ion titration

Interaction of metal ions with molecules showing photoinduced charge transfer (PCT) is well known in literature.[23,24] Both **mpae** and **mppe** contain 2,2′-bipyridyl subunit in their molecular architecture which is well known for its binding properties with transition and post-transition metal ions.[25] Our objective was to find out whether the effect of binding of metal ions with 2,2′-bipyridyl subunit conveyed to the anthracene/pyrene subunit through the ethylene linkage to significant amount so that the absorption or fluorescence signal changes drastically.

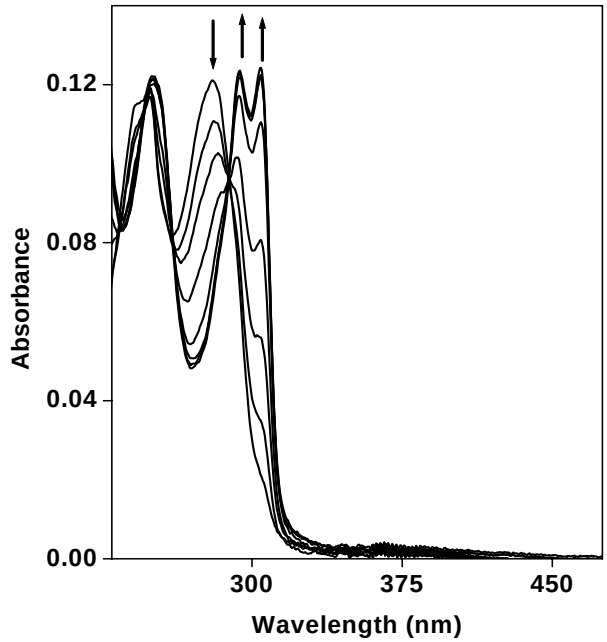

Fig. 3.8. Absorption spectral changes observed for **mpae**, on addition of Co^{2+} ion in CH_3CN. [**mpae**] = 5.8 μM; [Co^{2+}] = 0-6.3 μM.

The systems **mpae** and **mppe** were titrated with different metal ions in CH_3CN. In a typical titration, 5.8 μM of **mpae** is titrated with Co^{2+} and the absorption spectral changes are shown in fig. 3.8. The band at 280 nm disappears with simultaneous formation of new bands at 295 and 305 nm. However, the low energy band around 385 nm decreases only marginally. The spectral changes observed are similar for Mn^{2+}, Ni^{2+}, Cu^{2+}, Zn^{2+}, Cd^{2+} and Pb^{2+} ions. Binding constants are calculated using the change in absorbance at 305 nm and the equation described in section 2.9.1 and displayed in table 3.4.

Table 3.4. Binding constants (10^5 M^{-1}) of **mpae** with different metal ions in acetonitrile, calculated using absorption titration data.

Metal Ions	*K*
Mn^{2+}	11.4
Co^{2+}	54
Ni^{2+}	48.3
Cu^{2+}	13
Zn^{2+}	12.5
Cd^{2+}	3.4
Pb^{2+}	2.5

Fig. 3.9 depicts a representative absorption titration of **mppe** with Ni^{2+}. The most significant change is the formation of a new absorption broad band at 430 nm with concomitant decrease of the intensity of the 375 nm band. The formation of a new broad band at longer wavelength implies that on metal complexation, the charge transfer from pyrene to the metal bound 2,2′-

bipyridyl moiety becomes facile. The spectral changes observed are similar for Mn^{2+}, Co^{2+}, Cu^{2+}, Zn^{2+}, Cd^{2+} and Pb^{2+} ions. The change in the absorbance at 305 nm has been employed to calculate the binding constant of transition metal ions using the equation described in section 2.9.1 and shown in table 3.5.

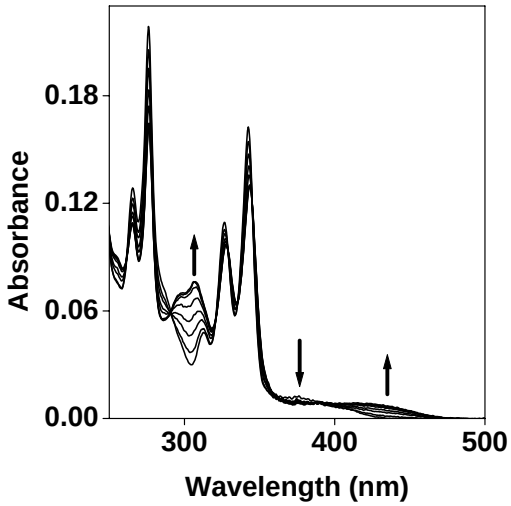

Fig. 3.9. Absorption spectral changes observed for **mppe**, on addition of Ni^{2+} ion in CH_3CN. [**mppe**] = 4.7 μM; [Ni^{2+}] = 0-7.1 μM.

Table 3.5. Binding constants (10^6 M^{-1}) of **mppe** with different metal ions in acetonitrile, calculated using absorption titration data.

Metal Ions	*K*
Mn^{2+}	3.3
Co^{2+}	3.9
Ni^{2+}	2.7
Cu^{2+}	2.4

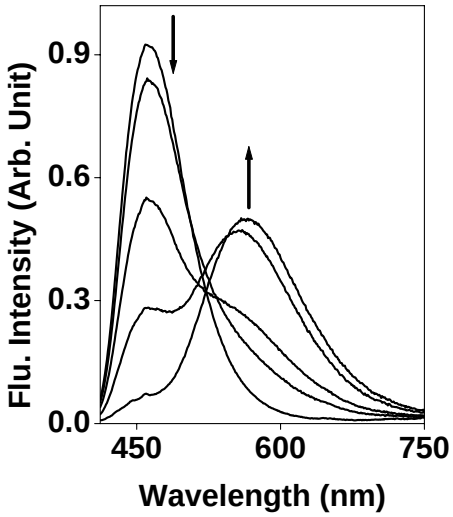

Fig. 3.10. Fluorescence spectral changes observed for **mppe** (λ_{exc} = 400 nm), on addition of Zn^{2+} ion in CH_3CN. [**mppe**] = 4.9 μM; [Zn^{2+}] = 0-6.6 μM.

The fluorescence of **mppe** is quenched on addition of the transition metal ions and formation of no new band is observed. However, post-transition metal ions such as Zn^{2+}, Cd^{2+} and Pb^{2+} behave differently, with the formation of a new fluorescence band at lower energy. In a typical titration, **mppe** was titrated with Zn^{2+} ion and change in fluorescence intensity is depicted in fig. 3.10. The binding constants of **mppe** with Zn^{2+}, Cd^{2+} and Pb^{2+}, calculated by employing the equations described in section 2.9.2, fluorescence enhancement (FE) and emission maxima of **mppe** in presence of each individual metal ion are shown in table 3.6. On binding with these metal ions, photoinduced charge transfer in the excited state becomes facile from relatively electron-rich pyrene to electron-deficient metal-bound 2,2′-bipyridyl moiety, leading to a new red-shifted emission band in the 550-580 nm region.

A similar large red-shift of the emission spectrum of compounds containing 1,4-diethynylated 2,5-dioctyloxyphenylene or phenylenevinylene linkage in presence of Zn^{2+} ion with respect to that of free compounds has been explained by emission from a charge transfer state.[16,17] A similar emission band is not observed in the presence of transition metal ions presumably due to fluorescence quenching effect of these metal ions. From table 3.5 and 3.6, it is observed that binding constants of **mppe** with Mn^{2+}, Co^{2+}, Ni^{2+}, Cu^{2+} and Zn^{2+} are of the order of 10^6 M^{-1} whereas, those for Cd^{2+} and Pb^{2+} are found one order of magnitude lower. This observation can be understood considering the fact that the ionic radii of the first five metal ions, which belong to period 4, are smaller than the latter two, which belong to period 5 and 6, respectively.

Table 3.6. Binding constants (10^5 M^{-1}), fluorescence enhancement (FE) and emission maxima of **mppe** with different metal ions in acetonitrile.[a]

Metal Ions	*K*	FE	λ_{max}^{em} (nm)
Zn^{2+}	15.2	16.5	565
Cd^{2+}	1.9	7.8	558
Pb^{2+}	1.1	6.1	577

[a] λ_{exc} = 440 nm, excitation and emission slit = 3 nm each.

We were interested to know whether **mppe** shows fluorescence OFF/ON signaling in presence of post-transition metal. The dyad **mppe** was titrated with Zn^{2+} in different solvents such as acetonitrile, tetrahydrofuran (THF) and acetonitrile-H_2O (95:5, v/v) mixture. The binding constants, fluorescence enhancement and emission maxima are shown in table 3.7. The fluorescence enhancement in THF is almost the same as that in CH_3CN and ~

10 times more than that in CH_3CN-H_2O mixture. Consequently, binding constants of **mppe** with Zn^{2+} in THF and CH_3CN are of the order of 10^6 M^{-1}, almost two orders of magnitude higher than that in CH_3CN-H_2O mixture. Water molecules in CH_3CN-H_2O mixture coordinate strongly with Zn^{2+} ions, thereby setting a competition with 2,2′-bipyridyl moiety of **mppe** for free coordination site of Zn^{2+} resulting in a lower binding constant.

Table 3.7. Binding constants (10^6 M^{-1}), fluorescence enhancement (FE) and emission maxima of **mppe** in presence of Zn^{2+} ion in different solvents.[a]

Solvents	*K*	FE	λ_{max}^{em} (nm)
THF	2.1	15.9	558
Acetonitrile	1.5	16.5	565
Acetonitrile-H_2O (95:5 v/v)	0.064	2.6	560

[a] λ_{exc} = 440 nm, excitation and emission slit = 3 nm each.

In case of titration of **mpae**, the fluorescence band around 485 nm is quenched gradually on addition of metal ions. This behavior is common for all metal ions used, irrespective of the nature of metal ions and no new red-shifted band is formed even with Zn^{2+}, Cd^{2+} or Pb^{2+}. This observation indicates that photoinduced charge transfer in the excited state from anthracene to metal-bound 2,2′-bipyridyl moiety is not possible in case of **mpae**.

3.4 Summary

We have investigated the photophysical behavior of two dyads, **mpae** and **mppe**, where anthracene and pyrene are appended with 2,2′-bipyridyl by an ethylene linkage. Absorption spectra of **mpae** and **mppe** are featured with a

broad absorption band of low ε value at lower energy. The absorption is attributed to charge transfer from 2,2′-bipyridyl subunit to anthracene/pyrene subunit at ground state. However, the extent of charge transfer is small at ground state as the band position is invariant to the solvent polarity. Emission spectra of both **mpae** and **mppe** comprise dual bands. Higher energy structured-peaks are due to emission from π, π^* excited singlet state localized at the anthracene/pyrene moiety and lower energy broad band is attributed to emission from intramolecular charge transfer (ICT) state.

A new lower energy absorption band for **mppe** in presence of transition (Mn^{2+}, Co^{2+}, Ni^{2+}, Cu^{2+}) and post-transition (Zn^{2+}, Cd^{2+}, Pb^{2+}) metal ions is formed whereas, no such new absorption can be observed for **mpae** under similar condition. **mppe** acts as a fluorescent OFF/ON switch in presence of Zn^{2+}, Cd^{2+} and Pb^{2+} with generation of a new red-shifted broad emission band.

3.5 References

1) *Handbook of Conducting Polymers*, 2nd ed.; Skotheim, T. A., Reynolds, J. R., Elsenbaumer, R. L., Eds.; Marcel Dekker: New York, 1997.
2) For a recent overview on π-conjugated materials see: *Acc. Chem. Res.* **1999**, *32* (3).
3) McQuade, D. T.; Pullen, A. E.; Swager, T. M. *Chem. Rev.* **2000**, *100*, 2537.
4) Walters, K. A.; Ley, K. D.; Cavalaheiro, C. S. P.; Miller, S. E.; Gosztola, D.; Wasielewski, M. R.; Bussandri, A. P.; van Willigen, H.; Schanze, K. S. *J. Am. Chem. Soc.* **2001**, *123*, 8329.

5) Zhu, S. S.; Caroll, P. J.; Swager, T. M. *J. Am. Chem. Soc.* **1996**, *118*, 8713.

6) Wang, B.; Wasielewski, M. R. *J. Am. Chem. Soc.* **1997**, *119*, 12.

7) Lopez, C.; Moutet, J.-C.; Saint-Aman, E. *J. Chem. Soc., Faraday Trans.* **1996**, *92*, 1527.

8) Wang, Q.; Yu, L. *J. Am. Chem. Soc.* **2000**, *122,* 11806.

9) Kimura, M.; Horai, T.; Hanabusa, K.; Shirai, H. *Adv. Mater.* **1998**, *10*, 459.

10) Zotti, G.; Zecchin, S.; Schiavon, G.; Berlin, A.; Penso, M. *Chem. Mater.* **1999**, *11*, 3342.

11) Harriman, A.; Hissler, M.; Ziessel, R. *Phys. Chem. Chem. Phys.* **1999**, *1*, 4203.

12) Hissler, M.; Harriman, A.; Khatyr, A.; Ziessel, R. *Chem. Eur. J.* **1999**, *5*, 3366.

13) Benniston, A. C.; Harriman, A.; Lawrie,D. J.; Mayeux, A.; Rafferty, K.; Russell, O. D. *Dalton Trans.* **2003**, 4762.

14) Rodriguez, A. L.; Peron, G.; Duprat, C.; Vallier, M.; Fouquet, E.; Fages, F. *Tetraheron Lett.* **1998***, 39*, 1179.

15) Soujanya, T.; Philippon, A.; Leroy, S.; Vallier, M.; Fages, F. *J. Phys. Chem. A* **2000**, *104,* 9408.

16) Leroy-Lhez, S.; Parker, A.; Lapouyade, P.; Belin, C.; Ducasse, L.; Oberle, J.; Fages, F. *Photochem. Photobiol. Sci.* **2004**, *3*, 949.

17) Leroy, S.; Soujanya, T.; Fages, F. *Tetrahedron Lett.* **2001**, *42*, 1665.

18) Ghosh, T.; Shukla, A. D.; Jose, D. A.; Kumar, D. K.; Maiya, B. G.; Samanta, A.; Das, A. *J. Biol. Inorg. Chem.* **2005**, *10*, 496.

19) Wasielewski, M. R.; Minsek, D. W.; Niemczyk, M. P.; Svec, W. A.; Yang, N. C. *J. Am. Chem. Soc.* **1990**, *112*, 2823.

20) Brun, A. M.; Harriman, A.; Tsuboi, Y.; Okada, T.; Mataga, N. *J. Chem. Soc., Faraday Trans.* **1995**, *91*, 4047.

21) Asahi, T.; Mataga, N. *J. Phys. Chem.* **1989**, *93*, 6575.

22) Berlman, I. B. *Handbook of Fluorescence Spectra of Aromatic Molecules*, 2nd edition, Academic Press: New York, 1971, p. 322.

23) Rurack, K.; Resch-Genger, U. *Chem. Soc. Rev.* **2002**, *31*, 116.

24) Valeur, B.; Leray, I. *Coord. Chem. Rev.* **2000**, *205*, 3.

25) Kaes, C.; Katz, A.; Hosseini, M. W. *Chem. Rev.* **2000**, *100*, 3553.

CHAPTER 4

Transition Metal Ions Signaling Behavior of Dipyridylquinoxalinazo Chemosensor

4.1 Introduction

The recognition and signaling events of analyte by chemosensor is an active area of research within the field of supramolecular chemistry.[1,2] Although, many fluorescent chemosensors have been developed in recent years for cations,[3-5] anions[6-8] and neutral molecules[9-11] the colorimetric chemosensors are somewhat less explored.[12-17] The real advantage of colorimetric chemosensor is that the recognition event is visible by naked eye with change in color and the detection can be real time and on a molecular scale.[1,2] The colorimetric chemosensors are designed such a way that the receptor and signaling units are either fused together into one unit or connected by some unsaturated groups. Generally, electron donor-acceptor moieties connected by π-conjugation are chosen as suitable system for this purpose. Recognition of analyte by the chemosensor is expected to affect the conjugation between electron-donor and acceptor segment of the molecule substantially and thereby give rise to drastic color changes upon recognition.

Using the above rationale, systems based on azobenzene,[18-21] naphthalimide,[22,23] azo-coupled calix[4]biscrowns[24,25] or phenoxazinone[26] have been used as colorimetric chemosensor for Na^+, K^+, Cs^+, Cu^{2+}, Ag^+, Hg^{2+} ions in recent years. Azo-dyes with nitrobenzene as electron-acceptor moiety and aza-crown or *o*-methoxyphenyliminodiacetate as electron-donor moiety have been employed as colorimetric reporter for potential recognition of Na^+, K^+ and Cu^{2+} ions.[18-21] The colorimetric cation sensing property of azo-dye

derivatives has been exploited only in few cases and just one report is available where transition metal ion, *viz.* Cu^{2+} is detected by color change using an azo-dye derivative.[21] The azo-dye derivatives are easy to prepare and color changes of such molecules with metal ion input are drastic. Hence, we intended to synthesize and study the transition metal ion binding property of the azo-dye derivative **dpqapd**, where dimethylamine acts as electron-donor and dipyridylquinoxaline as electron-acceptor. The sensing of transition metal ions (Co^{2+}, Ni^{2+}, Cu^{2+}, Zn^{2+} and Cd^{2+}) by **dpqapd** in CH_3CN is demonstrated by change in color.

4.2 Experimental section

The azo compound [4-(2,3-di-pyridin-2-yl-quinoxalin-6ylazo)-phenyl]-dimethylamine (**dpqapd**), and its precursors 6-nitro-2,3-di(2-pyridyl)quinoxaline (**ndpq**) and 2,3-di(2-pyridyl)-6-quinoxalinamine (**adpq**) were synthesized by following procedures.

6-Nitro-2,3-di(2-pyridyl)quinoxaline (ndpq)

2,2′-pyridil (212 mg, 1.0 mmol) was dissolved in glacial acetic acid (40 mL) and, a solution of 4-nitro-1,2-phenylenediamine (230 mg, 1.5 mmol) in acetic acid (30 mL) was added with stirring. The resulting mixture was heated at reflux under nitrogen atmosphere for overnight. Then, major part of acetic acid was distilled off under vacuum and the residue was taken up in a mixture of water (50 mL) and CH_2Cl_2 (50 mL). The residual acetic acid was neutralized by adding Na_2CO_3 and pH of the aqueous layer made basic. The organic layer was separated off and the aqueous layer was extracted with CH_2Cl_2 (3 x 30 mL). The organic layers were combined and dried over anhydrous sodium sulfate, filtered and evaporated to dryness. Neutral alumina

column chromatography (eluent: hexane/acetone, 4:1, v/v) afforded **ndpq** (270 mg, 82%) as a pale yellow solid. Anal. Calcd. For $C_{18}H_{11}N_5O_2$: C, 65.65; H, 3.34; N, 21.27. Found: C, 65.48; H, 3.42; N, 21.45. ^{1}H NMR (400 MHz, $CDCl_3$, TMS) δ, ppm: 7.28-7.31 (2H, m), 7.85-7.91 (2H, m), 8.05-8.09 (2H, m), 8.35-8.37 (3H, overlapping d and m), 8.59 (1H, dd, *J* = 3.2 Hz, 9.4 Hz), 9.13 (1H, d, *J* = 2.8 Hz) . LC-MS: *m/z* 329 (M^+).

2,3-Di(2-pyridyl)-6-quinoxalinamine (adpq)

To a solution of **ndpq** (165 mg, 0.5 mmol) in $CHCl_3$/methanol (1:4, v/v) mixture (50 mL) was added 10% palladium on activated carbon (Pd/C; 50 mg) as catalyst and then sodium tetrahydroborate (0.6 g) in portions at 0^{o}C. The reaction mixture was stirred for 17 h at room temperature and the solution changed from light yellow to brownish-red. Then Pd/C was filtered off and the filtrate was evaporated. The resultant solid was dissolved in water/$CHCl_3$ mixture. The organic layer was separated off and aqueous layer was extracted with $CHCl_3$ (3 x 30 mL). Removal of chloroform gave the crude product, which was purified by neutral alumina column chromatography (eluent: hexane/ethyl acetate, 2:3, v/v) to afford **adpq** (125 mg, 84%) as yellow solid. Anal. Calcd. For $C_{18}H_{13}N_5$: C, 72.24; H, 4.35; N, 23.41. Found: C, 72.48; H, 4.50; N, 23.18. ^{1}H NMR (400 MHz, $CDCl_3$, TMS) δ, ppm: 4.27 (2H, br s), 7.17-7.20 (1H, m), 7.20-7.22 (2H, m), 7.24 (1H, d, *J* = 3.2 Hz), 7.75-7.79 (2H, m), 7.83-7.86 (2H, m), 8.00 (1H, d, *J* = 8.8 Hz), 8.38-8.41 (2H, m). LC-MS: *m/z* 299 (M^+).

[4-(2,3-di-pyridin-2-yl-quinoxalin-6-ylazo)-phenyl]-dimethylamine (dpqapd)

adpq (90 mg, 0.3 mmol) was dissolved in 20 mL water/methanol mixture (1:1, v/v) and cooled at 0^oC. 5 mL solution of $NaNO_2$ (22 mg, 0.32 mmol) and HCl (0.2 mL, 12 M) in water/methanol mixture was added to previously cooled solution of **adpq** in small portions. This resultant solution was then added dropwise to a 15 mL solution of N,N-dimethylaniline (37 mg, 0.3 mmol) in water/methanol mixture, temperature of the solution being maintained at 0^oC. The reaction mixture was stirred for 1 hr at 0^oC and then, poured into 500 mL water of slightly alkaline pH. It was filtered under vacuum to afford a brownish-red solid. The crude material was purified on a neutral alumina column using hexane/acetone (7:3, v/v) as eluent to produce **dpqapd** as reddish-brown solid (52 mg, 40%). Anal. Calcd. For $C_{26}H_{21}N_7$: C, 72.39; H, 4.87; N, 22.74. Found: C, 72.50; H, 4.98; N, 22.56. ^1H NMR (400 MHz, $CDCl_3$, TMS) δ, ppm: 3.13 (6H, s), 6.80 (2H, d, *J* = 8.8 Hz), 7.23-7.25 (2H, m), 7.81-7.87 (2H, m), 7.98-8.04 (2H, m), 7.98 (2H, d, *J* = 8.8 Hz), 8.26 (1H, d, *J* = 8.8 Hz), 8.38-8.41 (3H, m), 8.63 (1H, d, *J* = 2 Hz). LC-MS: *m/z* 431 (M^+). UV-Visible (CH_3CN) λ_{max}, nm (ε, M^{-1} cm^{-1}): 240 (14400), 278 (16350), 464 (22700).

4.3 Results and discussion

4.3.1 Synthesis

The scheme leading to the synthesis of **dpqapd** has been shown in scheme 4.1. **dpqapd** was synthesized in three steps. Commercially available 2,2′-pyridil and 4-nitro-1,2-phenylenediamine were condensed in acetic acid to form **ndpq**, which was then reduced by $NaBH_4$ in presence of

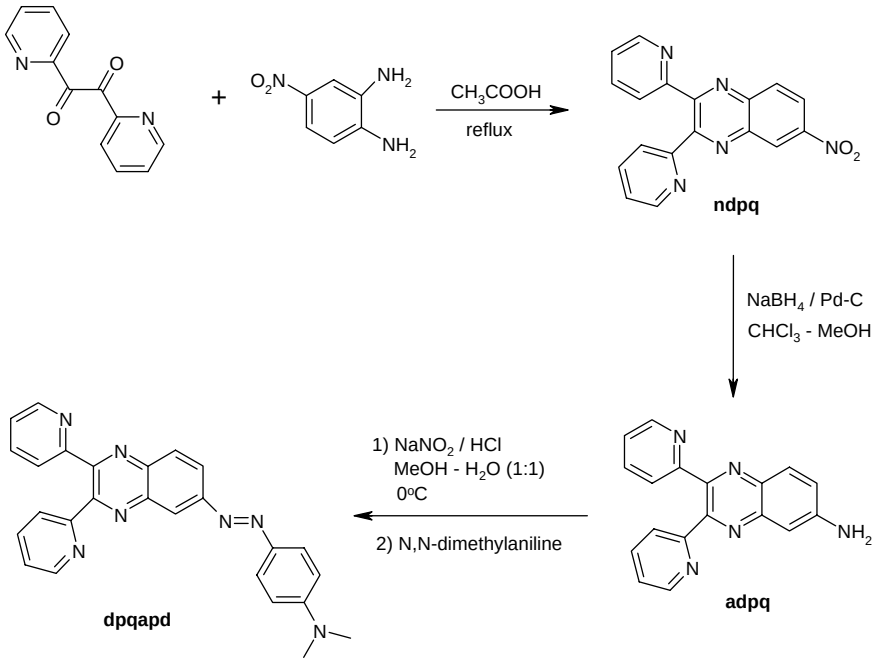

Scheme 4.1. Synthesis of **dpqapd**.

palladium/carbon (10%) catalyst to obtain **adpq**, the yield being good for both the steps. Diazotization of **adpq** followed by coupling with N,N-dimethylaniline afforded **dpqapd** as reddish-brown solid in low yield (40%). **dpqapd** and other two compounds have been characterized by elemental analysis, LC-mass and ^{1}H NMR spectroscopy.

4.3.2 Absorption spectral behavior

The absorption spectrum of **dpqapd** consists of three bands in CH_3CN, as shown in fig. 4.1. Two bands are observed in the UV region of absorption spectrum of **dpqapd** whereas, one band is observed in visible region and all

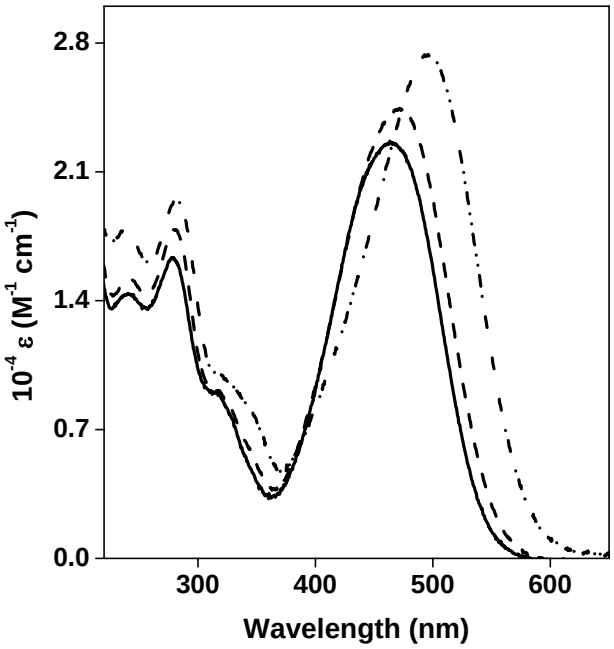

Fig. 4.1. Absorption spectrum of **dpqapd** in CH_3CN (——), MeOH (– – –), and 50 % MeOH-aqueous HEPES buffer (— · ·).

the bands have ε values of the order of 10^4 M^{-1} cm^{-1}. The higher energy bands around 240 and 280 nm are due to π, π^* transition and the lower energy one around 465 nm arises from intramolecular charge transfer (ICT) transition between electron-donating dimethylamine group and electron-withdrawing dipyridylquinoxaline group. To confirm the nature of transition of the bands, absorption spectrum of **dpqapd** has been recorded in methanol and 50% methanol-aqueous HEPES buffer (v/v). The position of the higher energy bands at 240 and 280 nm is insensitive to increasing the polarity of the solvents confirming the transitions as π, π^* in nature. The lower energy band

in the visible region is red-shifted with increase in the solvent polarity (λ_{max} = 465 nm (CH_3CN), 470 nm (MeOH), 495 nm (50% MeOH-aqueous HEPES buffer)). The ε value of the band is also increased with increase in solvent polarity. These observations support an intramolecular charge transfer transition between electron-donating dimethylamine group and electron-withdrawing dipyridylquinoxaline group at ground state.

4.3.3 Colorimetric sensing

The chemosensor **dpqapd** contains dipyridylquinoxaline and dimethylamine moieties in its molecular architecture, which can act as electron-acceptor and electron-donor, respectively. Binding of transition metal ion with dipyridylquinoxaline moiety would render it electron-deficient and enhance the feasibility of charge transfer from dimethylamine moiety. Hence, red-shift of the charge transfer band is expected. However, binding of metal ion with dimethylamine moiety would hamper the charge transfer in the molecule and blue-shift of the charge transfer band is expected.

The color change of **dpqapd** in CH_3CN on addition of different metal ions is shown in fig. 4.2. The experiment was carried out by using 10 μM **dpqapd** and 0.5 mM metal ion concentration. The original color of **dpqapd** is yellow which changes to light-pink in case of Ni^{2+}, Zn^{2+} and pink in case of Co^{2+}, Cd^{2+}. However, no color change is observed with Mn^{2+} and solution turns colorless with Cu^{2+}. The most significant observation of this experiment is that the color response of **dpqapd** is not the same for all the transition metal ions used. This indicates that the mode of binding may not be similar for all the metal ions.

None **+Mn^{2+}** **+Co^{2+}** **+Ni^{2+}** **+Cu^{2+}** **+Zn^{2+}** **+Cd^{2+}**

Fig. 4.2. Color changes of **dpqapd** on addition of different metal ions in CH_3CN. [**dpqapd**] = 10 μM, [metal ion] = 0.5 mM. From left to right: none, Mn^{2+}, Co^{2+}, Ni^{2+}, Cu^{2+}, Zn^{2+} and Cd^{2+}.

4.3.4 Absorption titration

The change in absorption spectrum of **dpqapd** in CH_3CN with addition of Ni^{2+} ion is shown in fig. 4.3. The band at 465 nm is red-shifted to 495 nm with gradual decrease in absorbance on addition of Ni^{2+} ion. Presence of an isosbestic point at 490 nm implies **dpqapd** and **dpqapd**–Ni^{2+} are in equilibrium in the course of titration and complexation between **dpqapd** and Ni^{2+} are 1:1 in nature. Similar change in absorption spectrum of **dpqapd** is observed on addition of Zn^{2+} ion also. However, the spectral changes are completely different with Cu^{2+} ion. The 465 nm absorption band decreases on addition of Cu^{2+} ion (Fig. 4.3). Also, a shoulder is found to form at 360 nm. Pyridine and quinoxaline nitrogen atoms are involved in binding with Ni^{2+} (or Zn^{2+}) ion in bidentate manner to form a five-member chelate ring. This makes dipyridylquinoxaline moiety sufficiently electron-deficient to draw electron density from donor dimethylamine moiety, making the charge transfer from the latter moiety more facile. Hence, the charge transfer band is red-shifted to 495 nm. In case of Cu^{2+} ion, the nitrogen atom of the dimethylamine moiety is involved in binding. Therefore, the charge transfer from dimethylamine is

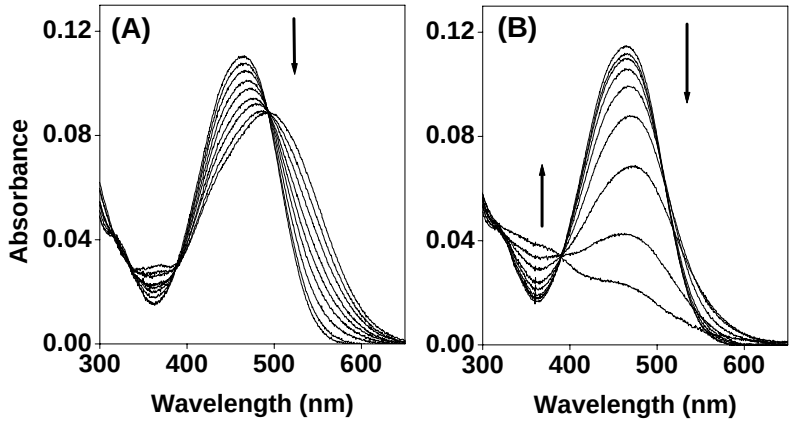

Fig. 4.3. Change in absorption spectrum of **dpqapd** on addition of (A) Ni^{2+} and (B) Cu^{2+} ions in CH_3CN. (A) [**dpqapd**] = 4.8 μM, [Ni^{2+}] = 0, 0.5, 1.3, 2.5, 4.0, 5.8, 7.9, 10.3, 13.1 μM. (B) [**dpqapd**] = 5 μM, [Cu^{2+}] = 0, 2.5, 4.0, 5.9, 8.4, 11.2, 14.7, 18.6, 26.2 μM.

gradually inhibited and almost completely stopped when all the dimethylamine moieties of **dpqapd** are complexed with Cu^{2+}, leading to the disappearance of the charge transfer absorption band. In a previously reported azo-benzene chemosensor, nitroegen atom of *o*-methoxyphenyliminodiacetate moiety was found to bind with Cu^{2+} ion, reducing the ability of the iminodiacetate moiety to participate in ICT.[21] The binding constants of **dpqapd** with Ni^{2+}, Zn^{2+} and Cu^{2+} ions, determined by decrease in absorbance at 465 nm and using equation described in section 2.9.1, are shown in table 4.1. The binding constant of **dpqapd** with Ni^{2+} is of the order of 10^5 M^{-1} and that with Zn^{2+} and Cu^{2+} is of the order of 10^4 M^{-1}.

Table 4.1. Binding constants (10^4 M^{-1}) of **dpqapd** with different metal ions in acetonitrile, calculated using decrease in absorbance at 465 nm.

Metal Ions	*K*
Ni^{2+}	12
Cu^{2+}	8.4
Zn^{2+}	9.3

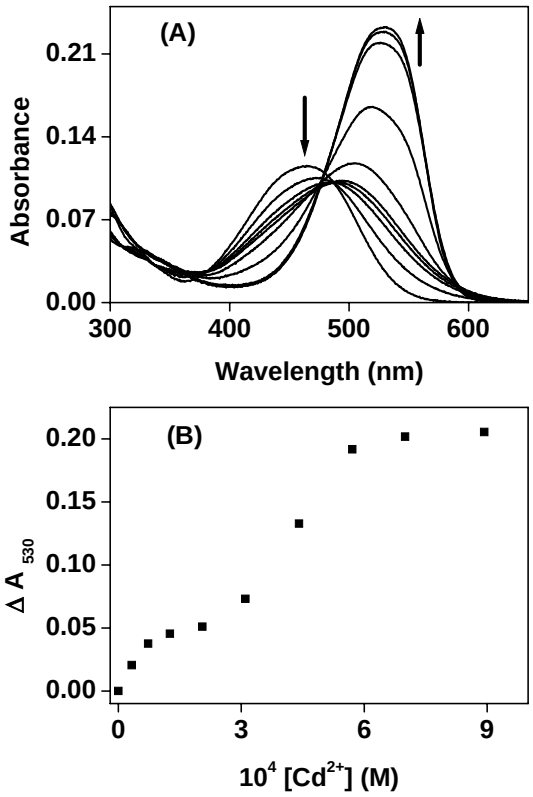

Fig. 4.4. (A) Absorption spectral change of **dpqapd** in CH_3CN on addition of Cd^{2+} ion. [**dpqapd**] = 5.1 μM. (B) Scatter plot of change in absorbance of **dpqapd** at 530 nm (ΔA_{530}) vs. [Cd^{2+}].

The titration of **dpqapd** with Cd^{2+} is featured by red-shift of the charge transfer band to 530 nm with drastic increase in absorbance, as shown in fig. 4.4. Isosbestic points at 485 and 475 nm are also observed. Similar spectral changes are observed for Co^{2+} ion as well. A scatter plot of change in absorbance at 530 nm vs. concentration of Cd^{2+} ion consists of two steps, which can be understood as follows (Fig. 4.4). Binding of one equivalent of Cd^{2+} ion with one pyridine and quinoxaline nitrogen atoms in bidentate fashion reflects the initial absorbance change at low Cd^{2+} ion concentration. At higher Cd^{2+} concentration, binding of another equivalent of Cd^{2+} with the free nitrogen atoms of other pyridine ring and quinoxaline ring in bidentate manner, inducing conformational changes in **dpqapd**, causes additional charge transfer from dimethylamine moiety and gives rise to a drastic increase in absorbance.

4.4 Summary

A new colorimetric chemosensor **dpqapd** for detection of transition metal ions has been synthesized by a three-step reaction in low yield. In the molecule, dipyridylquinoxaline and dimethylamine groups act as electron-acceptor and electron-donor moieties which are coupled by azo-benzene group. Absorption spectrum of **dpqapd** is featured by a charge transfer band in visible region whose position is sensitive to polarity of the solvent. **dpqapd** changes its color from yellow to light-pink with Ni^{2+}, Zn^{2+} and pink with Co^{2+}, Cd^{2+} in CH_3CN. However, no color change is observed with Mn^{2+} and the solution turns colorless with Cu^{2+}. The binding constants of **dpqapd** with metal ions are determined from absorption titration data, which are of the order of 10^5 M^{-1} with Ni^{2+} and 10^4 M^{-1} with Zn^{2+} and Cu^{2+}. The charge transfer band of **dpqapd** is red-shifted on addition of Ni^{2+} and Zn^{2+} whereas, the same band decreases gradually and finally vanishes on addition of Cu^{2+}.

The former two metal ions bind with the dipyridylquinoxaline moiety whereas, the latter one binds with the dimethylamine moiety. Binding of **dpqapd** with two equivalents of Cd^{2+} or Co^{2+} enhances charge transfer from dimethylamine moiety and intensity of the charge transfer band increases drastically.

4.5 References

1) *Fluorescent Chemosensors of Ion and Molecule Recognition*. Czarnik, A. W., Ed.; ACS Symp. Ser. 538; American Chemical Society: Washington DC, 1993.
2) Spichiger-Keller, U. E. *Chemical Sensors and Biosensors for Medicinal and Biological Applications*; Wiley-VCH: Weinheim, Germany, 1998.
3) Rurack, K.; Resch-Genger, U. *Chem. Soc. Rev.* **2002**, *31*, 116.
4) *Special Issue on 'Luminescent Sensors', Coord. Chem. Rev.* **2000**, *205*.
5) de Silva, A. P.; Gunaratne, H. Q. N.; Gunnlaugsson, T.; Huxley, A. J. M.; McCoy, C. P.; Rademacher, J. T.; Rice, T.E. *Chem. Rev.* **1997**, *97*, 1515.
6) *Supramolecular Chemistry of Anions*; Bianchi, A., Bowman-James, K., Garcia-Espana, E., Eds.; Wiley-VCH: New York, 1997.
7) Beer, P. D.; Gale, P. A. *Angew. Chem. Int. Ed.* **2001**, *40*, 486.
8) *Special Issue on 'Synthetic Anion Receptor Chemistry', Coord. Chem. Rev.* **2003**, *240*.
9) James, T. D.; Shinnoni, H.; Shinkai, S. *Chem. Commun.* **1997**, 71.
10) James, T. D.; Sandanayake, K. R. A. S.; Shinkai, S. *Nature* **1995**, *374*, 6520.
11) de Silva, A. P.; Gunaratne, H. Q. N.; Gunnlaugsson, T. *Tetrahedron Lett.* **1998**, *39*, 5077.

12) Lohr, H.-G.; Vogtle, F. *Acc. Chem. Res*. **1985**, *18*, 65.

13) McCleskey, S. C.; Metzger, A.; Simmons, C. S.; Anslyn, E. V. *Tetrahedron* **2002**, *58*, 621.

14) Sancenón, F.; Descalzo, A. B.; Martínez-Máñez, R.; Miranda, M. A.; Soto, J. *Angew. Chem. Int. Ed.* **2001**, *40*, 2640.

15) Wiskur, S. L.; Anslyn, E. V. *J. Am. Chem. Soc.* **2001**, *123*, 10109.

16) Yamaguchi, S.; Akiyama, S.; Tamao, K. *J. Am. Chem. Soc.* **2001**, *123*, 11372.

17) Pipoosananakaton, B.; Sukwattanasinitt, M.; Jaiboon, N.; Chaichit, N.; Tuntulani, T. *Tetrahedron Lett.* **2000**, *41*, 9095.

18) Gunnlaugsson, T.; Nieuwenhuyzen, M.; Richard, L.; Thoss, V. *Tetrahedron Lett.* **2001**, *42*, 4725.

19) Gunnlaugsson, T.; Leonard, J. P. *J. Chem. Soc., Perkin Trans. 2* **2002**, 1980.

20) Gunnlaugsson, T.; Nieuwenhuyzen, M.; Richard, L.; Thoss, V. *J. Chem. Soc., Perkin Trans. 2* **2002**, 141.

21) Gunnlaugsson, T.; Leonard, J. P.; Murray, N. S. *Org. Lett.* **2004**, *6*, 1557.

22) Jia, L.; Zhang, Y.; Guoa, X.; Qiana, X. *Tetrahedron Lett.* **2004**, *45*, 3969.

23) Xu, Z.; Qian, X.; Cui, J. *Org. Lett.* **2005**, *7*, 3029.

24) Kim, J. Y.; Kim, G.; Kim, C. R.; Lee, S. H.; Lee, J. H.; Kim, J. S. *J. Org. Chem.* **2003**, *68*, 1933.

25) Lee, S. H.; Kim, J. Y.; Ko, J.; Lee, J. Y.; Kim, J. S. *J. Org. Chem.* **2004**, *69*, 2902.

26) Descalzo, A. B.; Martınez-Manez, R.; Radeglia, R.; Rurack, K.; Soto, J. *J. Am. Chem. Soc.* **2003**, *125*, 3418.

CHAPTER 5

Fluoride Ion Sensors Based on Dipyrrolyl Derivatives: Synthesis, Optical and Electrochemical Sensing

5.1 Introduction

Anions play an important role in various industrial processes, energy transduction and enzymatic activity in organisms, clinical treatment of various disease states etc.[1-5] Sensing such anions is a challenging area in chemistry. Indeed, it is only recently that the coordination chemistry of anions is being developed, in contrast to that of cations. Among the many inorganic anions, fluoride ion is drawing a special attention due to its beneficial (e.g. prevention of dental caries and treatment of osteoporosis)[6,7] as well as detrimental (e.g. fluorosis)[8] roles. Thus, a wide variety of optical and electrochemical F^- sensors based on either positively charged or neutral organic receptors have been reported to date.[4,5] Of specific relevance to the present work are the recently reported pyrrole based sensors namely, calix[4]pyrrole[9,10] and dipyrrolylquinoxaline (DPQ)[11-19] families of compounds. The latter have the dual advantage of possessing a built-in chromophore and being readily accessible in two steps from commercially available materials. In addition, introduction of electron withdrawing groups at the pyrrole or quinoxaline subunits of the DPQ moiety is known to result in enhanced binding of the anion with the receptor.[11-14] Combing these attractive structural and spectroscopic features of dipyrrolyl derivatives will, therefore, provide ample opportunities to synthesize variously substituted DPQ and related class of motifs and develop anion sensors that suit individual application.

Our efforts have resulted in the synthesis of three new dipyrrolyl sensors **pdnqd**, **ppdcn** and **dpqa**, all of which are found to be avid binders of F^-. The highlights of the work described in this chapter are: (i) these DPQ/dipyrrolylpyrazine[18-20] (DPP) class of sensors show dramatic, binding-induced color changes in the presence of F^- and (ii) sensing of F^- by **pdnqd** and **ppdcn** can also be monitored by electrochemical methods.

5.2 Experimental section

The three new sensors investigated in this study were synthesized by single step reactions as detailed below.

2,3-di(1*H*-2-pyrrolyl)-7,12-dihydronaphtho[2,3-*f*]quinoxaline-7,12-dione (**pdnqd**)

1,2-di(1*H*-2-pyrrolyl)-1,2-ethanedione[11,21] (100 mg, 0.53 mmol) was dissolved in glacial acetic acid (40 mL) and a solution of 1,2-diaminoanthraquinone (190 mg, 0.8 mmol) in acetic acid (30 mL) was added with stirring. The resulting mixture was heated at reflux under nitrogen atmosphere for 12 h. Then, major part of acetic acid was distilled off under vacuum and the residue was taken up in a mixture of $CHCl_3$ (50 mL) and water (50 mL). The organic layer was separated off and the aqueous layer was extracted with $CHCl_3$ (3 x 30 mL). The organic layers were combined and washed successively with saturated aqueous sodium bicarbonate solution (50 mL), water (50 mL) and brine (50 mL). The solution was then dried over anhydrous sodium sulfate, filtered and evaporated to dryness. Silica gel column chromatography (eluent: $CHCl_3$/EtOAc, 96:4, v/v) afforded **pdnqd** (170 mg, 82%) as a red solid. Anal. Calcd. For $C_{24}H_{14}N_4O_2$: C, 73.84; H, 3.61;

N, 14.35. Found: C, 73.78; H, 3.65; N, 14.25. ^{1}H NMR (200 MHz, $(CD_3)_2SO$, TMS) δ, ppm: 6.19-6.25 (2H, m), 6.50-6.53 (1H, m), 6.64-6.66 (1H, m), 7.12-7.17 (2H, m), 7.88-8.00 (2H, m), 8.19-8.22 (2H, m), 8.25 (1H, d, *J* = 10 Hz), 8.40 (1H, d, *J* = 10 Hz), 11.16 (1H, br s), 11.87 (1H, br s). ^{13}C NMR (50 MHz, $(CD_3)_2SO$, TMS) δ, ppm: 114.7, 114.9, 118.4, 119.1, 128.3, 128.8, 130.5, 131.4, 131.7, 132.9, 133.3, 133.9, 137.1, 138.7, 138.9, 139.8, 140.1, 147.3 (some lines are overlapping, giving rise to less number of signals). FAB-MS: *m/z* 392 $(M+2H)^+$. IR (KBr pellet, cm^{-1}): 3376, 1665.

5,6-di(1*H*-2-pyrrolyl)-2,3-pyrazinedicarbonitrile (**ppdcn**)

1,2-di(1*H*-2-pyrrolyl)-1,2-ethanedione[11,21] (150 mg, 0.8 mmol) and 1,2-diaminomaleonitrile (121 mg, 1.12 mmol) were dissolved in ethanol (50 mL) and catalytic amount of $BF_3.Et_2O$ was added to this solution. It was then heated at reflux under nitrogen atmosphere for 8 h. The solvent was then removed and the residue was dissolved in CH_2Cl_2 and filtered. The filtrate was chromatographed over silica gel column (eluent: CH_2Cl_2/EtOAc, 99:1, v/v) to afford **ppdcn** (162 mg, 78%) as a yellow solid. Anal. Calcd. For $C_{14}H_8N_6$: C, 64.61; H, 3.10; N, 32.30. Found: C, 64.55; H, 3.02; N, 32.21. ^{1}H NMR (200 MHz, $CDCl_3$, TMS) δ, ppm: 6.30-6.34 (2H, m), 7.11-7.14 (2H, m), 7.35-7.39 (2H, m), 9.61 (2H, br s). ^{13}C NMR (50 MHz, $CDCl_3/CD_3OD$, 4:1, v/v, TMS) δ, ppm: 112.0, 115.4, 116.9, 126.6, 126.9, 127.9, 145.4. FAB-MS: *m/z* 260 $(M)^+$. IR (KBr pellet, cm^{-1}): 3314, 2243.

9-[2,3-di(1*H*-2-pyrrolyl)-6-quinoxalinyl]acridine (**dpqa**)

1,2-di(1*H*-2-pyrrolyl)-1,2-ethanedione[11,21] (100 mg, 0.53 mmol) and 9-(3,4-diaminophenyl)acridine[22] (184 mg, 0.64 mmol) were dissolved in glacial

acetic acid (40 mL) and the resulting mixture was heated at reflux under nitrogen atmosphere for 10 h. Then, major part of acetic acid was distilled off under vacuum and the residue was taken up in a mixture of $CHCl_3$ (50 mL) and water (50 mL). The organic layer was separated off and the aqueous layer was extracted with $CHCl_3$ (3 x 30 mL). The organic layers were combined and washed successively with saturated aqueous sodium bicarbonate solution (50 mL) and water (50 mL). The solution was then dried over anhydrous sodium sulfate, filtered and evaporated to dryness. Column chromatography over neutral alumina (eluent: CH_2Cl_2) afforded **dpqa** (150 mg, 65%) as yellowish-green solid. Anal. Calcd. For $C_{29}H_{19}N_5$: C, 79.63; H, 4.35; N, 16.02. Found: C, 79.81; H, 4.27; N, 16.18. ^{1}H NMR (400 MHz, $CDCl_3$, TMS) δ, ppm: 6.29-6.31 (1H, m), 6.32-6.34 (1H, m), 7.00-7.02 (1H, m), 7.05-7.07 (1H, m), 7.08-7.10 (2H, m), 7.42-7.46 (2H, m), 7.63 (1H, dd, *J* = 2 Hz, 8.4 Hz), 7.75-7.82 (4H, m), 8.00 (1H, d, *J* = 1.2 Hz), 8.10 (1H, d, *J* = 8.8 Hz), 8.32 (2H, d, *J* = 9.2 Hz), 9.68 (1H, br s), 9.77 (1H, br s). FAB-MS: *m/z* 438 $(M+H)^+$. IR (KBr pellet, cm^{-1}): 3414.

5.3 Results and discussion

5.3.1 Synthesis

Structurally, while sensors **pdnqd** and **dpqa** can be considered as DPQ derivatives having the quinine and acridine moieties as part of the extended π framework, compound **ppdcn** is a newly introduced sensor motif, *viz.* dipyrrolylpyrazine (DPP),[18-20] that is substituted with two cyano groups directly on its skeleton. The rationales behind the introduction of quinone or cyano group in these sensors are two folds: (i) these strongly electron-withdrawing groups are expected to render the pyrrole NH protons highly

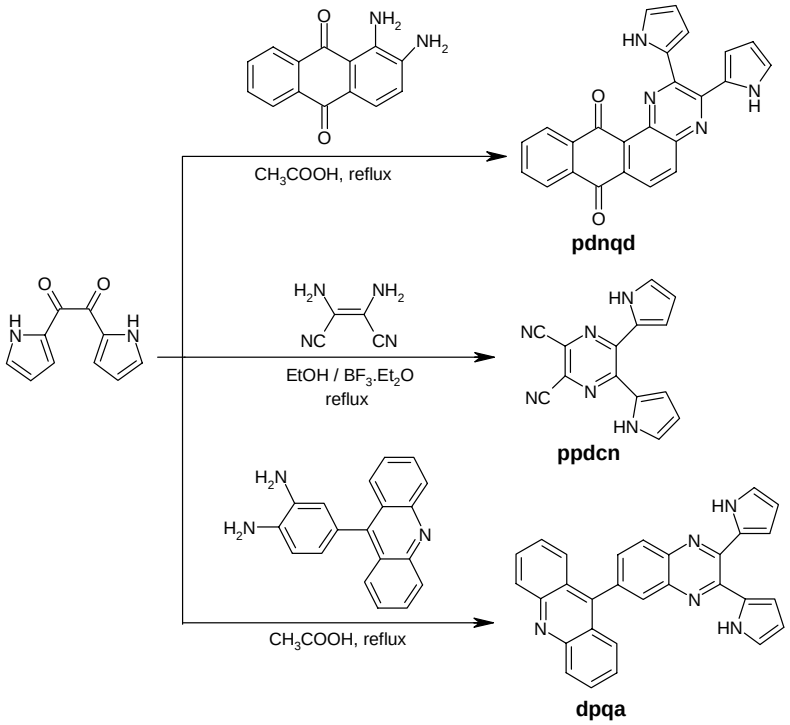

Scheme 5.1. Synthesis of sensors **pdnqd**, **ppdcn and dpqa**.

acidic and thereby enhance hydrogen-bonding ability of the anion sensors,[11-14] and (ii) both quinone and cyano substituents are redox active[23,24] and, hence, anion binding event can be monitored by the electrochemical methods as well.

The synthesis of sensors **pdnqd**, **ppdcn** and **dpqa** are illustrated in scheme 5.1. Reaction of easily synthesizable 1,2-di(1*H*-2-pyrrolyl)-1,2-ethanedione with 1,2-diaminoanthraquinone, 1,2-diaminomaleonitrile or 9-(3,4-diaminophenyl)acridine readily furnished sensors **pdnqd**, **ppdcn** and **dpqa** respectively, in good-to-moderate yield in each case. All the three compounds are sufficiently characterized for their purity and structural

integrity by elemental analysis, FAB-MS, IR, ^{1}H (1D and ^{1}H–^{1}H COSY) and ^{13}C NMR methods, as described in the experimental section.

5.3.2 Crystal structure of pdnqd

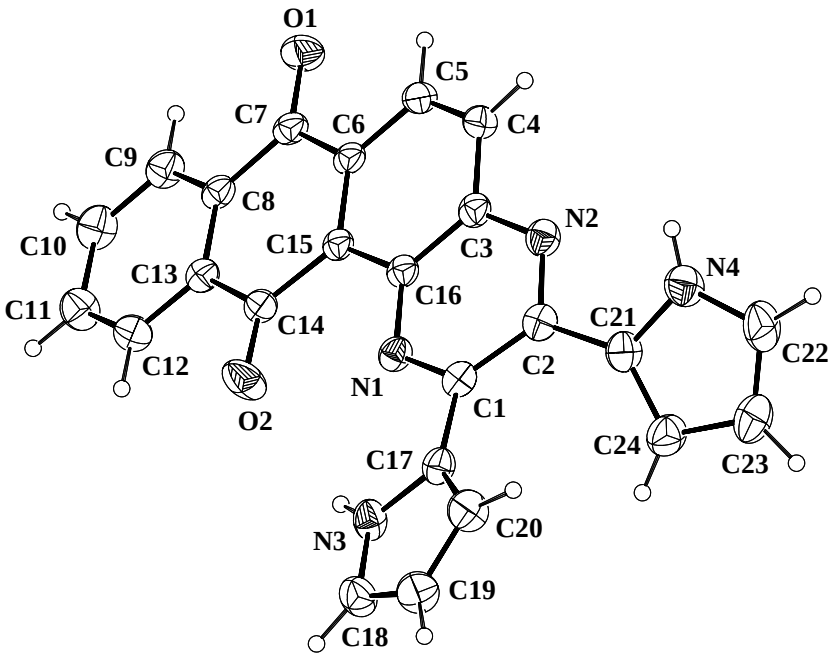

Fig. 5.1. Crystal structure of **pdnqd** with all heavy atoms labeled. The thermal ellipsoids were scaled to the 30% probability level.

The crystal structure of **pdnqd** is shown in fig. 5.1. The crystal was grown by diffusion of methanol vapor into a solution of **pdnqd** in N, N-dimethylformamide. Both pyrrole rings are in different plane than that of quinoxaline ring and make dihedral angles of 14^{o} and 30^{o} with the later. The spatial orientation of pyrrole rings are such that pyrrole NH moieties are in the same side of quinoxaline nitrogen atoms. The distance between N3 and O2

atoms is 3.73 Å which indicates the possibility of hydrogen-bonding interaction between them in solution state. However, no intramolecular or intermolecular hydrogen-bonding is observed in the solid state structure of **pdnqd**. Crystal data, bond lengths (Å) and bond angles (^{o}) are provided in appendix.

5.3.3 Spectral and electrochemical characterization of sensors

Infrared spectrum of sensor **pdnqd** shows peaks at 3376 and 1665 cm^{-1}, ascribable to the pyrrole NH and quinone carbonyl stretching frequencies, respectively. Similarly, the peaks appearing at 3314 and 3414 cm^{-1} in the spectrum of **ppdcn** and **dpqa** indicate the presence of pyrrole NH group, respectively. The cyano group of **ppdcn** shows a stretching frequency of 2243 cm^{-1}.

Table 5.1. Absorption, fluorescence data of **pdnqd**, **ppdcn** and **dpqa**.

Sensors	λ_{max}^{abs} (ε, M^{-1} cm^{-1})	λ_{max}^{em} (ϕ_f)
pdnqd [a]	290 (26650), 508 (12400)	693 (0.015) [c]
ppdcn [a]	338 (18700), 427 (18900)	541 (0.41) [d]
dpqa [b]	251 (108400), 302 (19150), 344 (13700), 360 (15400), 411 (17800)	513 (0.47) [d]

[a] Spectra were recorded in CH_2Cl_2. [b] Spectrum was recorded in CH_3CN.
[c] using 5,10,15,20-tetraphenylporphyrin (ϕ_f = 0.13 in CH_2Cl_2) as standard.[25]
[d] using 1,6-diphenyl-1,3,5-hexatriene (ϕ_f = 0.80 in cyclohexane) as standard.[26]

The absorption and fluorescence data of **pdnqd**, **ppdcn** and **dpqa** are summarized in table 5.1. All of them have a low energy absorption band in the visible region which is important in the context of color change on binding

with F^-. The fluorescence band of these sensors have been found to be broad, with full-widths at half-maximum (fwhm) were 3075 cm^{-1} (**pdnqd**), 3903 cm^{-1} (**ppdcn**) and 3663 cm^{-1} (**dpqa**). The fluorescence quantum yield (ϕ_f) of **dpqa** has highest value, followed by that of **ppdcn** and **pdnqd**.

Fig. 5.2 illustrates the ^1H NMR spectra of sensors **pdnqd** and **ppdcn**. The spectra (see Experimental section) were analyzed based not only on the chemical shift and integrated intensity data of the various peaks appearing in the 1D spectra but also on the proton connectivity patterns observed in the

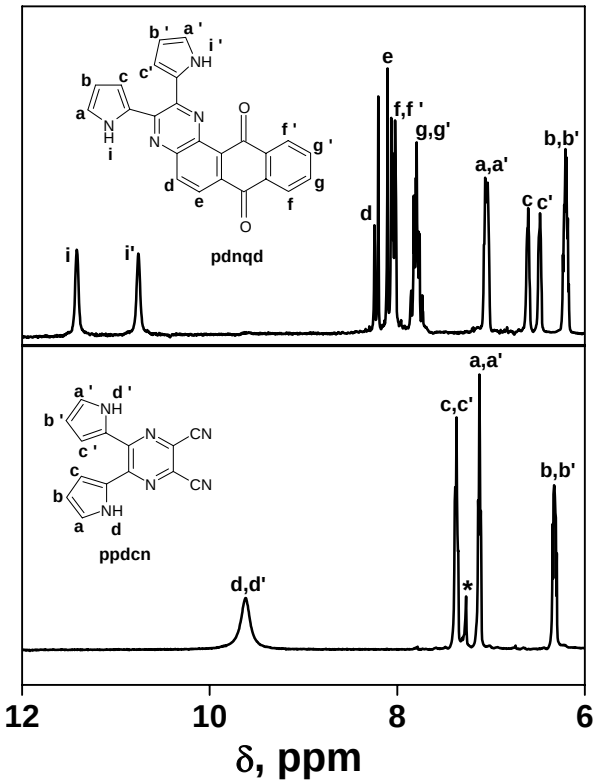

Fig. 5.2. ^1H NMR spectra of **pdnqd** ($(CD_3)_2SO$, TMS) and **ppdcn** ($CDCl_3$, TMS). * indicates the solvent signal for $CDCl_3$.

corresponding $^{1}H–^{1}H$ COSY spectra. The assignments made on the basis of these analyses are consistent with the structures of the new sensors. Interestingly, while the two β-pyrrole protons and two pyrrole NH protons of **pdnqd** (2.6 x 10^{-2} M in $(CD_3)_2SO$) resonate as two distinct multiplets and singlets respectively, the corresponding protons of **ppdcn** (3.8 x 10^{-2} M in $CDCl_3$) appear as one multiplet and singlet. These chemical shift data indicate that either the β-pyrrole proton and NH proton of one pyrrole ring of **pdnqd** are involved in hydrogen-bonding with quinine oxygen or, these protons may go within the shielding region of quinine moiety as pyrrole rings can rotate freely in solution state due to connection with quinoxaline ring by single bond.

Cyclic (CV) and differential-pulse (DPV) voltametric experiments were carried out using Pt as working and auxiliary electrodes and Ag as reference electrode.[23,24] Fc^{+}/Fc (Fc = ferrocene) couple was used to calibrate the redox potential values which are reported in V vs. SCE $E_{1/2}$ for the Fc^{+}/Fc couple. Fc^{+}/Fc couple was found to be 0.48 V vs. SCE in DMF, 0.1 M $TBAPF_6$ under our experimental conditions. In the cyclic voltammetric experiments, while sensor **pdnqd** showed one reversible (($E_{pa} - E_{pc}$) = ΔE_p = 70 mV and i_{pc}/i_{pa} = 0.98) and one quasi-reversible (ΔE_p = 138 mV and i_{pc}/i_{pa} = 0.7 in the scan rate over the range of 100-500 mV s^{-1}) current-voltage responses ($E_{1/2}$) at -0.53 and -0.77 V (vs. SCE) respectively, the other sensor **ppdcn** showed a quasi-reversible peak (ΔE_p = 94 mV) at -1.13 V at a scan rate of 100 mV s^{-1}.[27]

5.3.4 Anion sensing

We envisaged that given the novel built-in structural features, notably, the presence of highly electron-withdrawing groups in **pdnqd** and **ppdcn**, it

should be possible to monitor the fluoride ion binding properties of these sensors by colorimetric and electrochemical methods, thus enhancing the utility of these classes of compounds in anion sensing applications. Indeed, as will be discussed below, all the three sensors **pdnqd**, **ppdcn** and **dpqa** are avid binders of F^- in organic solvents and show dramatic, binding-induced changes in their optical signatures.

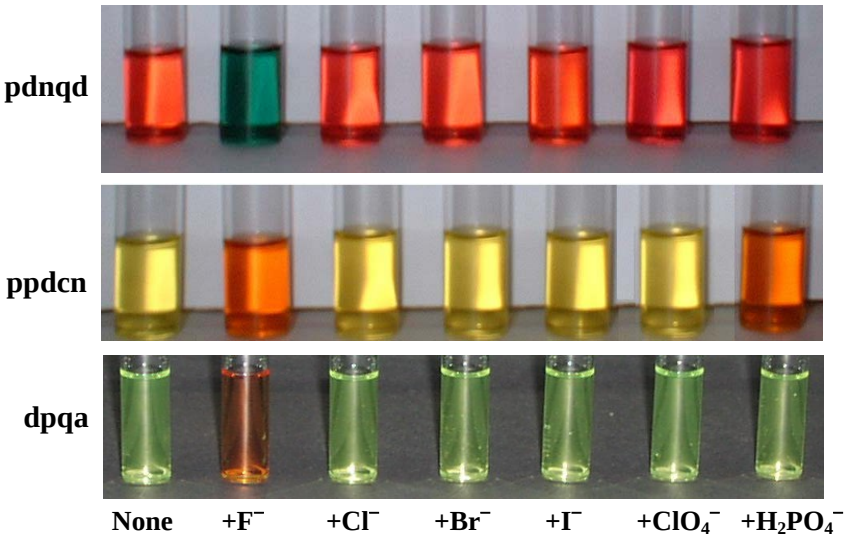

Fig. 5.3. Color changes observed for **pdnqd** (in CH_2Cl_2), **ppdcn** (in CH_2Cl_2) and **dpqa** (in CH_3CN) upon the addition of anions (as TBA^+ salts). From left to right: none, F^-, Cl^-, Br^-, I^-, ClO_4^- and $H_2PO_4^-$.

5.3.4.1 Colorimetric experiment

In the naked-eye colorimetric experiments, sensors **pdnqd**, **ppdcn** and **dpqa** show dramatic color changes from red to green (in CH_2Cl_2 or DMSO), yellow to orange-red (in CH_2Cl_2 or DMSO) and greenish-yellow to red (in CH_3CN), respectively in the presence of tetrabutylammonium fluoride (TBAF) (Fig. 5.3). While **pdnqd** and **dpqa** have been found to be insensitive

to the addition of any other anion employed during this study, **ppdcn** produced a faint orange-red color in the presence of $H_2PO_4^-$ but did not change its color upon addition of excess Cl^-, Br^-, I^- and ClO_4^-. These color changes suggest that all the three sensors are very specific binder of F^-.

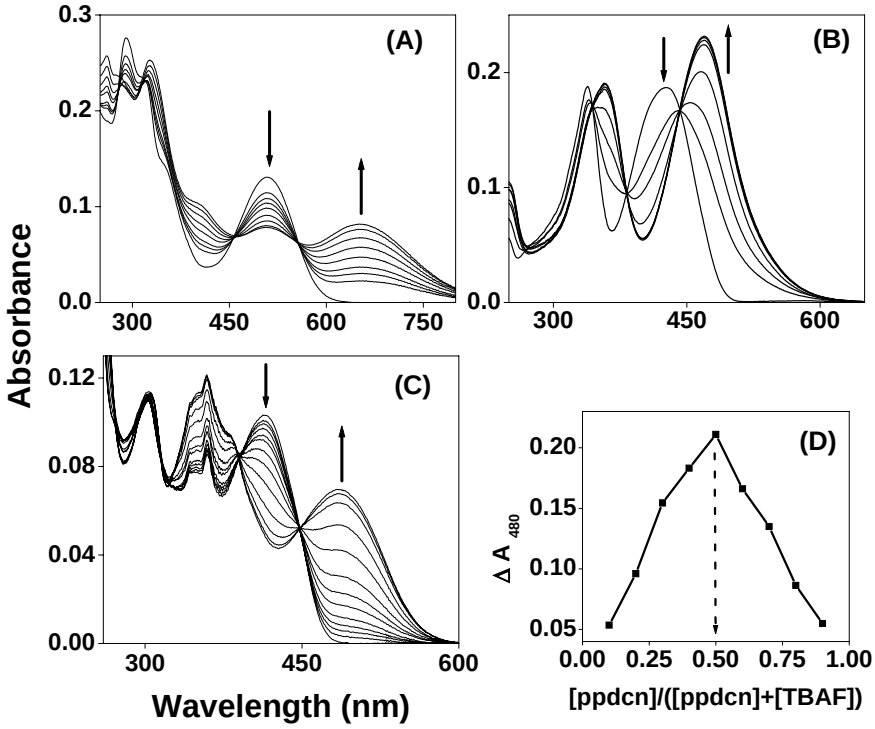

Fig. 5.4. Absorption spectral changes observed for (A) **pdnqd** (in CH_2Cl_2), (B) **ppdcn** (in CH_2Cl_2) and (C) **dpqa** (in CH_3CN) upon addition of F^- ion. (A) [**pdnqd**] = 10 μM, [TBAF] = (0, 1.7, 2.6, 3.5, 5.2, 7.7, 11.6, 16.6, 21.7) x 10^{-5} M. (B) [**ppdcn**] = 10 μM, [TBAF] = 0, 5.3, 8.8, 12.8, 17, 21.3, 30.1 μM. (C) [**dpqa**] = 5.7 μM, [TBAF] = (0, 0.9, 1.5, 2.1, 2.8, 3.6, 4.6, 5.6, 6.8, 8.2, 9.8, 11.6, 13.5) x 10^{-4} M. (D) The stoichiometric analysis of the fluoride complex **ppdcn**–F^- by Job's plot; [**ppdcn**] + [TBAF] = 5 x 10^{-5} M in CH_2Cl_2.

5.3.4.2 Absorption titration

Fig. 5.4 displays the changes in the absorption spectra of **pdnqd**, **ppdcn** and **dpqa** observed upon the addition of F^-. The band around 510 nm of **pdnqd** decreases upon addition of TBAF and new band appears at 650 nm. The band of **ppdcn** and **dpqa** around 430 and 410 nm decreases in the presence of F^- with concomitant increase of new band at 470 and 485 nm, respectively. Absorption spectra of titrations of all the three sensors contain isosbestic points which indicate that binding between the sensors and F^- is 1:1 in nature and the free sensors and sensor–F^- conjugates are in equilibrium in the course of titrations. The binding stoichiometry of **ppdcn** with F^- was determined by Job's plot analysis (Fig. 5.4). This stoichiometric analysis shows a 1:1 binding among **ppdcn** and F^-. The other two sensors **pdnqd** and **dpqa**, which consist of receptor moiety similar to that of **ppdcn**, are expected to bind with F^- in the 1:1 stoichiometry similarly.

Titrations were carried out for all the three sensors with the other anions investigated in this study and the binding constants extracted using the equation described in section 2.9.1 are summarized in table 5.2. The binding constant data shown in table 5.2 reveal that binding of F^- with **ppdcn** is strongest among the three sensors, with binding constant of the order of 10^5 M^{-1}. **pdnqd** and **dpqa** bind with F^- relatively weaker and the binding constants are one and two orders of magnitude lower than that of **ppdcn**, respectively. Although, $H_2PO_4^-$ shows relatively low binding constant with **ppdcn**, the two other sensors do not bind to any other anion except F^-. Thus, fluoride ion, being the smallest in size and having the strongest hydrogen-bond acceptor ability among all the anions investigated in this study, binds with all the three sensors **pdnqd**, **ppdcn** and **dpqa**. The higher F^- binding ability of

ppdcn over **pdnqd** is attributed to a consequence of the greater electron deficiency and enhanced hydrogen-bond donating character of the former derivative. This enhanced hydrogen-bond donating character of **ppdcn** is responsible for the ability of this sensor to bind, albeit weakly, to $H_2PO_4^-$. The other sensor **dpqa**, which lacks electron-withdrawing group present in **pdnqd** or **ppdcn**, binds with fluoride relatively weakly with binding constant of the order of 10^3 M^{-1}. In as much as this is true, we rationalize that it is the moderate binding ability of **pdnqd** and **dpqa** that leads to selective binding of F^- by these two sensors in contrast with **ppdcn**.

Table 5.2. Binding Constants (10^4 M^{-1}) of sensors **pdnqd**, **ppdcn** and **dpqa** with different anions, determined by absorption titration data.[a]

Sensor	F^-	Cl^-	Br^-	I^-	ClO_4^-	$H_2PO_4^-$
pdnqd [b]	1.6	ND	ND	ND	ND	ND
ppdcn [b]	16	ND	ND	ND	ND	0.046
dpqa [c]	0.52	ND	ND	ND	ND	ND

[a] ND denotes for 'Not Determined'. Change in absorption spectrum was not enough to calculate binding constants with these anions. [b] in CH_2Cl_2. [c] in CH_3CN.

An important additional observation made during these experiments is that the spectra (and also the color of the solution) of sensor–F^- conjugates revert back to the original spectra corresponding to those sensors in the absence of F^- upon addition of small aliquots of water/methanol. This not only suggests that the complexation between F^- and sensors is reversible in nature but also lends support to the proposition that hydrogen-bonding is involved in the binding between the sensors and F^-.

5.3.4.3 Fluorescence titration

Fluorescence titrations of **pdnqd** and **ppdcn** have been carried out with all the anions. Successive additions of F^- to CH_2Cl_2 solutions of **pdnqd** and **ppdcn** result in decrease of their fluorescence intensities with marginal changes in the emission maxima. This is illustrated in fig. 5.5, which shows the fluorescence spectra of **pdnqd** and **ppdcn** in the absence and presence of various concentrations of F^-. Treatment of the fluorescence intensity data using equation described in section 2.9.2 provided the binding constant values (**pdnqd**: 1.3 x 10^4 M^{-1} and **ppdcn**: 1.4 x 10^5 M^{-1}), which are comparable to those obtained by the absorption titration data. Fluorescence spectral profiles and the intensities of both **pdnqd** and **ppdcn** were found to be unsusceptible to the addition of other anions which indicate that anions other than F^- interact very little with both **pdnqd** and **ppdcn**.

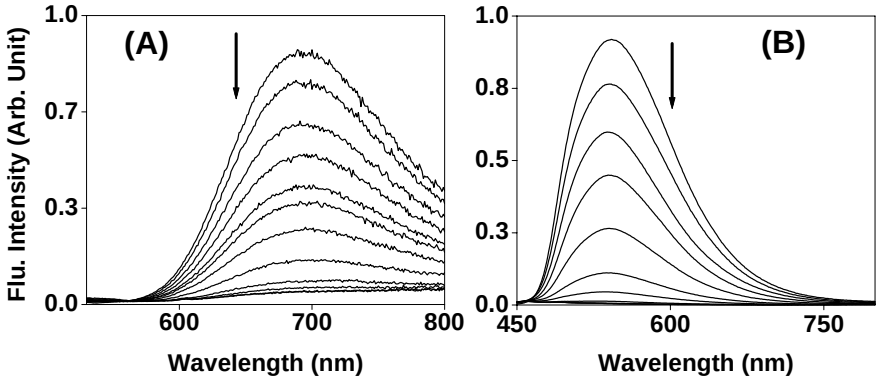

Fig. 5.5. Fluorescence spectral changes observed for (A) **pdnqd** and (B) **ppdcn,** upon addition of fluoride ion in CH_2Cl_2 ($\lambda_{exc.}$ = 510 and 430 nm, respectively); [**pdnqd**] and [**ppdcn**] = 10 μM. (A) [TBAF] = (0, 1.8, 3.7, 5.5, 7.4, 9.3, 12.1, 17.6, 26.6, 39.6) x 10^{-5} M. (B) [TBAF] = (0, 0.7, 1, 1.4, 1.7, 2.1, 2.8, 4.2) x 10^{-5} M.

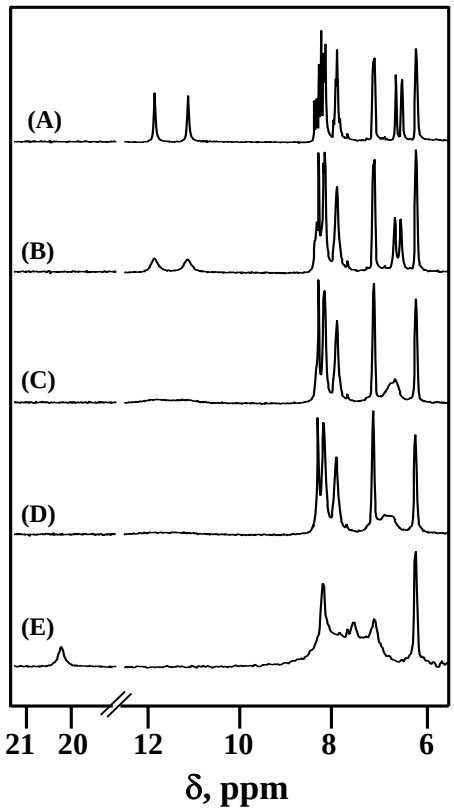

Fig. 5.6. ^{1}H NMR titration of **pdnqd** with TBAF in $(CD_3)_2SO$. [**pdnqd**] = 2.6 x 10^{-2} M; [**pdnqd**]:[F^-] in these traces are: (A) 1:0, (B) 1:0.2, (C) 1:0.6, (D) 1:1 and (E) 1:5.

5.3.4.4 ^{1}H NMR titration

Notwithstanding this observed agreement between the results of colorimetric, absorption and fluorescence titration experiments carried out with **pdnqd** and **ppdcn**, the reason operating behind the absorption spectral changes (and hence the color changes) by F^- and structural insight into the

sensor–F^- complexation are still unclear. ^{1}H NMR spectroscopy is a versatile tool to probe such issues and, we decided to probe the interaction of **pdnqd** and **ppdcn** with various anions by ^{1}H NMR titration method, the results of which are discussed below.

At the outset, it should be noted that no major changes in the ^{1}H NMR spectra of **pdnqd** and **ppdcn** have been noticed when anions (in excess and as tetrabutylammonium salts) other than F^- were added to $(CD_3)_2SO$ or $CDCl_3$ solutions containing these sensors. This observation is consistent with the inability of these same anions to produce changes in the absorption or fluorescence spectra of **pdnqd** and **ppdcn**. However, dramatic effects were observed in the spectral features of these sensors in the presence of F^-. Fig. 5.6 illustrates the ^{1}H NMR spectra of **pdnqd** (2.6×10^{-2} M in $(CD_3)_2SO$) in the absence (A) and presence (B-E) of various concentrations of TBAF. A cursory glance of these spectra reveals that the resonances ascribable to the NH protons of **pdnqd** (11.16 and 11.87 ppm) are initially broaden upon successive addition of TBAF and finally appear at ~20.2 ppm at [**pdnqd**]:[F^-] = 1:5. A similar broadening of the NH peak of **ppdcn** (9.61 ppm) was also noticed during the initial stages of the titration but, the peak completely disappeared from the spectral window (+25 to +5.5 ppm) at [**ppdcn**]:[F^-] = 1:1.5 (Fig. 5.7). In any case, the effect seen for the pyrrole NH proton resonances of **pdnqd** or **ppdcn** in the presence of F^- can be regarded as an evidence for the involvement of hydrogen-bonding between the two pyrrole NH protons of these sensors and F^-.

A careful examination of the ^{1}H NMR spectra of these sensors containing various concentrations of F^- reveals that both the α and β protons on the pyrrole rings (and quinoxaline protons of **pdnqd**) are also shifted

during the titrations. For example, the β protons of the pyrrole rings of **pdnqd** that were resonating at 6.65 and 6.52 ppm as two separate multiplets in the absence of F^-, slowly get broadened and resonate at ~6.9 ppm in the presence of excess F^-. A similar broadening of the β protons of **ppdcn** was also noticed during the titration with F^-.

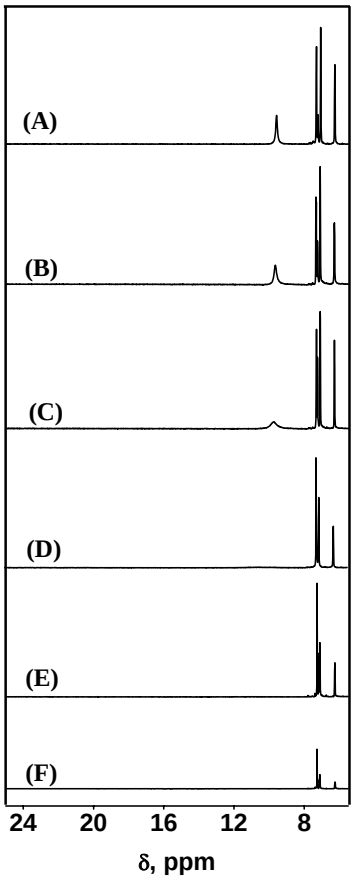

Fig. 5.7. ^{1}H NMR titration of **ppdcn** with TBAF in $CDCl_3$. [**ppdcn**] = 3.8 x 10^{-2} M; [**ppdcn**]:[F^-] in these traces are: (A) 1:0, (B) 1:0.045, (C) 1:0.1, (D) 1:0.5, (E) 1:1 and (F) 1:1.5.

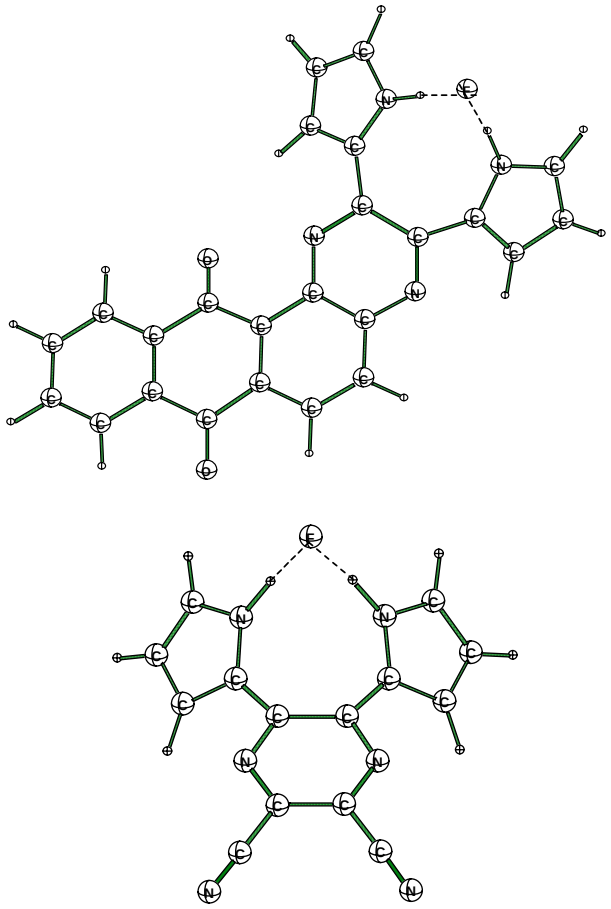

Fig. 5.8. Structures of **pdnqd**–F^- (top) and **ppdcn**–F^- (bottom) complexes (front view). Adapted from ref. 19.

These observations together with the interpretation made above for the pyrrole NH proton resonances can be rationalized in terms of a model proposed earlier for F^- binding by various DPQ derivatives.[11] In this model, binding of F^- is proposed to be facilitated by rotation of the pyrrole rings of **pdnqd** and **ppdcn** in such a way that both the NH protons orient towards the lone pairs of F^- and coordinate it simultaneously, forming two $NH^{\cdots}F^-$

hydrogen-bonds by the pyrrole NH protons in a ‘bidentate’ fashion, as shown in fig. 5.8.[19] This ‘bidentate’ type hydrogen-bonding between F^- and two pyrrole NH protons is in accordance with the observed 1:1 binding stiochiometry between **ppdcn** and F^- (section 5.3.4.2). The rotation of pyrrole rings is expected to assume them a ‘bite angle’ suitable for the size of F^- and to position them away from the quinoxaline/pyrazine chromophore leading to perturbation in the orbital overlap between the pyrrole and quinoxaline/pyrazine subunits. This F^- binding induced ‘intramolecular’ perturbation in the orbital overlap rationalizes the absorption and NMR spectral changes observed for **pdnqd** and **ppdcn** upon binding with the fluoride ion.

Theoretical studies carried out with the free sensors **pdnqd**, **ppdcn** and sensor–X^- (X = F, Cl, Br) conjugates also afforded important information regarding these systems.[19] Low energy barrier of rotation indicates that the pyrrole rings in **pdnqd** and **ppdcn** are relatively flexible in terms of rotation. The conformation corresponding to the crystal structures of **pdnqd** (section 5.3.2) and **ppdcn**[20] are the lowest energy conformers, as calculated by theory. The hydrogen-bonding between pyrrole NH protons of the sensors and F^- in ‘bidentate’ fashion is also supported by theoretical calculations. Other important outcome of the theoretical calculations is the grounds behind the selectivity of **pdnqd**/**ppdcn** with F^- over Cl^-/Br^-. The major factor for selectivity is the strength of hydrogen-bond between the charged halide ion and the two pyrrole NH protons. F^-, having the strongest hydrogen-bond acceptor ability among the halides, exhibits maximum affinities towards **pdnqd**/**ppdcn**. In addition to the basicity of the halide ions, the geometrical complementarity between **pdnqd**/**ppdcn** and the halide ion may also play a

significant role in governing the binding affinity. F^- is significantly smaller than the Cl^- and Br^- and therefore, fits relatively easily between the two pyrrole moieties of the sensors.

5.3.4.5 Electrochemical titration

As mentioned earlier, one of the main motivations in introducing quinone/cyano groups at the dipyrrolyl subunit has been to incorporate redox activity to this class of sensor molecules so that their anion sensing abilities can also be monitored by electrochemical methods. In this regard, it should be noted that electrochemical methods can, in principle, provide information

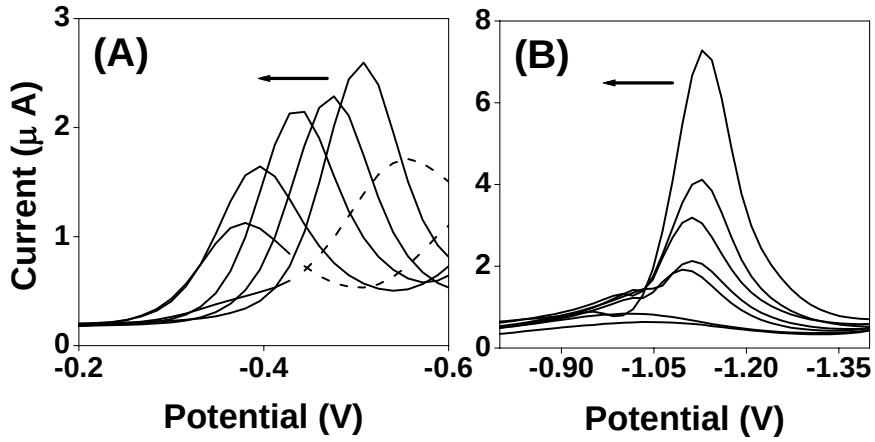

Fig. 5.9. Differential pulse voltammograms (DMF, 0.1 M $TBAPF_6$) of (A) **pdnqd** (0.5 mM) and (B) **ppdcn** (2 mM) in the presence of various concentrations of F^-. From right to left: (A) $[F^-]$ = (0, 0.6, 2.3, 4.6, 8.4, 21) x 10^{-4} M. (B) $[F^-]$ = (0, 0.3, 2.6, 7.4, 12.7, 22, 36.8) x 10^{-4} M. The dotted regions of the last two traces seen in (A) arise due to the second reduction peak of **pdnqd** that is anodically shifted during the titration with F^-.

about the binding properties of both the oxidized and reduced forms of the sensors. It should also be noted that, except for a solitary example, anion sensing by the previously reported DPQ derivatives has not been investigated by electrochemical methods.[13] Fig. 5.9 shows the DPV (DMF, 0.1 M $TBAPF_6$)[28] traces for **pdnqd** and **ppdcn** in the absence and presence of F^-. Addition of successive amounts of F^- results in the reduction of the peak current and anodic shift of the peak potential for both the sensors. The peak, in each case, disappeared completely at the end of the titration as in the case with a cobalt(III)-dipyridophenazine complex linked DPQ derivative reported earlier.[13] The complete disappearance of the peak for this latter complex in the presence of F^- has been interpreted in terms of a strong and, perhaps, electro-inactive complex formation between the sensor and F^-. In any case, the successive anodic shifts of the peak potential observed for **pdnqd** and **ppdcn** in the presence of F^- permits us to evaluate the ratio of the binding constants for neutral and the one-electron reduced sensor species as described below.[29]

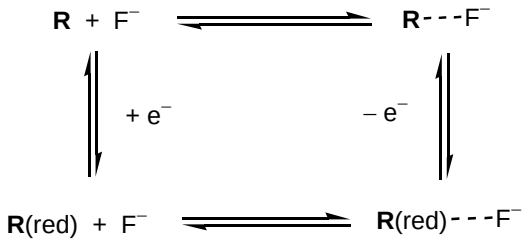

Scheme 5.2

The overall electrochemistry of **R**–F^- (**R** = **pdnqd** or **ppdcn**) system can be illustrated as shown in scheme 5.2. In this scheme, **R**(red) represents the one-electron reduced species of **R**. The scheme suggests that the redox data can be treated according to eq. 1.[30]

$$E_0^f - E_0^b = \frac{RT}{nF} \ln \frac{K(R)}{K(R(red))} \quad (1)$$

Here, E_0^f and E_0^b are the thermodynamic redox potentials for the free and fluoride-bound sensors, respectively, *n* is the number of electrons transferred, *K*(**R**)/*K*(**R**(red)) is the ratio of binding constants for neutral and the corresponding reduced species of **R**. Other parameters have their usual meaning. Substitution of appropriate values to suit the electrochemistry of **pdnqd** and **ppdcn** in the presence of F^- and from a limiting shifts of -128 mV (**pdnqd**) and -32 mV (**ppdcn**), the values of *K*(**R**)/*K*(**R**(red)) were calculated to be ~0.0062 and ~0.28, for **R** = **pdnqd** and **ppdcn**, respectively. These ratios, which are both less than unity, indicate that the one-electron reduced species of **pdnqd** and **ppdcn** are better F^- ion binders than the corresponding neutral species. If one considers that hydrogen-bonding between the pyrrole NH protons of neutral **pdnqd**/**ppdcn** are involved in the binding, the <1 ratios observed for *K*(**R**)/*K*(**R**(red)) suggest the pyrrole NH protons of the anionic species are more acidic than the neutral analogues. This apparent anomaly can perhaps be reconciled by recalling that in our model binding of fluoride leads to perturbation in the orbital overlap between the pyrrole and quinoxaline/pyrazine subunits. Perhaps, the anodic shifts of the peak potentials for the fluoride-bound sensors are a consequence of this perturbation in the orbital overlap. In this regard, it can be noted that the site of electron addition in these sensors is expected to be located at the quinoxaline/pyrazine moieties and not the pyrrole subunits of their structures. The pyrrole subunits orient themselves in different planes than the plane of quinoxaline/pyrazine moiety while making hydrogen-bonding with F^-. Thus, the shifts observed during the redox titrations are a composite of those due to F^- binding to the NH protons

and change in the electron density distribution at the electro-active centers of these sensors.

5.4 Summary

Three dipyrrolyl derivatives **pdnqd**, **ppdcn** and **dpqa** have been prepared by single step reactions easily. All the three sensors are specific to fluoride ion and they allow detection of F^- under optical conditions in organic solvents. The F^- binding event with **pdnqd** and **ppdcn** has been monitored by electrochemical methods as they contain electro-active quinine and cyano functionalities in their structures. ^{1}H NMR titration of **pdnqd** and **ppdcn** with F^- indicates that the pyrrole NH protons of both sensors interact with F^- by hydrogen-bond in 'bidentate' fashion. The selectivity of F^- over Cl^- or Br^- is attributed mainly to the fact that F^- is better hydrogen-bond acceptor than Cl^- or Br^- and partly to the complementarity of the geometries between the receptor moiety and F^-.

5.5 References

1) Stryer, L. *Biochemistry*, 4th Ed.; W. H. Freeman & Co.: New York, 1995.
2) *Riegel's Handbook of Industrial Chemistry*, 9th Ed.; Kent, J. A., Ed.; Van Nostrad Reinhold-Interantional Thomson Publishing: New York, 1992.
3) *Ullmann's Encyclopedia of Industrial Chemistry*, 6th Ed.; Bailey, J. E., Bohnet, M., Brinker, C. J., Cornils, B., Evans, T., Greim, H., Hegedus, L. L., Heitbaum, J., Keim, W., Kleemann, A., Kreysa, G., Loliger, J., McGuire, J. L., Mitsutani, A., Plass, L., Stephanopoulos, G., Werner,

D., Woditsch, P., Yoda, N., Eds.; 1999 Electronic Release; Wiley VCH: New York, 1999.

4) Atwood, J. L.; Steed, J. W. *Supramol. Chem.* **1997**, 147.
5) Beer, P. D.; Gale, P. A. *Angew. Chem. Int. Ed.* **2001**, *40*, 486.
6) Kirk, K. L. *Biochemistry of the Halogens and Inorganic Halides*, Plenum Press, New York, 1991, p. 58.
7) Kleerekoper, M. *Endochrinol. Metab. Clin. North Am*. **1998**, *27*, 441.
8) Wiseman, A. *Handbook of Experimental Pharmacology* XX/2, Part 2; Springer-Verlag: Berlin, 1970, p. 48-97.
9) Nielsen, K. A.; Jeppesen, J. O.; Levillain, E.; Becher, J. *Angew. Chem. Int. Ed.* **2003**, *42***,** 187.
10) Miyaji, H.; Sato, W.; Sessler, J. L. *Angew. Chem. Int. Ed.* **2000**, *39*, 1777.
11) Black, C. B.; Andrioletti, B.; Try, A. C.; Ruiperez, C.; Sessler, J. L. *J. Am. Chem. Soc.* **1999**, *121*, 10438.
12) Anzenbacher, P., Jr.; Try, A. C.; Miyaji, H.; Jursikova, K.; Lynch, V. M.; Marquez, M.; Sessler, J. L. *J. Am. Chem. Soc.* **2000**, *122*, 10268.
13) Mizuno, T.; Wei, W.-H.; Eller, L. R.; Sessler, J. L. *J. Am. Chem. Soc.* **2002**, *124*, 1134.
14) Anzenbacher, P., Jr.; Tyson, D. S.; Jursikova, K.; Castellano, F. N. *J. Am. Chem. Soc.* **2002**, *124*, 6232.
15) Sessler, J. L.; Maeda, H.; Mizuno, T.; Lynch, V. M.; Furuta, H. *Chem. Commun.* **2002**, 862.
16) Sessler, J. L.; Maeda, H.; Mizuno, T.; Lynch, V. M.; Furuta, H. *J. Am. Chem. Soc.* **2002**, *124*, 13474.
17) Aldakov, D.; Anzenbacher, P., Jr. *Chem. Commun.* **2003**, 1394.
18) Ghosh, T.; Maiya, B. G. *J. Chem. Sci.* **2004**, *116*, 17.

19) Ghosh, T.; Maiya, B. G.; Wong, M. W. *J. Phys. Chem. A* **2004**, *108*, 11249.

20) Sessler, J. L.; Pantos, G. D.; Katayev, E.; Lynch, V. M. *Org. Lett.* **2003**, *5*, 4141.

21) Behr, D.; Brandange, S.; Lindstrom, B. *Acta. Chem. Scand.* **1973**, *27*, 2411.

22) Plater, M. J.; Greig, I.; Helfrich, M. H.; Ralston, S. H. *J. Chem. Soc., Perkin Trans. 1* **2001**, 2553.

23) Ambroise, A.; Maiya, B. G. *Inorg. Chem.* **2000**, *39*, 4256.

24) Ambroise, A.; Maiya, B. G. *Inorg. Chem.* **2000**, *39*, 4264.

25) Quimby, D. J.; Lango, F. R. *J. Am. Chem. Soc.* **1975**, *97*, 5111.

26) Berlman, I. B. *Handbook of Fluorescence Spectra of Aromatic Molecules*, 2nd edition, Academic Press: New York, 1971, p. 322.

27) Nicholson, R. S.; Shain, I. *Anal. Chem.* **1964**, *36*, 706.

28) Addition of large excess of $TBAPF_6$ to DMF solutions containing **pdnqd** or **ppdcn** did not result in changes in their color and spectral (absorption and fluorescence) properties, indicating that PF_6^- ion does not bind to these sensors.

29) Medina, J. C.; Goodnow, T. T.; Rojas, M. T.; Atwood, J. L.; Lynn, B. C.; Kaifer, A. E.; Gokel, G. W. *J. Am. Chem. Soc*. **1992**, *114*, 10583.

30) Beer, P. D.; Gale, P. A.; Chen, G. Z. *J. Chem. Soc. Dalton Trans.* **1999**, 1897.

CHAPTER 6

Dipyrrolyl Derivative as both Fluoride and Transition Metal Ions Sensor

6.1 Introduction

Development of chemosensors capable of recognizing and sensing cations and anions is one of the most challenging fields, not only from the viewpoint of organic and supramolecular chemistry but also from its potential clinical applications.[1-8] Chemosensors consist of signaling (chromophore/fluorophore) and guest-binding (receptor) moieties, either separated by a spacer or integrated into one unit. Generally, N or O donor centers act as binding site for cations[1-3] and pyrrole, -OH, $-NH_2$, -CONH, $-NH_3^+$ etc. (capable of forming hydrogen-bond) or boron, silicon (capable of forming Lewis adduct) centers act as binding site for anions.[4-6] Simultaneous sensing of both types of charged analytes has been achieved by integrating cationic and anionic guest binding sites in a single molecule, where the cation binding site binds with a transition (Ni^{2+}, Cu^{2+}, Ag^+, Cd^{2+}) or alkali (Li^+, Na^+, K^+) or alkaline earth metal ion (Mg^{2+}, Ca^{2+}).[9-15]

During recent years, there is an upsurge in the field of colorimetric sensing of alkali, alkaline-earth and transition metal ions by organic molecules.[16-20] Among the cations, special attention is devoted to develop chemosensors for transitional metal ions: usually they symbolize an environmental concern when present in uncontrolled amount but at the same time some of them such as iron, cobalt, copper, zinc are present as essential element in biological systems. On the other hand, the halides, especially fluoride ion is of major interest among the anions due to its detrimental role (fluoresis and other diseases).[21,22] The recently reported pyrrole-based

sensors namely, calix[4]pyrrole,[23,24] dipyrrolylquinoxaline (DPQ)[25-31] and dipyrrolylpyrazine (DPP)[32-34] families of compounds have been used for anion sensing by exploiting the hydrogen-bond forming ability of pyrrole NH proton with anions, with subsequent change in color or fluorescence or redox potential. The last two types of sensors have the dual advantage of possessing a built-in chromophore and being readily accessible in two steps from commercially available materials.

We have recently embarked upon designing systems that can sense both anions and metal ions. To begin with, we concentrate on systems that can sense both fluoride and transition metal ions. In order to accomplish this goal, we have exploited fluoride ion signaling potential of the DPP derivatives and transition metal ion binding ability of the pyridine moiety. Amalgamating these approaches we have developed **dppp**, wherein a pyridine ring has been fused with the pyrazine frame. We demonstrate here unequivocally that it is indeed the nitrogen atom of the pyridine moiety that binds the transition metal ions. It is shown that this new DPP derivative binds the metal ions much more strongly compared to the previously reported DPP derivative **ppdcn** which lack the additional fused pyridine ring.[32-34] The sensing of F^- and metal ions (Co^{2+}, Ni^{2+}, Cu^{2+}, Zn^{2+} and Cd^{2+}) by **dppp** in acetonitrile is observable by change in color from yellowish-green to red in the case of former and to brown or light-brown in the later cases. The binding constants of the cations are found two orders of magnitude higher than that of F^-.

6.2 Experimental section

The dipyrrolyl derivative 2,3-di(1*H*-2-pyrrolyl)pyrido[2,3-*b*]pyrazine (**dppp**), the model compound pyrido[2,3-*b*]pyrazine (**pp**) and Ni(II) complex of **dppp** *i.e.* **$Ni(dppp)_2Cl_2$** were synthesized as detailed below.

2,3-di(1*H*-2-pyrrolyl)pyrido[2,3-*b*]pyrazine (**dppp**)

1,2-di(1*H*-2-pyrrolyl)-1,2-ethanedione[25,35] (190 mg, 1.0 mmol) was dissolved in toluene (40 mL), and a catalytic amount of $BF_3.Et_2O$ was added to it. A hot solution of 2,3-diaminopyridine (120 mg, 1.1 mmol) in toluene (30 mL) was added with stirring. The resulting mixture was heated at reflux under nitrogen atmosphere for 8 h. Then, toluene was distilled off under vacuum and the residue was taken up in a mixture of CH_2Cl_2 (50 mL) and water (50 mL). The organic layer was separated off and the aqueous layer was extracted with CH_2Cl_2 (3 x 30 mL). The organic layers were combined and was dried over anhydrous sodium sulfate, filtered and evaporated to dryness. Column chromatography over neutral alumina (eluent: CH_2Cl_2/MeOH, 99:1, v/v) afforded **1** (160 mg, 61%) as a yellow solid. Anal. Calcd. For $C_{15}H_{11}N_5$: C, 68.96; H, 4.21; N, 26.83. Found: C, 69.19; H, 4.28; N, 26.54. ^{1}H NMR (400 MHz, $CDCl_3$, TMS) δ, ppm: 6.25-6.28 (1H, m), 6.30-6.33 (1H, m), 7.04-7.06 (2H, m), 7.10-7.12 (1H, m), 7.17-7.19 (1H, m), 7.50 (1H, dd, *J* = 4.0 Hz, 8.0 Hz), 8.21 (1H, dd, *J* = 2.0 Hz, 8.0 Hz), 8.91 (1H, dd, *J* = 2.0 Hz, 4.0 Hz), 9.60 (1H, br s), 10.04 (1H, br s). ^{13}C NMR (50 MHz, $CDCl_3/CD_3OD$, 3:1, v/v, TMS) δ, ppm: 159.5, 152.8, 150.0, 148.7, 147.2, 138.7, 135.8, 129.7, 125.1, 124.8, 123.2, 116.5, 114.9, 111.2, 110.9. FAB-MS: *m/z* 262 $(M+H)^+$; UV-Visible (CH_3CN) λ_{max}, nm (ε, M^{-1} cm^{-1}): 204 (25200), 263 (18200), 312 (7100), 350 (7800), 421 (12350).

Pyrido[2,3-*b*]pyrazine (**pp**)

It was synthesized as per reported procedure shown in scheme 6.1.[36] Anal. Calcd. For $C_7H_5N_3$: C, 64.12; H, 3.82; N, 32.06. Found: C, 64.25; H, 3.96; N, 31.90. ^{1}H NMR (400 MHz, $CDCl_3$, TMS) δ, ppm: 7.77 (1H, dd, *J* = 3.6 Hz, 8.8 Hz), 8.51 (1H, dd, *J* = 2.0 Hz, 8.8 Hz), 8.70 (1H, d, *J* = 1.6 Hz), 9.10 (1H, d, *J* = 1.6 Hz), 9.22 (1H, dd, *J* = 2.0 Hz, 4.0 Hz). ^{13}C NMR (50 MHz, $CDCl_3$, TMS) δ, ppm: 154.3, 151.4, 147.8, 146.1, 138.6, 138.2, 125.4. LC-MS: *m/z* 131 (M^+); UV-Visible (CH_3CN) λ_{max}, nm (ε, M^{-1} cm^{-1}): 255 (1900), 301 (6750), 308 (7000), 314 (8950), 354 (200).

Dichlorobis(2,3-di(1H-2-pyrrolyl)pyrido[2,3-b]pyrazine))nickel(II) (**$Ni(dppp)_2Cl_2$**)

38 mg (0.14 mmol) of **dppp** was dissolved in methanol and 17 mg (0.07 mmol) of $NiCl_2$ (in methanol) was added to it. The solution was refluxed for 3 hours and the solvent was evaporated to dryness. The red solid was recrystallised from acetonitrile. Anal. Calcd. For $C_{30}H_{22}N_{10}NiCl_2$: C, 55.19; H, 3.37; N, 21.46. Found: C, 55.34; H, 3.42; N, 21.28.

6.3 Results and discussion

6.3.1 Synthesis

dppp, **pp** and **$Ni(dppp)_2Cl_2$** were synthesized by single step reactions, as illustrated in the scheme 6.1. Reaction between 1,2-di(1*H*-2-pyrrolyl)-1,2-ethanedione and 2,3-diaminopyridine produced **dppp** in ~60% yield. Sensor **dppp** can be considered structurally as a DPP derivative, well known for its potential as F^- sensor, having an additional pyridine ring fused with the pyrazine ring as part of its extended π framework. The justification behind the

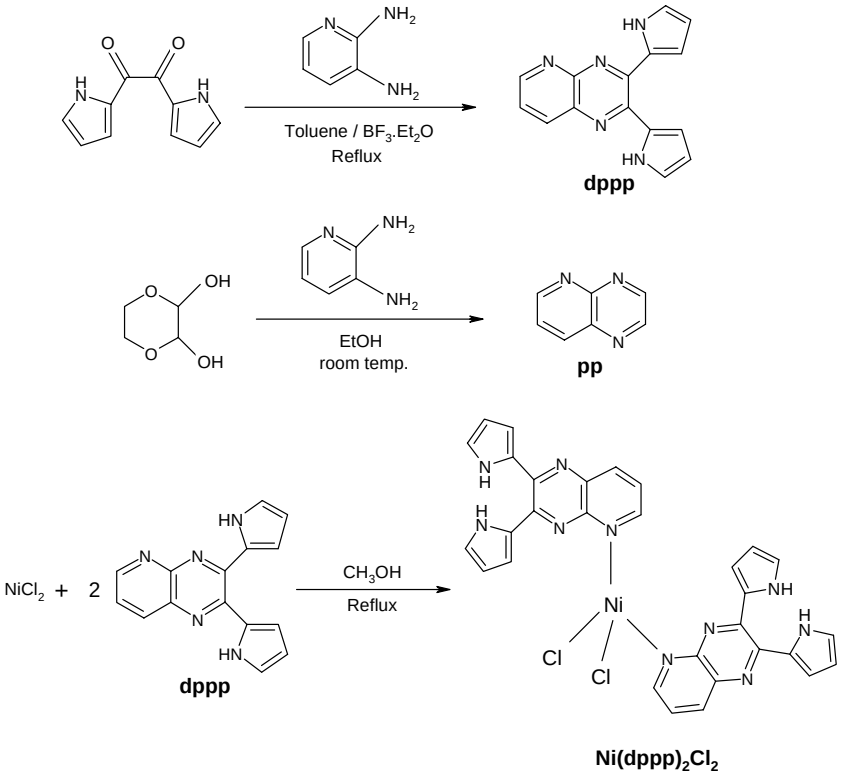

Scheme 6.1. Synthesis of **dppp**, **pp** and **$Ni(dppp)_2Cl_2$**.

fusion of the pyridine ring is to make **dppp** work as a cation sensor as well. This is because pyridine can act as cation binding centre in a sensor molecule.[37] In fact, a stronger metal binding property of **dppp** compared to a previously reported DPP derivative[32-34] supports our above justification.

6.3.2 Crystal structures of dppp and $Ni(dppp)_2Cl_2$

In order to determine whether one of the pyrazine nitrogen atoms or the pyridine nitrogen atom or both are involved in interaction with

the metal ions, Ni(II) complex of **dppp** *i.e.* **Ni(dppp)$_2$Cl$_2$** is synthesized and its structure is obtained by X-ray diffraction analysis. The single crystals of **dppp** and **Ni(dppp)$_2$Cl$_2$** were grown by slow evaporation of acetonitrile solutions.

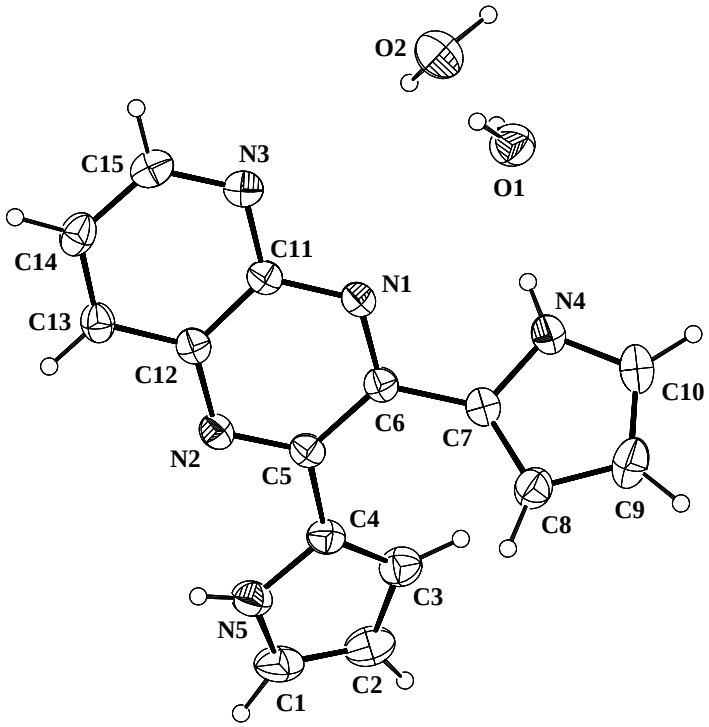

Fig. 6.1. X-ray structure of **dppp** with all heavy atoms labeled. The thermal ellipsoids were scaled to the 30% probability level.

The solid-state structure of **dppp** is shown as ORTEP diagram in fig. 6.1. In the case of **dppp**, two **dppp** molecules and four water molecules are present per unit cell. Intermolecular hydrogen-bonding is observed between the water molecules present in the crystal, pyrrole NH protons and, pyridine and pyrazine nitrogen atoms. Both the pyrrole rings are directed such that the

pyrrole NH moieties are on the same side of the pyrazine nitrogen atoms, the dihedral angles between pyrrole rings and pyridopyrazine plane being 23.2^{o} and 36.1^{o}.

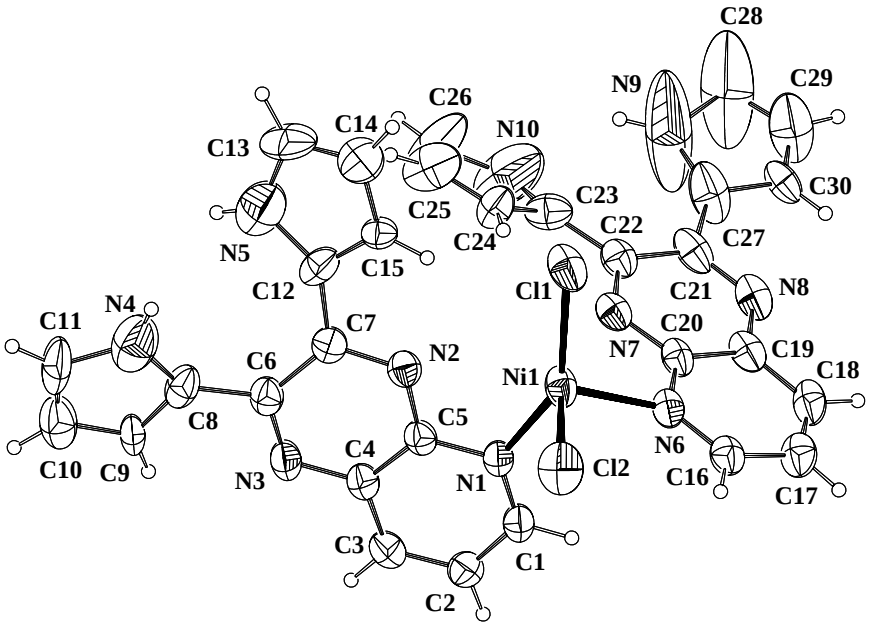

Fig. 6.2. X-ray structure of **Ni(dppp)$_2$Cl$_2$** with all heavy atoms labeled. The thermal ellipsoids were scaled to the 30% probability level.

The picture is quite different in the case of **Ni(dppp)$_2$Cl$_2$**, as shown by ORTEP diagram in fig. 6.2. There are two molecules of **Ni(dppp)$_2$Cl$_2$** in unit cell but no intermolecular hydrogen-bonding is observed like **dppp**. Ni(II) is coordinated with the pyridine nitrogen of **dppp** and Cl^{-}, having a distorted tetrahedral geometry with the pyridine N-Ni-N bond angle 96.9^{o} and Cl-Ni-Cl bond angle 99.7^{o}. The two pyrrole NH moieties are directed towards each other and both are in different planes than fused pyridopyrazine ring plane.

Here, all the dihedral angles between the pyrrole rings and pyridopyrazine ring of two ligands are different: 18.4^o and 20.6^o in one ligand and 10.7^o and 25^o in other one. It is also important to note that only the pyridine nitrogen is bonded with Ni(II), not the pyrazine nitrogen atoms. This observation is consistent with the recent finding of Manson, who has shown that the pyridine nitrogen of **pp** is involved in coordination with Cu^{2+}.[38] Crystallographic data, bond lengths (Å) and bond angles (^{o}) of **dppp** and **$Ni(dppp)_2Cl_2$** are provided in appendix.

6.3.3 Spectral characterization

The absorption spectra of **dppp** and **pp** in CH_3CN are depicted in fig. 6.3. It can be seen that the spectrum of **dppp** appears as somewhat structured but it lacks the fine structure of the spectrum of **pp**. Further, the lowest energy absorption band of **dppp** appears at a much longer wavelength relative to that of **pp**. These observations are consistent with an extended π-conjugation and N–H···N interaction between the pyrrole and pyrazine rings in **dppp**.

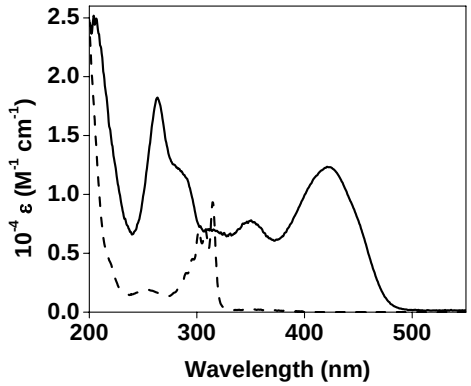

Fig. 6.3. Comparison of the absorption spectra of **dppp** (———) and **pp** (– – – –) in CH_3CN.

The influence of solvent on the absorption, fluorescence and fluorescence excitation spectra of **dppp** has been investigated in detail with a view to understanding the origin of the lowest energy transition in the absorption and fluorescence spectra. The fluorescence excitation spectrum of the system in any given solvent is found identical with the absorption spectrum in the same solvent. Fig 6.4 shows the fluorescence and fluorescence excitation spectra of the system. The most noticeable feature of these spectra

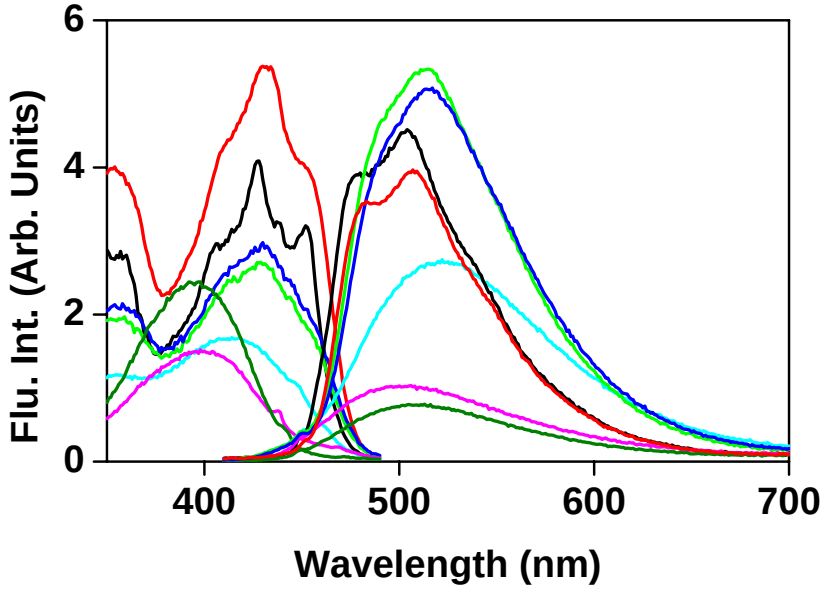

Fig. 6.4. Fluorescence excitation and fluorescence spectra of **dppp** in different solvents: cyclohexane ( ), toluene ( ), 1,4-dioxane ( ), tetrahydrofuran ( ), acetonitrile ( ), 2-propanol ( ) and methanol ( ). Conditions for fluorescence excitation spectra of **dppp** in different solvents: λ_{em} = 505 nm, excitation and emission slit = 2 nm. Conditions for fluorescence spectra of **dppp** in different solvents: λ_{exc} = 395 nm, O.D at 395 nm = 0.02, excitation and emission slit = 2 nm.

is the loss of structure in polar media. That the band positions are not so sensitive to the polarity of the medium suggest that the charge transfer contribution in these transitions is minimal. Reasonably high molar extinction coefficient of the absorption band and fairly high fluorescence efficiency of **dppp** suggest that the lowest energy transition in absorption and fluorescence is π, π* in nature. However, in protic media a blue-shift of the absorption band suggests that an n, π* state is in close proximity with the π, π* state.[39] Since the blue-shift is not observable in emission, it is evident that irrespective of the nature of the solvent, the emission always occurs from the π, π* state, which is the lowest excited state in the system.

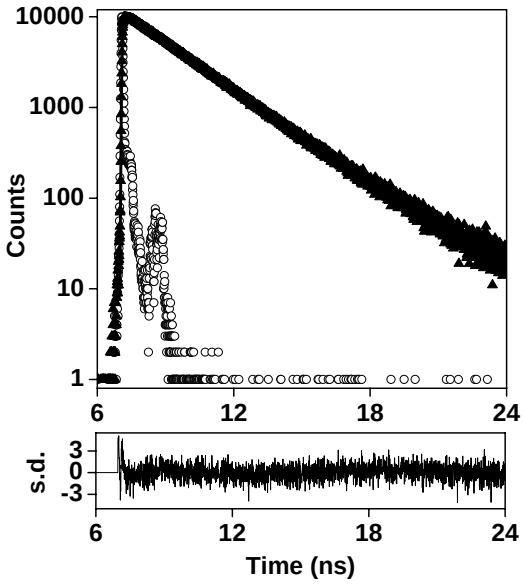

Fig. 6.5. Fluorescence decay behavior of **dppp** in acetonitrile. λ_{exc} = 375 nm, λ_{em} = 525 nm. The best fit to the data points (▲) is indicated by the solid line and lamp profile is represented by hollow circles.

dppp is found to be strongly fluorescent; the fluorescence quantum yield, ϕ_f value is estimated to be 0.29 in CH_3CN by using 1,6-diphenyl-1,3,5-hexatriene (ϕ_f = 0.80 in cyclohexane) as the standard.[40] We have also studied the fluorescence decay behavior of the system in tetrahydrofuran and acetonitrile. A single exponential fit to the decay profiles was found satisfactory from the χ^2 values and the residuals, as shown in fig. 6.5. The measured lifetimes are 2.5 ns in acetonitrile and 3.4 ns in tetrahydrofuran.

The ^{1}H NMR spectrum of sensor **dppp** is illustrated in Fig. 6.6. The spectrum was analyzed (see Experimental section) based not only on the chemical shift and integrated intensity data of the various peaks appearing in

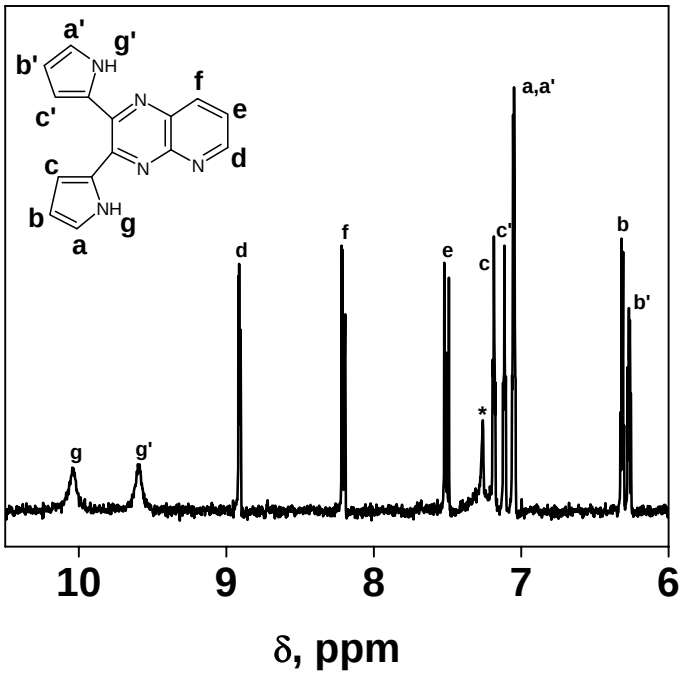

Fig. 6.6. ^{1}H NMR spectra of **dppp** ($CDCl_3$, TMS). * indicates the solvent signal for $CDCl_3$.

the 1D spectra but also on the proton connectivity patterns observed in the corresponding ^{1}H - ^{1}H COSY spectra. The four β-pyrrole protons resonate at four distinct signals as multiplets. While two of them (Hb and Hb′) appear at upfield, other two (Hc and Hc′) shift at downfield compared to Ha and Ha′ in ^{1}H NMR spectrum. Also, one of the two pyrrole NH protons appear 0.4 ppm downfield than the other. Non-equivalent magnetic environment for the pyrrole rings is created by virtue of intramolecular hydrogen-bonding between one of the pyrrole NH protons and pyrazine nitrogen, and electron withdrawing conjugation effect of pyridine. However, the two α-pyrrole protons (Ha and Ha′), being unaffected by such effect, appear together at 7.04-7.06 ppm.

6.3.4 Cation sensing

Typical changes in the absorption spectrum of **dppp** on addition of the metal salts in acetonitrile are shown in fig. 6.7. The band around 420 nm disappears and a new band appears at a much longer wavelength (λ_{max} = 495 nm). The presence of isosbestic point implies that **dppp** and **dppp**–Ni^{2+} are in equilibrium in the course of titration. The spectral changes observed are similar for Co^{2+}, Cu^{2+}, Zn^{2+} and Cd^{2+} ions. The change in the absorbance at 490 nm has been used to calculate the binding constant *K*, using the equation described in section 2.9.1. That the sensor **dppp** binds the transition metal ions with varying degree of strength is evident from the binding constant values shown in table 6.1. Ni^{2+} and Cu^{2+} bind more strongly (K ~ 10^6 M^{-1}), compared to Co^{2+} and Zn^{2+} for which the *K* values are one order of magnitude less. The metal ion binding is associated with a color change from yellowish-green to brown, as shown in fig. 6.7. In the case of Cd^{2+}, the color changes from

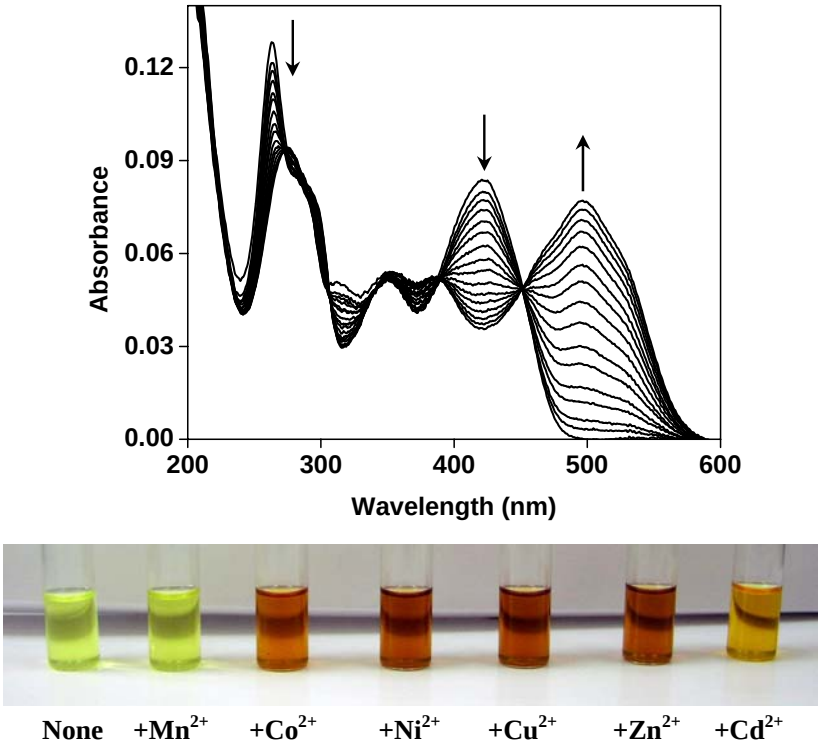

Fig. 6.7. Top: Absorption spectral changes observed for **dppp**, upon addition of Ni^{2+} ion in CH_3CN. [**dppp**] = 6.5 μM; [Ni^{2+}] = 0, 0.3, 0.7, 1.2, 1.7, 2.3, 3, 3.8, 4.6, 5.6, 6.6, 7.7, 9, 10.4, 12, 13.9 μM. Bottom: Color changes observed for **dppp** in CH_3CN upon the addition of cations (as ClO_4^- salts). From left to right: none, Mn^{2+}, Co^{2+}, Ni^{2+}, Cu^{2+}, Zn^{2+} and Cd^{2+}.

yellowish-green to light-brown, whereas no change in color of **dppp** is observed on addition of Mn^{2+}. That an additional pyridine ring does help metal ion binding is evident from the fact that our previously reported DPP derivative bearing cyano functionality, **ppdcn**[32-34] (chapter 5) does not show noticeable change in the absorption spectrum on addition of Mn^{2+}, Co^{2+}, Ni^{2+},

Zn^{2+} and Cd^{2+} ions. With Cu^{2+}, a decrease in absorbance of the 420 nm band is observed. This corresponds to a *K* value of 2.3 x 10^4 M^{-1}, which is two orders of magnitude less than that observed for the present system.

Table 6.1. Cation and anion binding constants (10^5 M^{-1}) for **dppp** in CH_3CN, determined by absorption titration data.

Ions	*K*
Mn^{2+}	ND [a]
Co^{2+}	3.2
Ni^{2+}	11
Cu^{2+}	15
Zn^{2+}	4.8
Cd^{2+}	0.68
F^-	0.049

[a] Change in absorption spectra was not enough to calculate binding constant.

6.3.5 Anion sensing

The change in absorption spectra of **dppp** on addition of F^- in CH_3CN solution is shown in fig. 6.8. Upon addition of tetrabutylammonium fluoride (TBAF), the 420 nm absorption band disappears, while a new band at 490 nm appears with an isosbestic point at 460 nm indicating equilibrium between **dppp** and **dppp**–F^- during the course of titration. The binding is associated with a color change from yellowish-green to red and is observable by naked eye. With other halogen anions and ClO_4^-, no color change was observed. This observation can be attributed to small size and strongest hydrogen-bond acceptor ability of the F^- compared to the other anions. The binding constant

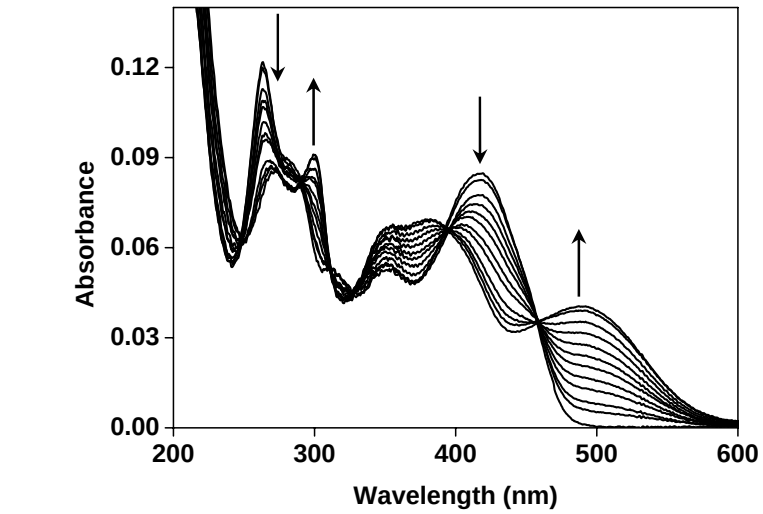

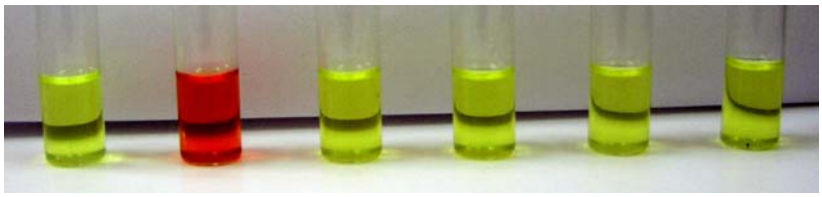

None **+F^-** **+Cl^-** **+Br^-** **+I^-** **+ClO_4^-**

Fig. 6.8. Top: Absorption spectral changes observed for **dppp**, upon addition of F^- ion in CH_3CN. [**dppp**] = 6.5 μM; [F^-] = (0, 2.3, 4, 6.3, 8.9, 12.2, 16.4, 21.2, 32.9, 42.1, 54.2, 68.9) x 10^{-5} M. Bottom: Color changes observed for **dppp** in CH_3CN upon the addition of anions (as TBA^+ salts). From left to right: none, F^-, Cl^-, Br^-, I^- and ClO_4^-.

for F^- complexation is estimated as 4.9 x 10^3 M^{-1}. The original spectrum of the sensor system is restored from that of sensor–F^- adduct upon addition of trace amount of water/methanol which not only suggests that the complexation between F^- and **dppp** is reversible in nature but also lends further support to

the involvement of hydrogen-bonding in the binding between the sensor and F^-. Comparison of the binding constant values reveals that **dppp** binds the cations much more strongly (*K* values are 2 orders of magnitude higher) compared to the F^-. The X-ray structure of **Ni(dppp)$_2$Cl$_2$** clearly reveals that the pyridine nitrogen atom is involved in binding of the metal ion. It is already well known that hydrogen-bonding interaction between F^- and pyrrole NH moieties is responsible for binding of F^-.[25-34] Binding between DPP moiety and F^- and subsequent color changes were explained with the help of a model and supported by theoretical calculations in previous chapter (chapter 5).[25,34]

Although, generation of a new absorption band around 500 nm is common to both cation and F^- titrations, careful examination of fig. 6.7 and 6.8 reveals that the spectra for the finally formed **dppp**–M^{2+} (M = Co, Ni, Cu, Zn, Cd) and **dppp**–F^- complexes are different. The appearance of a long wavelength band on absorption titration can perhaps be attributed to an enhanced conjugation between the pyrrole and pyridopyrazine rings on complexation. The X-ray crystallographic structure suggests that the dihedral angles between the pyrrole and pyridopyrazine rings are reduced to some extent on metal complexation allowing a better conjugation.

6.3.6 Sensing in the presence of competing ions

Since the present system consists of two distinct binding sites for the metal ions and F^-, we thought it appropriate to examine the effect of competing F^- ion on the binding ability of **dppp** for metal ion and vice versa. These experiments have been carried out in two different manners. First, we have titrated **dppp** with F^- (using TBAF) in the presence of 2 equivalents of metal ions, M^{2+}. Second, we have titrated **dppp** with M^{2+} in the presence of

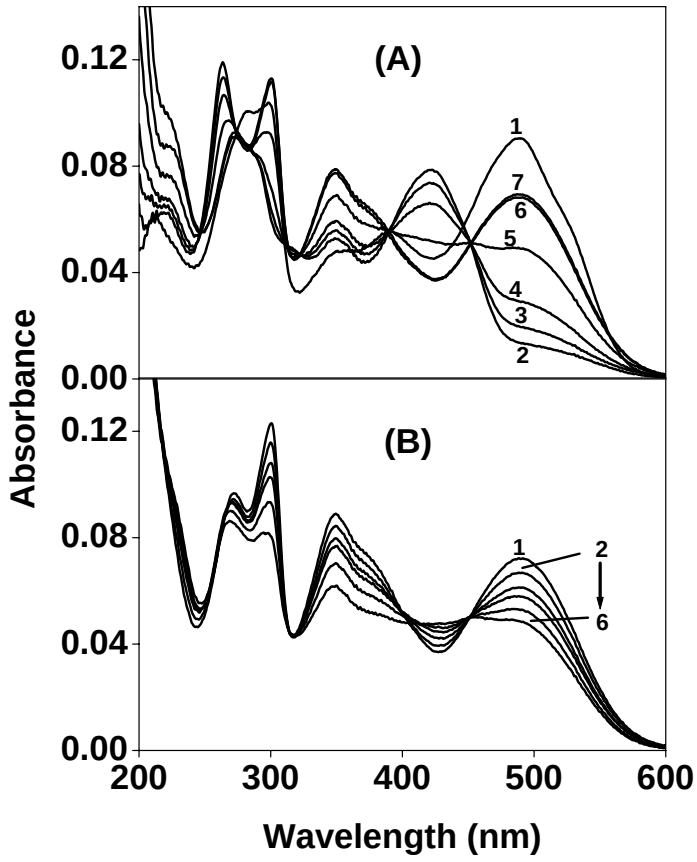

Fig. 6.9. Change in absorption spectra of (A) **dppp** (6.5 μM) on addition of Zn^{2+} ($[Zn^{2+}]$ = 13 μM, spectrum 1) and then, titration with TBAF, $[F^-]$ = (2, 10.1, 20.2, 40.1, 79.2, 154.5) x 10^{-5} M (spectra 2 to 7); (B) **dppp** (6.5 μM) on addition of TBAF ($[F^-]$ = 6.5 x 10^{-4} M, spectrum 1) and then, titration with Zn^{2+}, $[Zn^{2+}]$ = (0.4, 0.8, 1.2, 1.8, 3) x 10^{-5} M (spectra 2 to 6).

100 equivalents of TBAF. We chose Zn^{2+} and F^- for the dual sensing experiment as the Zn^{2+} salts are colorless and it is possible to observe distinct

changes due to metal complexation/decomplexation without any interference from the color of the salts. The spectral changes are shown in fig. 6.9. As can be seen, initial titration of **dppp** and two equivalents of Zn^{2+} with TBAF results in a drastic reduction of the intensity of the 500 nm band suggesting sequestering of the metal ion to form ion pair with F^- ion in solution, as has been recently observed in some cases.[41,42] However, as expected, when sequestering of the metal ion is complete, further addition of F^- ion leads to expected enhancement of the intensity of the 500 nm band due to complexation of F^- ion. The binding constant of **dppp** with F^- in the presence of 2 equivalents of Zn^{2+} is estimated as 550 M^{-1}, which is almost one order of magnitude less than that observed in the absence of competing metal ion. In the second experiment, which is carried out in the presence of 100 equivalents of F^-, addition of Zn^{2+} ion leads to a gradual reduction of the intensity of the 500 nm band due to the sequestering of F^- ion. The fact that the concentration of F^- ion in solution is far in excess of the Zn^{2+} ion, the condition in which all the F^- is completely uncomplexed is never met in this case and hence, enhancement of the 500 nm band intensity at a later stage, as has been noticed in the previous experiment, is not observed in this case. Moreover, presence of large concentration of F^- in the solution engages the metal ions in ion pair formation in solution rather than engaging them in complexation. We repeated similar experiments with other metal ions such as Ni^{2+} and Cu^{2+} that do not have such high affinity towards F^-. With these metal ions, the sharp drop of absorption shown in fig. 6.9 could not be observed because of high binding constant of **dppp** with the metal ions and low affinity of these metal ions with F^-. Nevertheless, it is evident that although **dppp** contains distinct binding sites for both anion and cation, simultaneous binding of both the species, as

observed exploiting allosteric effect,[43,44] through-bond electrostatic effect[45,46] or to the host as an associated ion-pair,[41] is not possible in this case unless the total concentration of the two species is much less than what a particular binding site can accommodate.

6.4 Summary

The DPP derivative, **dppp** has been synthesized and characterized by different methods. The crystal structures of **dppp** and **Ni(dppp)$_2$Cl$_2$**, which are essential for an understanding of the change in orientation of pyrrole rings on metal complexation and determining the coordinating site of the metal, have been determined. The binding constants of **dppp** with several transition metal ions have been found to be two orders of magnitude higher than that for the F^- in acetonitrile. The sensing of the metal ions and F^- is visible by naked eye observation of the color change of the system.

6.5 References

1) *Supramolecular Chemistry*; Lehn, J. M., Ed.; VCH: Weinheim, 1995.
2) de Silva, A. P.; Gunaratne, H. Q. N.; Gunnlaugsson, T.; Huxley, A. J. M.; McCoy, C. P.; Rademacher, J. T.; Rice, T. E. *Chem. Rev.* **1997**, *97*, 1515.
3) *Special Issue on 'Luminescent Sensors', Coord. Chem. Rev.* **2000**, *205*.
4) *Supramolecular Chemistry of Anions*; Bianchi, A., Bowman-James, K., Garcia-Espana, E., Eds.; Wiley-VCH: New York, 1997.
5) Beer, P. D.; Gale, P. A. *Angew. Chem. Int. Ed.* **2001**, *40*, 486.
6) *Special Issue on 'Synthetic Anion Receptor Chemistry', Coord. Chem. Rev.* **2003**, *240*.

7) Spichiger-Keller, U. E. *Chemical Sensors and Biosensors for Medical and Biological Applications*; Wiley-VCH: Berlin, 1998.
8) Wolfbeis, O. S. In *Biomedical Optical Instrumentation and Laser-Assisted Biotechnology*; Verga Scheggi, A. M., Ed.; Kluwer: Dordrecht, 1996; p 327.
9) Gale, P. A. *Coord. Chem. Rev.* **2003**, *240*, 191.
10) Mahoney, J. M.; Stucker, K. A.; Jiang, H.; Carmichael, I.; Brinkmann, N. R.; Beatty, A. M.; Noll, B. C.; Smith, B. D. *J. Am. Chem. Soc.* **2005**, *127,* 2922.
11) Turner, D. R.; Spencer, E. C.; Howard, J. A. K.; Tocher, D. A.; Steed, J. W. *Chem. Commun.* **2004**, 1352.
12) Tobey, S. L.; Anslyn, E. V. *J. Am. Chem. Soc.* **2003**, *125,* 14807.
13) Plieger, P. G.; Tasker, P. A.; Galbraith, S. G. *Dalton Trans.* **2004**, 313.
14) Smith, C. B.; Stephens, A. K. W.; Wallwork, K. S.; Lincoln, S. F.; Taylor, M. R.; Wainwright, K. P. *Inorg. Chem.* **2002**, *41*, 1093.
15) Zhou, L.-L.; Sun, H.; Li, H.-P.; Wang, H.; Zhang, X.-H.; Wu, S.-K.; Lee, S.-T. *Org. Lett.* **2004**, *6*, 1071.
16) Talanova, G. G.; Hwang, H.-S.; Talanov, V. S.; Bartsch, R. A. *Anal. Chem.* **2001**, *73*, 5260.
17) Ros-Lis, J. V.; Martinez-Manez, R.; Rurack, K.; Sancenon, F.; Soto, J.; Spieles, M. *Inorg. Chem.* **2004**, *43*, 5183.
18) Arunkumar, E.; Ajayaghosh, A.; Daub, J. *J. Am. Chem. Soc.* **2005**, *127,* 3156.
19) Gunnlaugsson, T.; Leonard, J. P.; Murray, N. S. *Org. Lett.* **2004**, *6*, 1557.
20) Jia, L.; Zhang, Y.; Guo, X.; Qian, X. *Tetrahedron Lett.* **2004**, *45*, 3969.

21) Kirk, K. L. *Biochemistry of the Halogens and Inorganic Halides*, Plenum Press, New York, 1991; p. 58.

22) Wiseman, A. *Handbook of Experimental Pharmacology* XX/2, Part 2; Springer-Verlag: Berlin, 1970; p. 48-97.

23) Nielsen, K. A.; Jeppesen, J. O.; Levillain, E.; Becher, J. *Angew. Chem. Int. Ed.* **2003**, *42***,** 187.

24) Miyaji, H.; Sato, W.; Sessler, J. L. *Angew. Chem. Int. Ed.* **2000**, *39*, 1777.

25) Black, C. B.; Andrioletti, B.; Try, A. C.; Ruiperez, C.; Sessler, J. L. *J. Am. Chem. Soc.* **1999**, *121*, 10438.

26) Anzenbacher, P., Jr.; Try, A. C.; Miyaji, H.; Jursikova, K.; Lynch, V. M.; Marquez, M.; Sessler, J. L. *J. Am. Chem. Soc.* **2000**, *122*, 10268.

27) Mizuno, T.; Wei, W.-H.; Eller, L. R.; Sessler, J. L. *J. Am. Chem. Soc.* **2002**, *124*, 1134.

28) Anzenbacher, P., Jr.; Tyson, D. S.; Jursikova, K.; Castellano, F. N. *J. Am. Chem. Soc.* **2002**, *124*, 6232.

29) Sessler, J. L.; Maeda, H.; Mizuno, T.; Lynch, V. M.; Furuta, H. *Chem. Commun.* **2002**, 862.

30) Sessler, J. L.; Maeda, H.; Mizuno, T.; Lynch, V. M.; Furuta, H. *J. Am. Chem. Soc.* **2002**, *124*, 13474.

31) Aldakov, D.; Anzenbacher, P., Jr. *Chem. Commun.* **2003**, 1394.

32) Sessler, J. L.; Pantos, G. D.; Katayev, E.; Lynch, V. M. *Org. Lett.* **2003**, *5*, 4141.

33) Ghosh, T.; Maiya, B. G. *J. Chem. Sci.* **2004**, *116*, 17.

34) Ghosh, T.; Maiya, B. G.; Wong, M. W. *J. Phys. Chem. A* **2004**, *108*, 11249.

35) Behr, D.; Brandange, S.; Lindstrom, B. *Acta. Chem. Scand.* **1973**, *27*, 2411.

36) Venuti, M. C. *Synthesis* **1982**, 61.

37) de Silva, A. P.; Dixon, I. M.; Gunaratne, H. Q. N.; Gunnlaugsson, T.; Maxwell, P. R. S.; Rice, T. E. *J. Am. Chem. Soc.* **1999**, *121*, 1393.

38) Manson, J. L. *Inorg. Chem.* **2003**, *42*, 2602.

39) Turro, N. J. *Modern Molecular Photochemistry*; Benjamin/Cummings Publishing: California, 1978, pp. 108.

40) Berlman, I. B. *Handbook of Fluorescence Spectra of Aromatic Molecules*, 2nd edition, Academic Press: New York, 1971, p. 322.

41) Shukla, R.; Kida, T.; Smith B. D. *Org. Lett.* **2000**, *2*, 3099.

42) Tumcharern, G.; Tuntulani, T.; Coles, S. J.; Hursthouse, M. B.; Kilburn, J. D. *Org. Lett.* **2003**, *5*, 4971.

43) Kubik, S.; Goddard, R. *J. Org. Chem.* **1999**, *64*, 9475.

44) Beer, P. D.; Hopkins, P. K.; Mckinney, J. D. *J. Chem. Soc., Chem. Commun.* **1999**, 1253.

45) Beer, P. D.; Cooper, J. B. *J. Chem. Soc., Chem. Commun.* **1998**, 129.

46) Tozawa, T.; Misawa, Y.; Tokita, S.; Kubo, Y. *Tetrahedron Lett.* **2000**, *41*, 5219.

CHAPTER 7

DNA Interaction and Photocleavage Activities of Mixed-Ligand Complexes of Ruthenium(II) Containing New Photo- or Electro-active Ligands

7.1 Introduction

The photochemical and electrochemical properties of ruthenium (II) complexes continue to receive considerable attention largely due to their potential applications in various research areas including solar energy conversion, luminescence sensing, biotechnology, electroluminescence displays, photochemical molecular devices etc.[1-5] In recent years, ruthenium(II) polypyridyl complexes are also being employed in studies with DNA, with views to design and develop synthetic restriction enzymes, new drugs, and DNA foot printing agents.[6-10] These complexes have been found to be particularly useful for the above-mentioned purposes because of their potential to bind DNA *via* multitude of interactions and to cleave the duplex by virtue of their intrinsic chemical, electrochemical and photochemical reactivity.

Presently, a great deal of attention is centered around DNA interactions of ruthenium(II) complexes containing modified **bpy**/**phen** ligands (**bpy** = 2,2′-bipyridyl and **phen** = 1,10-phenanthroline), where the modification of the **bpy**/**phen** is done in such a way that it augments the intercalative interaction of the complexes.[2,7-14] The synthesis, characterization and DNA binding and photocleavage proclivities of a series of mixed-ligand ruthenium(II) complexes incorporating modified **phen** ligands possessing quinone/cyano substituent in their π-framework has been recently reported where the

extended π-framework and also the highly electron withdrawing substituent(s) present in these ligands not only ensured strong intercalative DNA binding, but also effected efficient DNA photocleavage by the corresponding ruthenium(II) complexes.[15-18]

Earlier studies show that **[Ru(bpy)$_2$(sq)]$^+$** -based (**sq** is semiquinone) complexes act as a mild oxidant towards organic substrate.[19-22] Detrimental roles of intermediate semiquinone radicals forming oxidized cellular macromolecules including lipids, proteins and DNA inside cells are well known[23-26] and thus **[Ru(bpy)$_2$(sq)]$^+$** -based complexes are expected to behave as an non-innocent molecule towards DNA.

With these in our mind, we have investigated DNA binding and photocleavage/redox properties of six new mixed-ligand ruthenium(II) complexes that incorporate photoactive modified **bpy** *viz.* (E)-1-[2-(4-methyl-2-pyridyl)-4-pyridyl]-2-(1-naphthyl)-1-ethene (**mpne**), (E)-1-(9-anthryl)-2-[2-(4-methyl-2-pyridyl)-4-pyridyl]-1-ethene (**mpae**), (E)-1-[2-(4-methyl-2-pyridyl)-4-pyridyl]-2-(1-pyrenyl)-1-ethene (**mppe**) or electroactive semiquinone *viz.* 4-(4-pyridyl)-1,2-benzenedioleto(+I) (**sq-py**), 1,10-phenanthroline-5,6-dioleto(+I) (**sq-phen**), 1,2-benzenedioleto(+I) (**bsq**) ligands.

7.2 Experimental section

The ruthenium(II) complexes of three photoactive ligands *viz.* **[Ru(bpy)$_2$(mpne)](PF$_6$)$_2$**, **[Ru(bpy)$_2$(mpae)](PF$_6$)$_2$**, **[Ru(bpy)$_2$(mppe)](PF$_6$)$_2$** and, three electroactive ligands *viz.* **[Ru(bpy)$_2$(sq-py)]PF$_6$**, **[Ru(bpy)$_2$(sq-phen)]PF$_6$** and **[Ru(phen)$_2$(bsq)]PF$_6$** were synthesized by a published procedure whose structures are shown in fig. 7.1.[27] In the latter three complexes, 4-(4-pyridyl)-1,2-benzenediol (**catpy**), 5,6-dihydroxy-1,10-

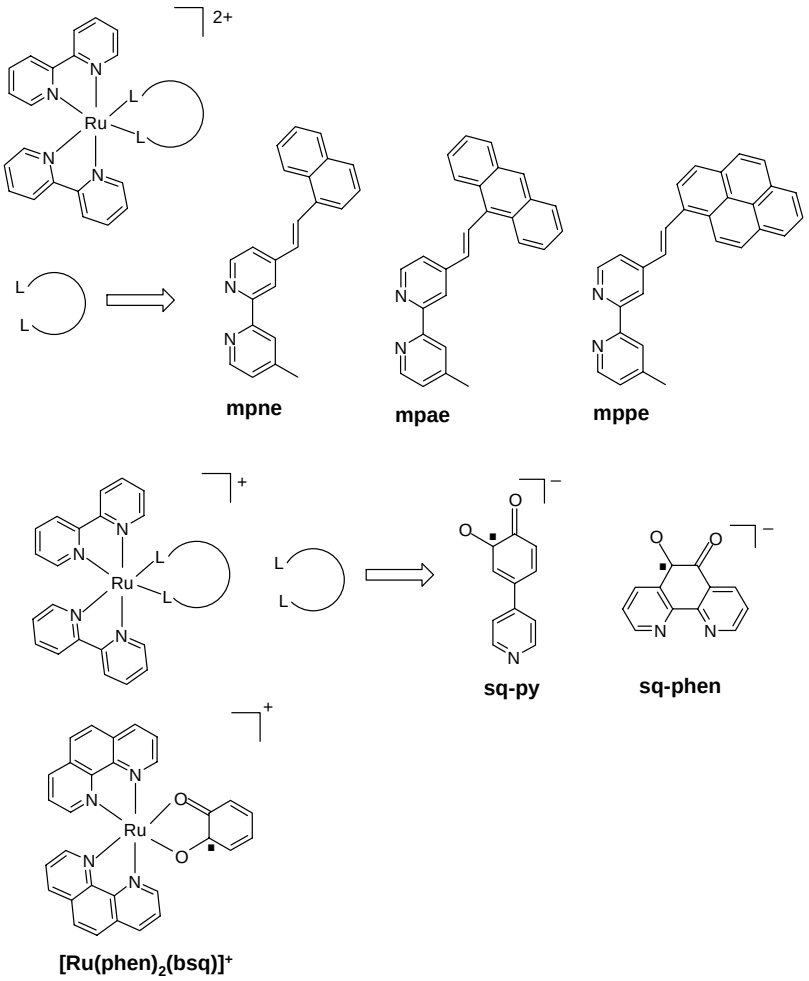

Fig. 7.1. Molecular structure of the ruthenium (II) complexes.

phenanthroline (**catphen**) and 1,2-benzenediol (**cat**) ligands are actually bound to the metal center as the corresponding semiquinone species, *viz*.: 4-(4-pyridyl)-1,2-benzenedioleto(+I) (**sq-py**), 1,10-phenanthroline-5,6-dioleto(+I)

(**sq-phen**) and 1,2-benzenedioleto(+I) (**bsq**), thus making the overall charge of the complexes to be equal to formally +1 in each case.

Analytical data of the ligands and complexes are provided below. **mpne**: Calcd. for $C_{23}H_{18}N_2$: C, 85.68; H, 5.63; N, 8.69%. Found: C, 85.5; H, 5.6; N, 8.6 %. ^{1}H NMR (200 MHz, $CDCl_3$, TMS) δ, ppm: 2.46 (3H, s), 7.14-7.22 (2H, m), 7.45-7.61 (4H, m), 7.76-7.90 (3H, m), 8.22 (1H, d; *J* = 16.4 Hz), 8.23-8.28 (2H, m), 8.59 (2H, d, *J* = 5 Hz), 8.62 (1H, d; *J* = 5 Hz). EI-MS: *m/z* 322 (M^+). **[Ru(bpy)$_2$(mpne)](PF$_6$)$_2$**: Calcd. for $RuC_{43}H_{34}N_6P_2F_{12}$: C, 50.56; H, 3.33; N, 8.23 %. Found: C, 51.1; H, 3.5; N, 8.2 %. ^{1}H NMR (200 MHz, CD_3CN, TMS) δ, ppm: 2.45 (3H, s), 7.19-7.48 (6H, m), 7.55-7.7 (7H, m), 7.75-7.8 (3H,m), 7.88 (2H, d, *J* = 5.6 Hz), 7.94-8.11 (7H, m), 8.40-8.59 (6H, m). FAB-MS: *m/z* 879 (M^+ - PF_6), 735 (M^+ - 2PF_6). **[Ru(bpy)$_2$(mpae)](PF$_6$)$_2$**: Calcd. for $RuC_{47}H_{36}N_6P_2F_{12}$: C, 52.47; H, 3.38; N, 7.81%. Found: C, 53.2; H, 3.5; N, 7.1 %. ^{1}H NMR (200 MHz, CD_3CN, TMS) δ, ppm: 2.42 (3H, s), 7.18-7.23 (3H, m), 7.33-7.42 (6H, m), 7.54 (2H, d, *J* = 5.8 Hz), 7.72 (4H, d, *J* = 5.8 Hz), 7.88 (2H, dd, *J* = 3.6 Hz), 7.99 (2H, t, *J* = 8 Hz), 8.03 (2H, m), 8.07 (2H, t, *J* = 7.8 Hz), 8.27 (2H, dd, *J* = 3.6 Hz), 8.35 (2H, s), 8.46-8.5 (6H, m). FAB-MS: *m/z* 930 (M^+ - PF_6), 785 (M^+ - 2PF_6). **[Ru(bpy)$_2$(mppe)](PF$_6$)$_2$**: Calcd. for $RuC_{49}H_{36}N_6P_2F_{12}$: C, 53.53; H, 3.28; N, 7.64%. Found: C, 54.3; H, 3.3; N, 7.4 %. ^{1}H NMR (200 MHz, CD_3CN, TMS) δ, ppm: 2.4 (3H, s), 7.35 (1H, d, *J* = 16.2 Hz), 7.53 (2H, d, *J* = 6.8 Hz), 7.57-7.9 (12H, m), 8.1-8.6 (16H, m), 8.66 (2H, d, *J* = 5.6 Hz). FAB-MS: *m/z* 954 (M^+ - PF_6), 809 (M^+ - 2PF_6). **[Ru(bpy)$_2$(sq-py)]PF$_6$**: Calcd. for $RuC_{31}H_{23}N_5O_2PF_6$: C, 50.06; H, 3.10; N, 9.42%. Found: C, 49.9; H, 3.2; N, 9.3%. FAB-MS: *m/z* 598 (M^+ - PF_6). IR (KBr pellet, cm^{-1}): 1729 (br, C=O), 1445 (semiquinone stretching), 841 (PF_6). **[Ru(bpy)$_2$(sq-phen)]PF$_6$**: Calcd. for $RuC_{32}H_{22}N_6O_2PF_6$: C, 49.99; H, 2.86; N,

10.94%. Found: C, 49.4; H, 3.0; N, 10.6%. FAB-MS: *m/z* 623 (M^+ - PF_6). IR (KBr pellet, cm^{-1}): 1722 (C=O), 1612, 1590 (C=C, C=N), 1445 (semiquinone stretching), 838 (PF_6). **[Ru(phen)$_2$(bsq)]PF$_6$**: Calcd. for $RuC_{30}H_{20}N_4O_2PF_6$: C, 50.44; H, 2.80; N, 7.84%. Found: C, 51.6; H, 2.7; N, 7.9%. FAB-MS: *m/z* 714 (M^+), 569 (M^+ - PF_6). IR (KBr pellet, cm^{-1}): 1726 (C=O), 1448 (semiquinone stretching), 839 (PF_6).

7.3 Results and discussion

7.3.1 Spectral and electrochemical characterization

7.3.1.1 EPR spectra

All the three ruthenium(II)-semiquinone complexes **[Ru(bpy)$_2$(sq-py)]$^+$**, **[Ru(bpy)$_2$(sq-phen)]$^+$** and **[Ru(phen)$_2$(bsq)]$^+$** were found to be EPR active due to the semiquinone nature of the coordinated dioxolene ligand.

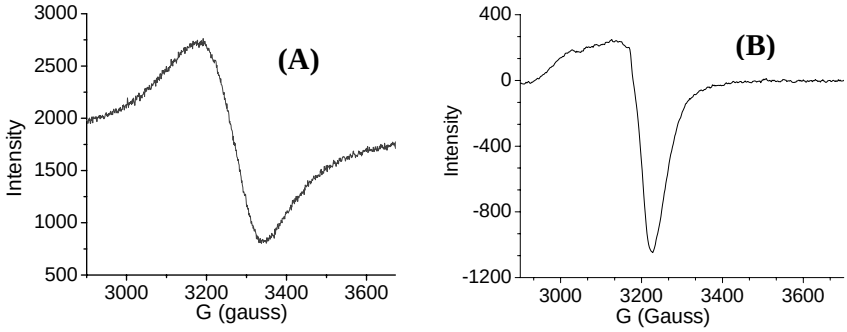

Fig. 7.2. EPR spectra of **[Ru(bpy)$_2$(sq-phen)]PF$_6$** recorded (A) as powder at room temperature and (B) as frozen CH_2Cl_2-toluene glass at 77K.

These complexes showed a featureless room temperature EPR spectrum consisting of a broad free radical signal centered at g ~ 2.003 ($\Delta H_{P,P}$ ~ 180 G) in

CH_3CN. Spectra recorded at 77K (frozen CH_2Cl_2-toluene glass) are anisotropic with $g_\perp$ ~1.98 and $g_\parallel$ ~ 2.05; no hyperfine structures could be resolved in these spectra. Spectra for the three complexes are essentially same and representative spectra for **$[Ru(bpy)_2(sq\text{-}phen)]^+$** are shown in fig. 7.2 and the g values are summarized in table 7.1. Nonetheless, we believe that the anisotropicity observed in the low temperature spectra are due to the fact that the molecular orbital containing the unpaired electron of the semiquinone fragment is partially localized on the ruthenium(II) center as is the case with the previously reported metal-bound semiquinone complexes.[19,20,28,29]

Table 7.1. Redox potential [a] and EPR (at room temperature [b] and 77K [c]) data of ruthenium(II) complexes.

Complexes	Redox potential		EPR	
	Oxidation $E_{1/2}$ (V vs Ag/AgCl)	Reduction $E_{1/2}$ (V vs Ag/AgCl)	298K g_{avg}	77K $g_\perp, g_\parallel$
$[Ru(bpy)_2(mpne)](PF_6)_2$	+0.83	-1.51, -1.68, -2.13	–	–
$[Ru(bpy)_2(mpae)](PF_6)_2$	+0.84	-1.53, -1.65, -2.10	–	–
$[Ru(bpy)_2(mppe)](PF_6)_2$	+0.86	-1.49, -1.66, -2.08	–	–
$[Ru(bpy)_2(sq\text{-}py)]PF_6$	+1.04, +0.18	-0.36, -1.81, -1.98	2.003	1.98, 2.05
$[Ru(bpy)_2(sq\text{-}phen)]PF_6$	+1.1, +0.27	-0.4, -1.87, -2.0	2.003	1.983, 2.043
$[Ru(phen)_2(bsq)]PF_6$	+1.08, +0.22	-0.38, -1.9, -2.0	2.003	1.982, 2.004

[a] in CH_3CN, 0.1 M $TBAPF_6$. [b] in CH_3CN. [c] frozen CH_2Cl_2-toluene glass.

7.3.1.2 Electrochemistry

Redox features of each investigated complex were probed by the cyclic and square wave voltammetric methods in CH_3CN using a conventional three-electrode cell assembly. A saturated Ag/AgCl as reference and platinum as working and auxiliary electrodes were used for this purpose. Ferrocene was used internal standard and all potentials are quoted versus the ferrocenium/ferrocene (Fc^+/Fc) couple. Tetrabutylammonium hexafluorophosphate ($TBAPF_6$, 0.1 M) was used as supporting electrolyte for the electrochemical measurements and electrode potential values reported for various redox processes were typically evaluated at a scan rate of 100 mV s^{-1}.

The redox potential data of the complexes are displayed in table 7.1. **$[Ru(bpy)_2(mpne)]^{2+}$**, **$[Ru(bpy)_2(mpae)]^{2+}$** and **$[Ru(bpy)_2(mppe)]^{2+}$** showed anticipated redox processes typical for **$[RuL_3]^{2+}$** -type complexes where L is a polypyridyl ligand. However, it is worth mentioning, that reduction of the **mpne**/**mpae**/**mppe** is more facile than that for other two coordinated **bpy**-units and generally occurs at ~ -1.5 V. Thus, for these ligands LUMO is lower than that for the **bpy** ligands. This observation explains the bathochromic shift of the MLCT transition ($d(\pi_{Ru})$-$\pi^*_{L'}$) (L′ is **mpne**/**mpae**/**mppe**) band (~ 460 nm) compared to the corresponding band of **$[Ru(bpy)_3]^{2+}$** (452 nm).

For **$[Ru(phen)_2(bsq)]^+$**, **$[Ru(bpy)_2(sq\text{-}py)]^+$** and **$[Ru(bpy)_2(sq\text{-}phen)]^+$**, in addition to anticipated $Ru^{III/II}$ -based and ruthenium(II)-bound **bpy** or **phen** based redox couples, two additional redox processes are also observed. These additional redox processes are assigned to dioxolene-based redox couples, *viz*: 1,2-diol/semiquinone (~ -0.4 V) and semiquinone/quinone (~ 0.2 V) couples. These metal-bound dioxolene based redox processes are found to be more reversible in protic solvents. For free 1,2-benzenediol, the redox processes are

at best quasi reversible even in protic solvents and the 1,2-diol/semiquinone redox processes are more difficult by at least 0.4 V with respect to those for the coordinated dioxolene fragment. Thus, coordination of the semiquinone-fragment of all the three semiquinone-derivatized ligands in **[Ru(phen)$_2$(bsq)]$^+$**, **[Ru(bpy)$_2$(sq-py)]$^+$** and **[Ru(bpy)$_2$(sq-phen)]$^+$** makes reduction of semiquinone-fragment to corresponding 1,2-diolate-fragment facile by at least 0.4 V. Similarly, the oxidation of the semiquinone-fragment in these complexes to the corresponding quinone-fragment is difficult by at least 0.3 V. Such shifts in potentials seem reasonable if it is considered that the semiquinone-fragments are connected to ruthenium(II) center.

7.3.1.3 Absorption and fluorescence spectra

The absorption and fluorescence spectral data of the ruthenium(II) complexes are summarized in table 7.2. The **bpy** and aromatic hydrocarbon subunits are conjugatively connected in **mpne**, **mpae** and **mppe**, unlike the case with the similar type of ligands reported by Wilson and co-workers,[30] in which the same two subunits are connected *via* aliphatic spacers. For **[Ru(bpy)$_2$(mpne)]$^{2+}$**, absorption spectrum in the 240-500 nm region is quite similar to that of **[Ru(bpy)$_3$]$^{2+}$**, as shown in fig. 7.3. Assignment for ^1L_a or ^1L_b bands for the coupled naphthalene chromophore was found to be difficult due to the intense **bpy**-based n-π^* transition appearing at 250 nm, π-π^* transition at 285 nm and d(π_{Ru})-π^*(bpy) transition at 460 nm. Absorption band at 350 nm is presumably due to the substituted **bpy**-based intra-ligand charge transfer process. However, in the 220-240 nm region of this complex, spectral features are dominated by naphthalene-based (^1B_b) transition. For **[Ru(bpy)$_2$(mpae)]$^{2+}$**, spectral pattern is not very different from that observed for

Table 7.2. Absorption [a] and fluorescence [b] data of ruthenium(II) complexes.

Complexes	λ_{max}^{abs} (log ε)			λ_{max}^{em} (ϕ_f)
	Ligand Transition		MLCT	
	Hydrocarbon based	**bpy**/**phen** based		
[Ru(bpy)$_2$(mpne)]$^{2+}$	213 (4.85) 244 (4.58) 349 (4.30)	288 (4.89)	460 (4.33)	639 (0.005)
[Ru(bpy)$_2$(mpae)]$^{2+}$	251 (4.18)	287 (4.47)	454 (3.70)	630 (0.05)
[Ru(bpy)$_2$(mppe)]$^{2+}$	239 (4. 90) 382 (4.60) 416 (4.63)	294 (4.92)	461 (sh)	617 (0.003)
[Ru(bpy)$_2$(sq-py)]$^{+}$	243 (4.20), 288 (4.49), 345 (3.79)		429 (3.66) 464 (3.64) 954 (3.63)	–
[Ru(bpy)$_2$(sq-phen)]$^{+}$	245 (4.27), 286 (4.56)		449 (3.86) 941 (3.66)	–
[Ru(phen)$_2$(bsq)]$^{+}$	222 (4.46), 262 (4.54)		420 (3.71) 958 (2.77)	–

[a] Except for **[Ru(phen)$_2$(bsq)]$^{+}$**, the spectrum of which was recorded in water, each spectrum was run using CH_3CN as the solvent. sh is shoulder. [b] Quantum yield was calculated using **[Ru(bpy)$_3$]$^{2+}$** (ϕ_f = 0.062 in CH_3CN) as standard.[31]

[Ru(bpy)$_2$(mpne)]$^{2+}$; except that assignment of not so clearly resolved bands at around 360-390 nm is not so straight forward. Pyrene is known to absorb strongly at 340 (^1L_a), 275 (^1B_b) and 240 (^1B_a) nm and these bands are overlapped with the less intense bands arising from the '**Ru(bpy)$_3$**'–chromophore in **[Ru(bpy)$_2$(mppe)]$^{2+}$**. Two absorption bands seen at ~ 380 and 415 nm are based on the **mppe** fragment. The ε values for the pyrene based transitions are either comparable or higher than that for '**Ru(bpy)$_3$**'-subunit based transitions and mostly dominate the overall spectrum for

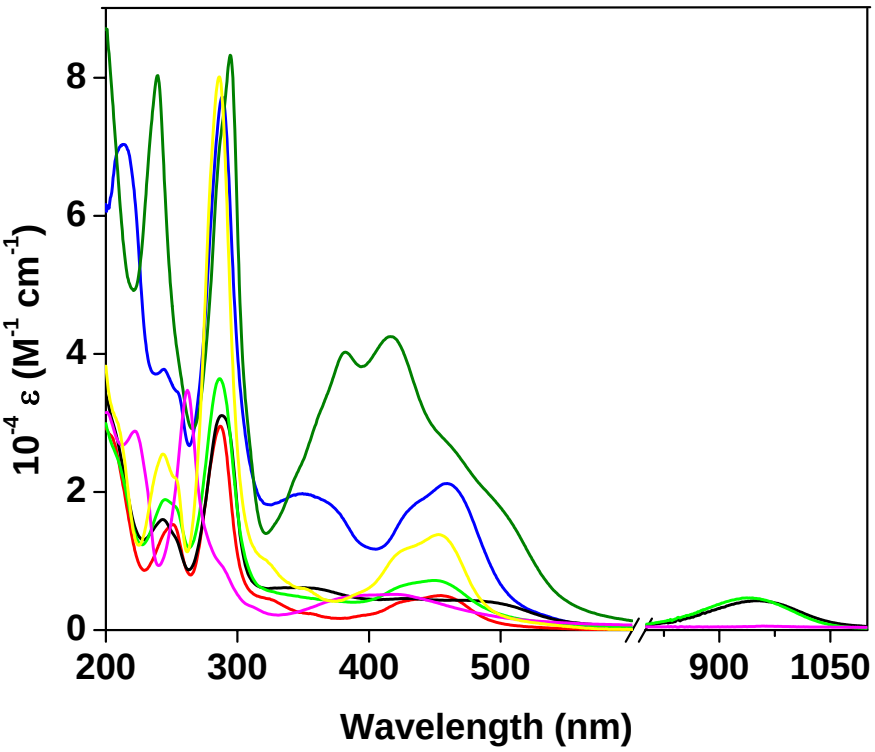

Fig. 7.3. Absorption spectra of **[Ru(bpy)$_2$(mpne)]$^{2+}$** ( ), **[Ru(bpy)$_2$(mpae)]$^{2+}$** ( ), **[Ru(bpy)$_2$(mppe)]$^{2+}$** ( ), **[Ru(bpy)$_2$(sq-py)]$^{+}$** ( ), **[Ru(bpy)$_2$(sq-phen)]$^{+}$** ( ), **[Ru(phen)$_2$(bsq)]$^{+}$** ( ) and **[Ru(bpy)$_3$]$^{2+}$** ( ). All spectra were recorded in CH_3CN, except for the last two complexes the spectra of which were recorded in water.

[Ru(bpy)$_2$(mppe)]$^{2+}$. For **[Ru(bpy)$_2$(mpae)]$^{2+}$** and **[Ru(bpy)$_2$(mppe)]$^{2+}$**, d(π_{Ru})-π*(bpy)-based MLCT band appear around 455 and 460 (shoulder) nm, respectively.

Absorption spectra for **catpy** and **catphen** show strong absorption bands between 220-340 nm; but an unambiguous assignment for these bands

is not possible. Moreover, in the corresponding isolated complexes of these ligands, the binding modes are in the form of semiquinone and this makes it even more difficult to correlate and assign the transitions in either the ligands or the complexes. However, **phen**-centered n-π^* and π-π^* transitions in **[Ru(phen)$_2$(bsq)]$^+$** appear around 220 and 260 nm, respectively and spectrum in this region is not complicated by the any significant absorption band that arises from the coordinated semiquinone-fragment. The **bpy**-centered n-π^* and π-π^* transitions for **[Ru(bpy)$_2$(sq-py)]$^+$** and **[Ru(bpy)$_2$(sq-phen)]$^+$** are located at ~ 245 and ~ 285 nm, respectively. For **[Ru(bpy)$_2$(sq-py)]$^+$**, band at ~ 345 nm is presumably arises from a transition based on coordinated **sq-py** moiety. Characteristic MLCT transitions of the d(π_{Ru})-π^*(bpy/phen) are seen around 465, 450 and 420 nm for **[Ru(bpy)$_2$(sq-py)]$^+$**, **[Ru(bpy)$_2$(sq-phen)]$^+$** and **[Ru(phen)$_2$(bsq)]$^+$**, respectively and those of the type d(π_{Ru})-π*(sq-py), d(π_{Ru})-π*(sq-phen) and d(π_{Ru})-π*(bsq) appear in the region 940-960 nm. As discussed earlier by Lever and coworkers, we attribute these latter transitions as d(π_{Ru})-π*(sq_{SOMO})-based MLCT transition.[19,20,28,29]

[Ru(bpy)$_2$(mpne)]$^{2+}$, **[Ru(bpy)$_2$(mpae)]$^{2+}$** and **[Ru(bpy)$_2$(mppe)]$^{2+}$** are found to be fluorescent when excited between 450 and 460 nm in CH_3CN solutions and fluorescence quantum yields (ϕ_f) were calculated using **[Ru(bpy)$_3$]$^{2+}$** as the standard (ϕ_f = 0.062 in CH_3CN).[31] On the other hand, the three semiquinone bound mixed-ligand ruthenium(II) complexes are non-fluorescent under identical experimental conditions.

The absorption data suggest that it is possible to monitor the DNA binding at both the high (400-500 nm) and low (900-1000 nm) energy MLCT bands of **[Ru(phen)$_2$(bsq)]$^+$**, **[Ru(bpy)$_2$(sq-py)]$^+$** and **[Ru(bpy)$_2$(sq-phen)]$^+$** by the absorption titration method, and that the wavelength range available for

the same purpose is restricted to 400-500 nm for **[Ru(bpy)$_2$(mpne)]$^{2+}$**, **[Ru(bpy)$_2$(mpae)]$^{2+}$** and **[Ru(bpy)$_2$(mppe)]$^{2+}$**. On the other hand, the fluorescence data suggest that DNA interactions of the latter three complexes can also be probed by the fluorescence titration method.

7.3.2 DNA binding

It should be noted here that because all the complexes reported here have been isolated in their racemic forms, their DNA binding behaviors described below are a composite effect of the two enantiomers. It should also be noted here that **[Ru(bpy)$_2$(mppe)]$^{2+}$** (either chloride or PF_6^- salt) was thrown out from the solution as a precipitate upon addition of DNA. Whenever DNA solution was added to a solution of **[Ru(bpy)$_2$(mppe)]$^{2+}$** for fluorescence or absorption titration, orange-red colored particles were formed inside the cuvette, which disturbed the recording of absorption and emission spectra with increasing scattering. Thus it was impossible to study its interaction with the duplex. Addition of DNA may be forcing the **[Ru(bpy)$_2$(mppe)]$^{2+}$** complex, which contains bulky, hydrophobic pyrene group attached to its ligand structure, to be precipitated out from solution due to more hydrophilic nature of the solution. In all the other cases, chloride salt of the complexes, the absorption spectra of which in aqueous solution are almost identical to the spectra of the corresponding PF_6^- salts in CH_3CN, were employed in studies with DNA. The only difference is that the ε values of chloride salts in aqueous solution are less than the corresponding ε values of PF_6^- salts in acetonitrile.

Buffer A (5 mM Tris, pH 7.1, 50 mM NaCl) was used for the absorption and fluorescence titration experiments. Absorption titration

experiments were carried out by varying the DNA concentration (0-100 μM) and maintaining the complex concentration constant (2-30 μM). Absorption spectra were recorded after each successive addition of DNA and equilibration (*ca.* 10 min). In the presence of increasing amounts of calf thymus (CT) DNA, each complex showed decrease in absorbance (hypochromicity) and red-shifted MLCT peak maxima with the presence of isosbestic points in the absorption spectra. For **[Ru(bpy)$_2$(mpne)]$^{2+}$** and **[Ru(bpy)$_2$(mpae)]$^{2+}$**,

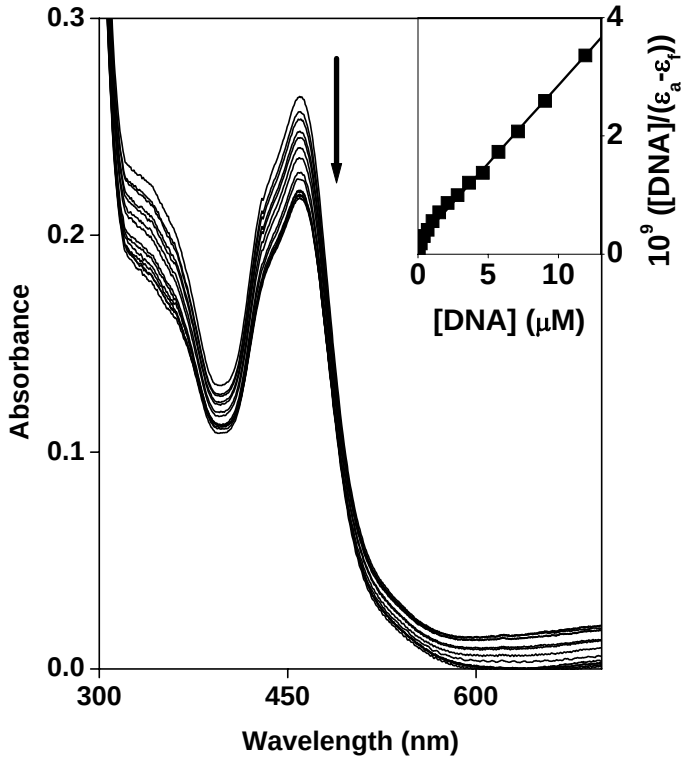

Fig. 7.4. Absorption titration of **[Ru(bpy)$_2$(mpne)]$^{2+}$** with CT DNA in buffer A. [Complex] = 16 μM. The inset figure shows the best fitting straight line of the data for calculation of binding constant.

hypochromicity and bathochromic shifts observed in the presence of DNA are 22%, 13% and 2, 1 nm, respectively. A representative absorption titration of **[Ru(bpy)$_2$(mpne)]$^{2+}$** with DNA is depicted in fig. 7.4. The binding constants (K_b), calculated using the equation described in section 2.10.1, are summarized in table 7.3. The value of K_b, as determined by the absorption titration method, for the standard complex **[Ru(phen)$_3$]$^{2+}$** with DNA is 5.5 x 10^3 M^{-1} whereas, that for other standard complex **[Ru(bpy)$_3$]$^{2+}$** has been reported to be too low to be measured with a reasonable level of accuracy.[32] Binding constants for all the complexes reported in this work are higher than that of these standard complexes by at least two orders of magnitude.

Table 7.3. DNA binding constants (10^5 M^{-1}) and melting temperature data.

Complexes	K_b	T_m (^{o}C)	σ_T (^{o})
[Ru(bpy)$_2$(mpne)]$^{2+}$	13	64	25
[Ru(bpy)$_2$(mpae)]$^{2+}$	3.6	61	21

For **[Ru(phen)$_2$(bsq)]$^+$**, **[Ru(bpy)$_2$(sq-py)]$^+$** and **[Ru(bpy)$_2$(sq-phen)]$^+$**, in addition to the hypochromicity and bathochromic shifts of the MLCT band at around 450 nm, almost complete bleaching of the absorption band at the near IR (NIR) region was observed. Hypochromicity and bathochromic shift values for the 450 nm band for these three complexes were found to be 20%, 7%, 19%, and 21, 4, 4 nm, respectively. Fig. 7.5 shows change in absorption spectra of **[Ru(bpy)$_2$(sq-phen)]$^+$** on titration with CT DNA in buffer A. At

this point, this was almost essential to ascertain whatever the observed bleaching in absorbance in the NIR region is due to the binding of the ruthenium(II) complex in the DNA strand or due to some other chemical reaction. To check this, we added ethidium bromide solution at the end of above absorption titration of **[Ru(bpy)$_2$(sq-phen)]$^+$** with CT DNA. Ethidium bromide is known to be a strong intercalator of DNA[33,34] and expected to release the bound ruthenium(II)-semiquinone complex from the DNA. In that case, one should expect the NIR band to restore with almost original intensity provided the bleaching of NIR band was due to binding to the DNA molecule,

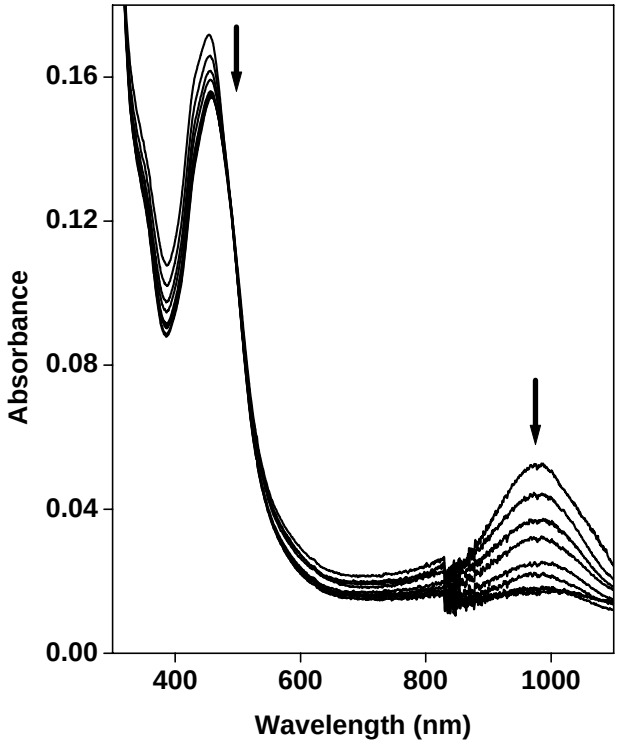

Fig. 7.5. Absorption titration of **[Ru(bpy)$_2$(sq-phen)]$^+$** with CT DNA in buffer A. [Complex] = 30 μM, [DNA] = 0-100 μM.

but not for some other chemical reaction. However, NIR band was not restored on addition of ethidium bromide. This helped us to conclude in favor of some other chemical reaction.

It is known from the earlier studies that the intense NIR band of these complexes is sensitive to the redox state of the coordinated dioxolene moiety. Electrochemical studies reveal that the redox potential for the 1,2-diol/semiquinone redox couple for the ruthenium(II)-semiquinone complexes is easily accessible (table 7.1) and thus can be reduced easily both chemically and electrochemically.[19-22] Now, DNA is known to have a 2-deoxy-D-ribose unit, which may behave as an enough strong reductant for the semiquinone fragment of the Ru(II)-complexes. Keeping this redox behavior of the ruthenium(II)-semiquinone complexes in mind we studied the spectral change of the **$[Ru(bpy)_2(sq\text{-}phen)]^+$** complex in aqueous buffer medium with time after addition of excess of glucose solution. The observed change is very much similar to the one shown in the Fig. 7.5. Thus, it seems reasonable to us to conclude that the observed hypochromicity of the NIR band at 950 nm for **$[Ru(phen)_2(bsq)]^+$** or **$[Ru(bpy)_2(sq\text{-}phen)]^+$** or **$[Ru(bpy)_2(sq\text{-}py)]^+$** is due to the formation of corresponding 1,2-diol derivative, **$Ru(phen)_2(cat)$** or **$Ru(bpy)_2(catphen)$** or **$Ru(bpy)_2(catpy)$**, respectively. Independent experiment shows that the observed second order rate constant for the redox reaction between **$[Ru(bpy)_2(sq\text{-}phen)]^+$** ($37.5 \times 10^{-6}$ M) and CT DNA (3×10^{-4} M) was found to be $(9.0\pm0.1) \times 10^{-3}$ s^{-1}, when reaction was carried out at the specified condition: ionic strength = 50 mM NaCl, pH = 7.1, [Tris] = 5 mM. Spectroelectrochemical studies with the related **$[Ru(bpy)_2(sq^*)]^+$**-class of compounds (**sq*** signifies various substituted semiquinone derivative) reveal that when these complexes are reduced to the corresponding 1,2-diol

form, in addition to the complete bleaching of the NIR band (>900 nm), little hypochromicity is observed for the MLCT band at 450 nm[19-22] and it is much less than the observed hypochromicity observed in the present study. This enhanced hypochromicity at the 450 nm absorption band presumably signifies the binding of the ruthenium(II)-semiquinone complexes to the DNA molecule.

However, we are not in the position to make any comment how much hypochromicity attributed to binding with DNA and how much for reduction of semiquinones to 1,2-diols, and whether this actually precedes the observed reduction process or which is the rate determining step–binding or reduction? Our preliminary studies showed that relative rate for the bleaching of the NIR band for three different ruthenium(II)-semiquinone complexes follows the order: **$[Ru(phen)_2(bsq)]^+$** ~ **$[Ru(bpy)_2(sq\text{-}phen)]^+$** > **$[Ru(bpy)_2(sq\text{-}py)]^+$**. If one considers that '**$Ru(bpy)_2$**' or '**$Ru(phen)_2$**'-fragment cannot bind with the DNA strand,[32] then pyridine unit of the **sq-py** or phen unit of the **sq-phen** is the better candidate to have a more efficient interaction which is contradictory to the observed rate of bleaching of the NIR band. Thus, the oxidation of the 2-deoxy-D-ribose unit may precede the binding step.

In the fluorescence titration experiments, aqueous buffer (buffer A) solution of the metal complex was titrated with DNA in the same fashion mentioned in case of absorption titration, exciting the sample at 460 nm and monitoring the intensity at the emission maximum. Fluorescence intensity of **$[Ru(bpy)_2(mpne)]^{2+}$** increases with increasing addition of DNA, as shown in fig. 7.6. In aqueous buffer medium, fluorescence of **$[Ru(bpy)_2(mpne)]^{2+}$** is quenched due to predominating nonradiative deactivation pathways. Intercalation of **$[Ru(bpy)_2(mpne)]^{2+}$** with DNA double helix causes the

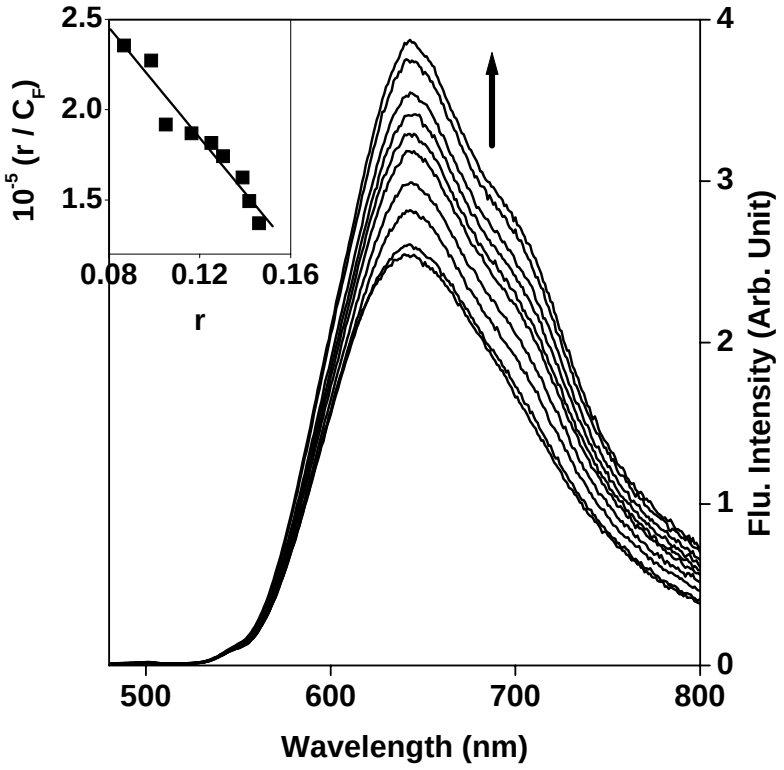

Fig. 7.6. Fluorescence titration of **$[Ru(bpy)_2(mpne)]^{2+}$** with CT DNA in buffer A. [Complex] = 11 μM, [DNA] = 0-250 μM, λ_{exc} = 460 nm. The inset shows the best fit of the data for calculation of binding constant.

molecule to enter in a less polar environment from a more polar one. So, radiative pathways dominate over nonradiative pathways and hence, an enhancement of fluorescence intensity is observed.[35,36] The binding constant for **$[Ru(bpy)_2(mpne)]^{2+}$**, estimated by the fluorescence titration method (fig. 7.6, inset) using equation described in section 2.10.2, is found to be 4 x 10^5 M^{-1} with n = 3. The binding constant obtained by fluorescence titration

method is lower than that by the absorption titration method. The varying K_b values obtained by two titration methods could be due to different methods of measurements (i.e. absorption and fluorescence titration), as has been recently suggested by Wu et. al.[37] On the other hand, there is very little change in the fluorescence intensity for **[Ru(bpy)$_2$(mpae)]$^{2+}$** on adding even large excess of DNA.

Thermal denaturation experiments were carried out by monitoring the absorption of CT DNA at 260 nm at various temperatures, in the presence (2-5 μM) and absence of each complex in buffer B (1 mM phosphate, pH 7.0, 2 mM NaCl). The melting temperature (T_m) and the curve width (σ_T) are calculated and reported in table 7.3.[38,39] DNA thermal melting is a measure of stability of DNA double helix with temperature; an increase in thermal melting temperature (T_m) indicates an interaction between DNA and metal complex. In the present case, thermal melting studies are carried out at [DNA]/[complex] = 25 and T_m and σ_T values were determined by monitoring the absorbance of DNA at 260 nm as a function of temperature. The T_m of DNA in the absence of any added drug was found to be 60±1^{o}C, under our experimental conditions. Under the same set of conditions, presence of **[Ru(bpy)$_2$(mpne)]$^{2+}$**, and **[Ru(bpy)$_2$(mpae)]$^{2+}$** increased the T_m by 4^{o}C and 1°C, respectively and are given in table 7.3. For ruthenium(II)-semiquinone complexes, situation is complicated due the redox reaction between the coordinated semiquinone moiety and the sugar fragment of the DNA molecule and thus, it is difficult to evaluate any precise T_m and σ_T values.

Based on the hypochromicity and bathochromic shifts of the MLCT bands observed, high K_b value, enhancement of fluorescence during emission titration, and the increase in the T_m and σ_T values in the thermal denaturation

experiments, we suggest that **[Ru(bpy)$_2$(mpne)]$^{2+}$** interacts with the DNA *via* the intercalative mode,[2,15-18,40-42] with the naphthalene part of **mpne** ligand intercalated between the base pairs. Thus, ruthenium(II)-bound **bpy** ligands in **[Ru(bpy)$_2$(mpne)]$^{2+}$** act only as 'spectator ligands'[32] and it is the other ligand (**mpne**) that is involved in the intercalation with the DNA. Nonetheless, other binding models including groove binding can not be neglected altogether.[40] The other complex, **[Ru(bpy)$_2$(mpae)]$^{2+}$**, may be interacting with DNA by groove binding mode, which is well understandable by lower K_b value (of the order of 10^5), little change in emission intensity and almost no change in thermal melting temperature of DNA. In this regard, it is interesting that the K_b, T_m and emission titration data suggest that **[Ru(bpy)$_2$(mpne)]$^{2+}$** binds DNA strongly than **[Ru(bpy)$_2$(mpae)]$^{2+}$**. If one considers that anthracene has more extended π-surface than naphthalene for insertion into the base-pairs of DNA, this observation is quite unexpected. It is thus possible that the naphthalene ring in **[Ru(bpy)$_2$(mpne)]$^{2+}$** is ideally exposed for intercalation than the anthracene subunit in **[Ru(bpy)$_2$(mpae)]$^{2+}$** which might be experiencing steric clashes during its approach towards the DNA.[43-48] Among the complexes containing the semiquinone ligands, observed rate constant values for the reduction of the ruthenium(II)-semiquinone complexes to the corresponding ruthenium(II)-1,2-diol system, follow the order: **[Ru(phen)$_2$(bsq)]$^+$** ~ **[Ru(bpy)$_2$(sq-phen)]$^+$** > **[Ru(bpy)$_2$(sq-py)]$^+$**. For complexes **[Ru(phen)$_2$(bsq)]$^+$** and **[Ru(bpy)$_2$(sq-py)]$^+$**, the ligands **bsq** and **sq-py** do not have extended π-conjugated systems as it is in **[Ru(bpy)$_2$(sq-phen)]$^+$**. The ligand **sq-phen** in **[Ru(bpy)$_2$(sq-phen)]$^+$** possesses relatively better extended π-conjugated system than the previous two ligands; but it is well known fact that **phen** is a minor contributor for intercalative mode of

binding with DNA in the case of **[Ru(phen)$_3$]$^{2+}$**.[32] So, it can be inferred that these three complexes may be interacting with DNA by groove binding mode.

7.3.3 DNA photocleavage

For the gel electrophoresis experiments, supercoiled pBR 322 DNA (100 μM in nucleotide phosphate) was treated with the metal complex (10 μM) in Tris-HCl buffer and the mixture was incubated for 1 h. in the dark. Photocleavage experiments were carried out for the pre-incubated (dark, 1 h.) samples by irradiating them at 450 (±5) nm for 1 h. in each case.

DNA photocleavage experiments were conducted with **[Ru(bpy)$_2$(mpne)]$^{2+}$** and **[Ru(bpy)$_2$(mpae)]$^{2+}$** - the only two photoactive complexes investigated in this study. Control experiments suggested that untreated pBR 322 DNA does not show any cleavage in the dark and even upon irradiation by 450 nm light, as shown in fig. 7.7. Similarly, both the complexes were not detectably active in the dark experiments. In the light experiments, while **[Ru(bpy)$_2$(mpae)]$^{2+}$** was found to be totally ineffective in cleaving the DNA, **[Ru(bpy)$_2$(mpne)]$^{2+}$** show evident photocleavage, as illustrated in fig. 7.7. The photocleavage ability of this complex is almost twice than that seen for the parent reference compound, *viz.* **[Ru(bpy)$_3$]$^{2+}$** under the similar set of experimental conditions of drug and light dose. Thus, it is interesting that despite having a lower fluorescence quantum yield (ϕ_f = 0.005), **[Ru(bpy)$_2$(mpne)]$^{2+}$** efficiently photocleaves DNA as opposed to the inability to do so by **[Ru(bpy)$_2$(mpae)]$^{2+}$**, the fluorescence quantum yield of which is at least an order of magnitude higher (ϕ_f = 0.05) than that of **[Ru(bpy)$_2$(mpne)]$^{2+}$**. This observation can be rationalized as follows: (i) the fluorescence intensity of **[Ru(bpy)$_2$(mpne)]$^{2+}$** increases in the presence of

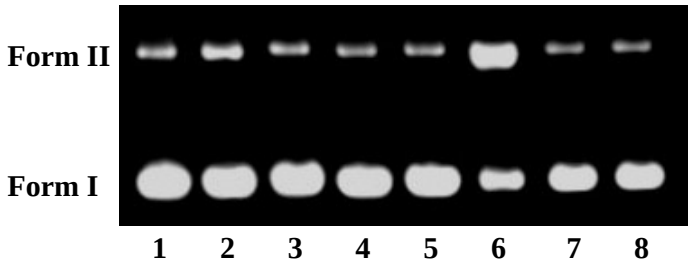

Fig. 7.7. Light induced nuclease activity of **[Ru(bpy)$_2$(mpne)]$^{2+}$**. Lanes 1, 2, 3 and 4 (Dark experiments, incubation for 1 h): control pBR 322 DNA, DNA + **[Ru(bpy)$_2$(mpne)]$^{2+}$**, DNA + **[Ru(bpy)$_2$(mpae)]$^{2+}$** and DNA + **[Ru(bpy)$_3$]$^{2+}$**, respectively. Lanes 5, 6, 7 and 8 (light experiments, incubation for 1 h in dark followed by irradiation at 450 (±5) nm for 1 h): control pBR 322 DNA, DNA + **[Ru(bpy)$_2$(mpne)]$^{2+}$**, DNA + **[Ru(bpy)$_2$(mpae)]$^{2+}$** and DNA + **[Ru(bpy)$_3$]$^{2+}$**, respectively. [DNA] = 100 μM (nucleotide phosphate) and [complex] = 10 μM in all cases.

DNA but **[Ru(bpy)$_2$(mpae)]$^{2+}$** does not show any such DNA-induced fluorescence enhancement and (ii) the K_b of **[Ru(bpy)$_2$(mpne)]$^{2+}$** is nearly an order of magnitude higher than that for **[Ru(bpy)$_2$(mpae)]$^{2+}$**.

'Inhibitor' studies carried out to reveal the mechanism of DNA photocleavage of **[Ru(bpy)$_2$(mpne)]$^{2+}$** indicated that $OH^{\bullet}$ might be involved in the nicking reaction, which is illustrated in fig. 7.8. Purging the reaction mixture with N_2 (15 min, to remove O_2) does not inhibit the reaction and also DABCO-a $^1O_2$ 'quencher', does not inhibit the photocleavage by the complex. The case is similar for Tiron (4,5-dihydroxy-1,3-benzenedisulphonic acid, disodium salt monohydrate), which too, does not inhibit the photocleavage by the complex, thereby indicating that superoxide anion (O_2^{-}) is not involved in

the cleavage mechanism. On the other hand, DMSO and mannitol, which scavenge $OH^{\bullet}$ were found to partially inhibit the photocleavage under our experimental conditions. Most probably, the ruthenium(II) centre together with the naphthalene moiety of **mpne** ligand and also with the help of the irradiated light are responsible to generate $OH^{\bullet}$ radical in aqueous buffer medium which is involved in subsequent DNA cleavage.

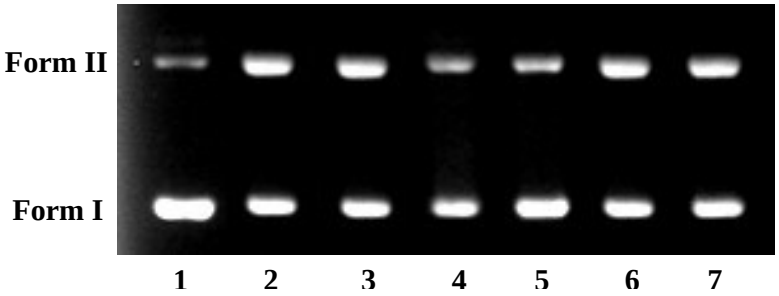

Fig. 7.8. Effects of 'inhibitors' on the light-induced nuclease activity of **$[Ru(bpy)_2(mpne)]^{2+}$**. Lane 1: control pBR 322 DNA, Lane 2: DNA + **$[Ru(bpy)_2(mpne)]^{2+}$**. Lanes 3-7: DNA + **$[Ru(bpy)_2(mpne)]^{2+}$** in the presence of N_2 atmosphere, DMSO (200 mM), mannitol (100 mM), DABCO (20 mM) and Tiron (2 mM), respectively. [DNA] = 100 μM (nucleotide phosphate) and [complex] = 10 μM in all cases. All the samples were irradiated for 1h. at 450 (±5) nm after incubation for 1h. in dark.

Although, the three ruthenium(II)-semiquinone complexes are found to be non-luminescent but they show nucleases activity even in dark with pBR 322 DNA to some extent, which is displayed in fig. 7.9. However, irradiation of light does not enhance the cleavage efficiency of DNA by these complexes. The control experiment shows the cleavage ability of these complexes are

more than the untreated pBR 322 DNA lane and parent reference compound ($\mathbf{[Ru(bpy)_3]^{2+}}$) lane under dark condition. This observation is explainable if a chemical reaction has taken place between these complexes and DNA even in dark. This, in turn, also supports the explanation for bleaching of the band around 950 nm during the absorption titration of $\mathbf{[Ru(bpy)_2(sq\text{-}phen)]^{+}}$ with CT DNA due to oxidation of 2-deoxy-D-ribose unit of DNA by semiquinone fragment of the ruthenium(II) complex.

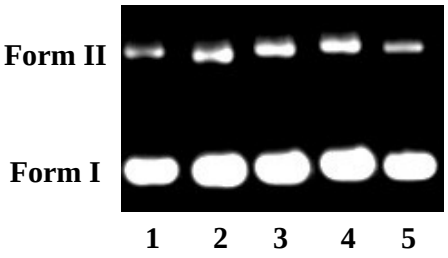

Fig. 7.9. Nuclease activity of ruthenium(II)-semiquinone complexes in dark condition (incubation for 1 h. in dark). Lanes 1-5: control pBR 322 DNA, DNA + $\mathbf{[Ru(phen)_2(bsq)]^{+}}$, DNA + $\mathbf{[Ru(bpy)_2(sq\text{-}phen)]^{+}}$, DNA + $\mathbf{[Ru(bpy)_2(sq\text{-}py)]^{+}}$, and DNA + $\mathbf{[Ru(bpy)_3]^{2+}}$, respectively. [DNA] = 100 μM (nucleotide phosphate) and [complex] = 10 μM in all cases.

7.4 Summary

DNA binding and photocleavage/redox properties of six new, mixed-ligand ruthenium(II) complexes have been investigated, where **bpy** or **phen** are present as ‘spectator ligands’. While three of these complexes possess luminescent, photoactive hydrocarbon ligands, the other three contain electroactive, semiquinone type ligands. These latter complexes are EPR active as they contain unpaired electron on the semiquinone ligands. All the

complexes are strong binders of DNA with binding constants being at least two orders more than that of **$[Ru(bpy)_3]^{2+}$** or **$[Ru(phen)_3]^{2+}$**. Hypochromicity observed for the low energy MLCT band (> 900 nm) of the ruthenium(II)-semiquinone complexes in the presence of DNA arises due to reduction of semiquinone by sugar part (deoxyribose) of DNA. It was also observed that **$[Ru(bpy)_2(mpne)]^{2+}$** showed considerable photocleavage activity but **$[Ru(bpy)_2(mpae)]^{2+}$** is totally ineffective in cleaving DNA under the same set of experimental conditions although, the former has quantum yield 10 times less than the latter one. The inhibitor studies indicate that the reactive oxygen species $OH^{\bullet}$ radical is involved in the DNA photocleavage of **$[Ru(bpy)_2(mpne)]^{2+}$**. Although, the ruthenium(II)-semiquinone complexes show nuclease activity even in dark with pBR 322 DNA to some extent due to the oxidation of 2-deoxy-D-ribose unit of DNA by semiquinone fragment of the ruthenium(II) complex but, irradiation of light does not enhance the cleavage efficiency of DNA by these complexes.

7.5 References

1. Ji, L.-N.; Zou, X.-H.; Liu, J.-G. *Coord. Chem. Rev.* **2001**, *216-217*, 513.
2. Erkkila, K. E.; Odom, D. T.; Barton, J. K. *Chem. Rev.* **1999,** *99*, 2777.
3. Xiong, Y.; Ji, L.-N. *Coord. Chem. Rev.* **1999**, *185-186*, 711.
4. Kelly, S. O.; Barton, J. K. in Sigel, A.; Sigel, H.; Eds.; *Metal ions in Biological Systems*; Marcel Dekker: New York, 1998; vol. 39; pp 211-249.
5. Mesmaeker, A. K.-De.; Lecomte, J. P.; Kelly, J. M. in Mattay, J.; Ed.; *Topics in Current Chemistry*; 1996**,** vol. 177, pp 25-76.
6. Kane-Maguire, N. A. P.; Wheeler, J. F. *Coord. Chem. Rev.* **2001**, *211*, 145.

7. Kaes, C.; Katz, A.; Hosseini, M. W. *Chem. Rev*. **2000,** *100*, 3553.
8. Armitage, B. *Chem. Rev*. **1998,** *98*, 1171.
9. Sigman, D. S.; Mazumder, A.; Perrin, D. M. *Chem. Rev*. **1993,** *93*, **2295.**
10. Armond, M. K. De; Carlin, C. M. *Coord. Chem. Rev.* **1981**, *36*, 325.
11. Turro, C.; Bossmann, S. H.; Jenkins, Y.; Barton, J. K.; Turro, N. J.; *J. Am. Chem. Soc.* **1995**, *117*, 9026.
12. Friedman, A. E.; Kumar, C. V.; Turro, N. J.; Barton, J. K. *Nuclic Acids Res.* **1991**, *19*, 2595.
13. Hartshorn, R. M.; Barton, J. K. *J. Am. Chem. Soc.* **1992**, *114*, 5919.
14. Murphy, C. J.; Barton, J. K. *Methods Enzymol*. **1993**, *226*, 576.
15. Ambroise, A.; Maiya, B.G. *Inorg. Chem.* **1999**, *38*, 842.
16. Ambroise, A.; Maiya, B.G. *Inorg. Chem.* **2000**, *39*, 4256.
17. Ambroise, A.; Maiya, B.G. *Inorg. Chem.* **2000**, *39*, 4264.
18. Sastri, C. V.; Eswaromoorthy, D.; Giribabu, L.; Maiya, B. G. *J. Inorg. Biochem.* **2003**, *94*, 138.
19. Ghosh, D.; Shukla, A. D.; Banerjee, R.; Das, A. *J. Chem. Soc. Dalton Trans.* **2002**, 1220 (and references therein).
20. Shukla, A. D.; Das, A. *Polyhedron* **2000**, *19*, 2605.
21. Shukla, A. D.; Ganguly, B.; Dave, P. C.; Samanta, A.; Das, A. *Chem. Commun.* **2002**, 2648.
22. Jose, A. D.; Shukla, A. D.; Krishnakumar, D.; Ganguly, B.; Das, A.; Ramakrishna, G.; Ghosh, H. N. *Inorg. Chem.* **2005**, *44*, 2414.
23. Flowers, L.; Ohnishi, S. T.; Penning, T. M. *Biochemistry* **1997**, *36*, 8640.
24. Bolton, J. L.; Trush, M. A.; Penning, T. M.; Dryhurst, G.; Monks, T. J. *Chem. Res. Toxicol.* **2000**, *13*, 135.

25. Schelvis, J. P. M.; Ramsey, M.; Sokolova, O.; Tavares, C.; Cecala, C.; Connell, K.; Wagner, S.; Gindt, Y. M. *J. Phys. Chem. B* **2003**, *107*, 12352.
26. Yang, C. H.; Chen, W. F.; Jong, M. C.; Jong, B. J.; Chang, J. C.; Waring, M. J.; Ma, L.; Sheh, L. *J. Am. Chem. Soc.* **2004**, *126*, 8104.
27. Ghosh, T.; Shukla, A. D.; Jose, D. A.; Kumar, D. K.; Maiya, B. G.; Samanta, A.; Das, A. *J. Biol. Inorg. Chem.* **2005**, *10*, 496.
28. Barthram, A. M.; Cleary, R. L.; Kowallick, R.; Ward, M. D. *Chem. Commun*. **1998**, 2695.
29. Haga, M.; Dodsworth, E. S.; Lever, A. B. P. *Inorg. Chem.* **1986**, *25*, 447.
30. Wilson, G. J.; Launikonis, A.; Sasse, W. H. F.; Mau, A. W.-H. *J. Phys. Chem. A* **1997**, *101*, 4860.
31. Juris, A.; Balzani, V.; Barigelletti, F.; Campagna, S.; Belser, P.; Zelewsky, A. V. *Coord. Chem. Rev.* **1988,** *84*, 85.
32. Pyle, A. M.; Rehmann, J. P.; Meshoyrer, R.; Kumar, C. V.; Turro, N. J.; Barton, J. K. *J. Am. Chem. Soc.* **1989**, *111*, 3051.
33. Wang, A. H-J. *Current Opinion in Structrural Biology* **1992,** *2*, 361.
34. Wang, J. G. *J. Mol. Biol.* **1974**, *89*, 783.
35. Friedman, A. E.; Chambron, J.-C.; Sauvage, J.-P.; Turro, N. J.; Barton, J. K. *J. Am. Chem. Soc.* **1990**, *112*, 4960.
36. Moucheron, C.; Mesmaeker, A. K.-De.; Choua, S. *Inorg. Chem.* **1997**, *36*, 584.
37. Wu, J.; Du, F.; Zhang, P.; Khan, I. A.; Chen, J.; Liang, Y. *J. Inorg. Biochem.* **2005**, *99*, 1145.
38. Kelly, J. M.; Tossi, A. B.; McConnell, D. J.; OhUigin, C. *Nucl. Acid. Res*. **1985**, *13*, 6017.

39. Marmur, J.; Doty, P. *J. Mol. Biol*. **1962**, *5*, 109.
40. Long, E. C.; Barton, J. K. *Acc. Chem. Res.* **1990**, *23*, 271.
41. Thorp, H. H. *Adv. Inorg. Chem.* **1995**, *43*, 127.
42. Norden, B.; Lincoln, P.; Akerman, B.; Tuite, E. in Sigel, A.; Sigel, H.; Eds.; *Metal ions in Biological Systems*; Marcel Dekker: New York, 1996; vol. 33; pp 177-252.
43. Goldstein, B. M.; Barton, J. K.; Berman, H. M. *Inorg. Chem.* **1986**, *25*, 842.
45. Morgan, R. J.; Chatterjee, S.; Baker, A. D.; Strekas, T. C. *Inorg. Chem.* **1991**, *30*, 2687.
46. Tysoe, S. A.; Morgan, R. J.; Baker, A. D.; Strekas, T. C. *J. Phys. Chem.* **1993**, *97*, 1707.
47. Xu, H.; Zheng, K. C.; Chen, Y.; Li, Y. Z.; Lin, L. J.; Li, H.; Zhang, P. X.; Ji, L. N. *J. Chem. Soc., Dalton Trans.* **2003**, 2260.
48. Zhen, Q. X.; Zhang, Q. L.; Liu, J. G.; Ye, B. H.; Ji, L. N.; Wang, L. *J. Inorg. Biochem.* **2000**, *78*, 293.

CHAPTER 8

Conclusion

Synthesis, characterization and signaling of easily synthesizable molecules containing 2,2′-bipyridyl, quinoxalinyl or pyrazinyl moieties in the presence of cation or anion and DNA binding and photocleavage activities of some new ruthenium(II) complexes that incorporate modified 2,2′-bipyridyl (bpy) containing photoactive naphthalene, anthracene, pyrene or electroactive semiquinone ligands are the main theme of the studies described in this thesis.

In Chapter 1 of the thesis, the recent literature related to cation sensing, anion sensing, ion-pair sensing and DNA binding and photocleavage by metal complexes have been reviewed. The literature survey presented in this chapter is not intended to be exhaustive, but is only representative, with emphasis being laid on those examples that bear relevance to the main theme of the present thesis. Chapter 2 provides a general description of the synthesis of various compounds as well as various techniques and methodologies used in the research work. Chapters 3 to 7 constitute the research works performed during the present study. Conclusions, in accordance with the investigations carried out, observations and rational explanations, have been drawn and described chapter-wise in the following sections. A brief outline about the possible future scopes that can be accomplished in continuation and extension of the present study has been suggested at the end of this chapter.

8.1 Dual Emission of Anthracene/Pyrene-(2,2′-bipyridine) Dyads and Fluorescence OFF/ON Signaling of Pyrene-(2,2′-bipyridine) Dyad with Post-Transition Metal Ions

The photophysical behavior of two dyads **mpae** and **mppe** where anthracene or pyrene is appended with 2,2′-bipyridyl by an ethylene linkage (Fig. 8.1) has been investigated. Both **mpae** and **mppe** show a broad absorption band with low ε value at around 380 nm, which is attributed to charge transfer transition from 2,2′-bipyridyl subunit to anthracene/pyrene subunit in the ground state. However, the extent of charge transfer is small in the ground state as the position of this absorption band is invariant to solvent polarity. Retention of absorption profile of free anthracene in **mpae** and free pyrene structured-peaks in **mppe** indicates also little charge transfer at ground state. Steady state emission spectra of both **mpae** and **mppe** comprise dual bands. Higher energy structured-peaks arise for emission from the π, π^* excited singlet state of anthracene or pyrene and lower energy broad band is attributed to emission from the intramolecular charge transfer (ICT) state. Red-shift of lower energy emission band with increased solvent polarity for both **mpae** and **mppe** supports the intramolecular charge transfer character of the emitting state. That the long and short lifetime components are associated with emission from the π, π^* state and intramolecular charge transfer state, respectively are evident from the amplitudes of bi-exponential fluorescence decay profiles of **mppe**. However, the pattern of the variation of lifetime with **mpae** is not properly understood.

In presence of transition (Mn^{2+}, Co^{2+}, Ni^{2+}, Cu^{2+}) and post-transition (Zn^{2+}, Cd^{2+}, Pb^{2+}) metal ions, charge transfer in **mppe** becomes more facile from relatively electron-rich pyrene to 2,2′-bipyridyl moiety, as the metal ion

binding with the latter moiety makes it electronically deficient, leading to the formation of new absorption band around 430 nm. **mppe** also acts as a fluorescent OFF/ON sensor for Zn^{2+}, Cd^{2+} and Pb^{2+} with generation of a new broad emission band in low energy region. Formation of similar emission band with **mppe** in the presence of transition metal ions is not observed presumably due to fluorescence quenching effect of these metal ions. In the case of **mpae**, no new red-shifted absorption or emission band, as seen with **mppe**, could be observed with the transition or post-transition metal ions. Binding constants of **mpae** and **mppe** with Mn^{2+}, Co^{2+}, Ni^{2+}, Cu^{2+} and Zn^{2+} are measured to be of the order of 10^6 M^{-1} whereas, those with Cd^{2+} and Pb^{2+} are found one order of magnitude lower.

8.2 Transition Metal Ions Signaling Behavior of Dipyridylquinoxalinazo Chemosensor

New colorimetric chemosensor **dpqapd** for transition metal ions has been synthesized where dipyridylquinoxaline and dimethylamine groups, coupled by azo-benzene group (Fig. 8.1), act as electron-acceptor and electron-donor moieties. Absorption spectrum of **dpqapd** is featured by a charge transfer band in the visible region, the position of which is sensitive to polarity of the solvent.

dpqapd changes its color from yellow to light-pink with Ni^{2+}, Zn^{2+} and pink with Co^{2+}, Cd^{2+} in CH_3CN. However, no color change is observed with Mn^{2+} and the solution turns colorless with Cu^{2+}. The binding constant of **dpqapd** with metal ions, determined from absorption titration data, indicates that Ni^{2+} binds strongly than Zn^{2+} and Cu^{2+} ions.

The charge transfer band of **dpqapd** shifts towards red on addition of Ni^{2+} and Zn^{2+} whereas, the same band intensity gradually decreases on

addition of Cu^{2+}. Pyridine and quinoxaline nitrogen atoms bind with Ni^{2+} (or Zn^{2+}) ion in bidentate manner to form five-member chelate ring, which renders dipyridylquinoxaline moiety electron-deficient and charge transfer becomes more facile, leading to red-shift of the lower energy band. Cu^{2+} ion binds with the nitrogen atom of dimethylamine moiety, leading to inhibition of charge transfer from dimethylamine.

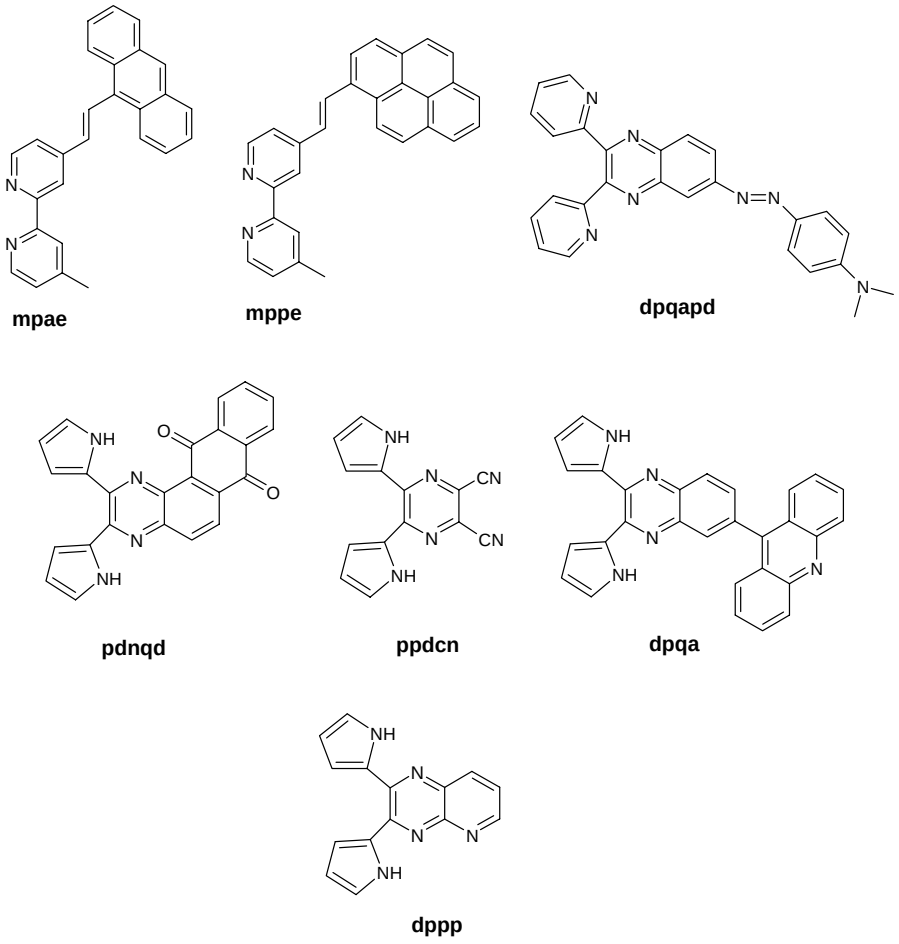

Fig. 8.1

Titration of **dpqapd** with Co^{2+} or Cd^{2+} causes significant red-shift and drastic increase in absorbance of the charge transfer band, with two isosbestic points. The scatter plot of change in absorbance at 530 nm vs. concentration of added Co^{2+} or Cd^{2+} consists of two steps which is somewhat unusual than the normal trend. Binding of Cd^{2+} (or Co^{2+}) ion is perhaps associated with some conformational change in the system for higher concentration of Cd^{2+} or Co^{2+} ion.

8.3 Fluoride Ion Sensors Based on Dipyrrolyl Derivatives: Synthesis, Optical and Electrochemical Sensing

Three dipyrrolyl derivatives **pdnqd**, **ppdcn** and **dpqa** (Fig. 8.1) were prepared by single step reactions which show dramatic, binding-induced changes in their optical signatures with F^-. However, no change in color is observed with Cl^-, Br^-, I^-, or ClO_4^-, thus rendering these three specific fluoride ion sensors. The solid state structure of **pdnqd** has been determined by single crystal X-ray diffraction analysis. Introduction of strongly electron-withdrawing quinone or cyano groups in **pdnqd** and **ppdcn** makes the pyrrole NH protons highly acidic, which enhances the hydrogen-bonding ability of these sensors. The other sensor **dpqa**, which lacks electron-withdrawing group present in **pdnqd** or **ppdcn**, binds with fluoride relatively weakly. That the reversible nature of complexation between F^- and sensors and involvement of hydrogen-bonding in the binding between the sensors and F^- are evident from the restoration of original spectra (and also the color of the solution) corresponding to those sensors in the absence of the anion from that of sensor–F^- conjugates upon addition of small aliquots of water/methanol.

pdnqd and **ppdcn**, which contain electro-active quinine and cyano functionalities, show reduction of the peak current and anodic shift of the peak potential on addition of successive amount of F^- ion in differential pulse voltammetry. The shifts observed during the redox titrations are a composite of those due to F^- binding to the NH protons and change in the electron density distribution at the electro-active centers of these sensors.

^{1}H NMR titration of **pdnqd** and **ppdcn** with F^- indicates that the pyrrole NH protons of both sensors interact with F^- by hydrogen-bond in 'bidentate' fashion. The selectivity of F^- over Cl^- or Br^- is attributed mainly to the fact that F^- is better hydrogen bond acceptor than Cl^- or Br^- and partly to the complementarity of the geometries between the receptor moiety and F^-.

8.4 Dipyrrolyl Derivative as both Fluoride and Transition Metal Ions Sensor

The dipyrrolylpyrazine (DPP) derivative, **dppp** has been synthesized and characterized by different methods (Fig. 8.1). The crystal structures of **dppp** and **Ni(dppp)$_2$Cl$_2$**, which are essential for an understanding of the change in orientation of pyrrole rings on metal complexation and determining the coordinating site of the metal, have been determined. It is important to note that only pyridine nitrogen is bonded with Ni(II), not the pyrazine nitrogen atoms.

The sensing of transition metal ions (Co^{2+}, Ni^{2+}, Cu^{2+}, Zn^{2+} and Cd^{2+}) and F^- by **dppp** is clearly visible by change in color of the system from yellowish-green to red in the case of former and to brown or light-brown in the latter cases. The binding constants of **dppp** with transition metal ions have been found to be two orders of magnitude higher than that for the F^-.

While hydrogen-bonding interaction between F^- and pyrrole NH moieties is responsible for binding of F^- with **dppp**, the binding of cation involves pyridine nitrogen of **dppp**. That an additional pyridine ring does help metal ion binding is evident from the fact that our previously reported DPP derivative **ppdcn**, bearing cyano functionality, does not show noticeable change in the absorption spectrum on addition of Mn^{2+}, Co^{2+}, Ni^{2+}, Zn^{2+} and Cd^{2+} ions and with Cu^{2+}, a binding constant which is 100 times lower than that of **dppp** is obtained.

Even though **dppp** possesses two separate binding sites for F^- and metal ions, it is observed that the presence of the metal ions (Ni^{2+}, Co^{2+}, Zn^{2+}) influences the binding of the anion (F^-) and vice versa due to sequestering of the metal ion to form ion-pair with F^- ion in organic medium. The binding constant values of an ion in the presence of oppositely charged species are measured to be significantly lower.

8.5 DNA Interaction and Photocleavage Activities of Mixed-Ligand Complexes of Ruthenium(II) Containing New Photo- or Electro-active Ligands

DNA binding and photocleavage/redox properties of six new, mixed-ligand ruthenium(II) complexes have been investigated, where 2,2′-bipyridyl or 1,10-phenanthroline are present as ‘spectator ligands’ (Fig. 8.2). While three of these complexes possess luminescent, photoactive hydrocarbon ligands, the other three contain electroactive, semiquinone type ligands. These latter complexes are EPR active as they contain unpaired electron on the semiquinone ligands.

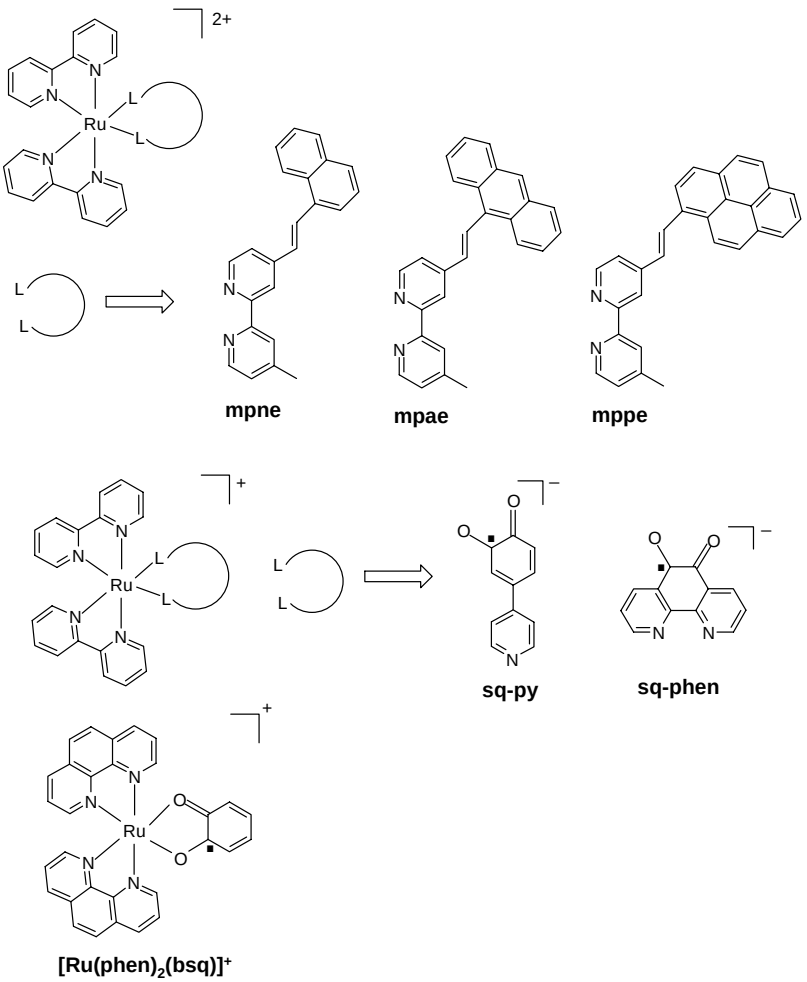

Fig. 8.2

All the complexes are strong binders of DNA with binding constants being at least two orders more than that of **$[Ru(bpy)_3]^{2+}$** or **$[Ru(phen)_3]^{2+}$**. Decrease in absorbance (hypochromicity) observed for the low energy MLCT band (> 900 nm) of the ruthenium(II)-semiquinone complexes in the presence of DNA arises due to oxidation of sugar (deoxyribose) unit of DNA by semiquinone fragment of the ruthenium(II) complex.

It was also observed that **[Ru(bpy)$_2$(mpne)]$^{2+}$** showed considerable photocleavage activity but **[Ru(bpy)$_2$(mpae)]$^{2+}$** is totally ineffective in cleaving DNA under the same set of experimental conditions although, the former has quantum yield 10 times less than the latter one. This may be due to stronger intercalative binding of DNA with the former complex than the latter one. The inhibitor studies indicate that the reactive oxygen species $OH^{\bullet}$ radical is involved in the DNA photocleavage of **[Ru(bpy)$_2$(mpne)]$^{2+}$**. The ruthenium(II)-semiquinone complexes did not show any photocleavage activity, as they are totally non-luminescent. However, they show nucleases activity even in dark with pBR 322 DNA to some extent which is caused by the oxidation of 2-deoxy-D-ribose unit of DNA by semiquinone fragment of the ruthenium(II) complex.

8.6 Future scope

It is evident from this study that the dyad **mppe** is capable of generating red-shifted fluorescence in presence of post-transition metal ions. Small molecules of the type of **mppe** can be used as building blocks for π-conjugated polymers where the metal binding sites (2,2′-bipyridyl) would alter the electronic and/or optical properties by complexation with different metal ions. Such polymers have immense importance and vast application in material science, electronics and photonic technologies. On the other hand, the colorimetric sensing of transition metal ions displayed by **dpqapd** can be exploited in detection of these metal ions in medical diagnostics such as serum studies or analytical chemistry.

We have observed that the colorimetric sensing of F^- by **pdnqd**, **ppdcn**, **dpqa** and **dppp** involves hydrogen-bonding interaction between

pyrrole NH protons and F^-. In aqueous medium, since F^- also competes with the water molecules for hydrogen-bond formation, more number of pyrrole NH protons are necessary to make a stronger hydrogen-bonding interaction with F^-. An encapsulated F^- by pyrrole NH protons may be useful in aqueous medium. Extended 'claw'-like molecules containing multi-pyrrole groups can be synthesized from the above molecules and used for binding of F^- or other anions in aqueous medium. Pyridine or other cation binding site, which is in the vicinity of the anion binding site, can strengthen the anion binding by contact ion-pair recognition due to columbic interaction between oppositely charged ions. Expanded **dppp** molecule, where greater number of pyrrole groups are closer to pyridine moiety, may be useful for ion-pair recognition in aqueous medium.

DNA binding and photocleavage/redox properties of six new, mixed-ligand ruthenium(II) complexes have been investigated, where 2,2′-bipyridyl or 1,10-phenanthroline are present as 'spectator ligands'. The complexes bearing fluorophore groups can be used as photonucleases whereas ruthenium(II)-semiquinone complexes can be used as potential but mild redox agents for selective chemical modification of the DNA molecule.

Appendix

Table 1. Crystallographic data for **pdnqd**, **dppp** and **Ni(dppp)$_2$Cl$_2$**.

Compound/Complex	**pdnqd**	**dppp**	**Ni(dppp)$_2$Cl$_2$**
Chemical formula	$C_{24}H_{14}N_4O_2$	$C_{15}H_{11}N_5.$ $2H_2O$	$NiC_{30}H_{22}Cl_2N_{10}$
Formula weight	390.39	297.32	652.19
Crystal system	Monoclinic	Triclinic	Triclinic
Space group	Pbca	$P\bar{1}$	$P\bar{1}$
a (Å)	7.483(2)	6.7615(6)	6.9445(4)
b (Å)	14.924(4)	9.3751(9)	12.8462(8)
c (Å)	31.974(9)	12.2200(11)	17.3296(11)
α (^{o})	90.00	83.376(2)	110.3790(10)
β (^{o})	90.00	89.496(2)	90.8100(10)
γ (^{o})	90.00	75.250(2)	94.5210(10)
V (Å^3)	3570.5(18)	743.92(12)	1443.28(15)
Z	8	2	2
μ (mm^{-1})	0.096	0.093	0.898
T / K	298	298	298
Reflections collected	31602	8661	13866
Unique reflections	3132	3453	5058
Reflections [$I \geq 2\sigma(I)$]	2195	2678	3143
Parameters	279	219	388
$R1$, $wR2$ [$I \geq 2\sigma(I)$]	0.0419, 0.0970	0.0651, 0.1874	0.0724, 0.1991
$R1$, $wR2$ [all data]	0.0697, 0.1106	0.0792, 0.2003	0.1103, 0.2241
Goodness-of-fit on F^2	1.024	1.059	1.040
Largest peak and hole (e Å^{-3})	0.198, -0.148	1.034, -0.304	0.566, -0.532

Table 2. Bond lengths (Å) and angles (°) for **pdnqd**.

O1-C7	1.226(2)	O2-C14	1.218(2)
N1-C1	1.318(2)	N1-C16	1.358(2)
C8-C9	1.390(3)	C8-C13	1.397(2)
C8-C7	1.480(3)	C13-C12	1.388(3)
C13-C14	1.491(3)	C15-C6	1.401(2)
C15-C16	1.428(2)	C15-C14	1.498(2)
N3-C18	1.347(2)	N3-C17	1.371(2)
C6-C5	1.408(3)	C6-C7	1.485(3)
C16-C3	1.416(2)	C1-C2	1.448(3)
C1-C17	1.459(3)	N2-C2	1.322(2)
N2-C3	1.363(2)	C3-C4	1.407(3)
C17-C20	1.372(3)	C5-C4	1.359(3)
C9-C10	1.375(3)	C12-C11	1.379(3)
C10-C11	1.381(3)	C18-C19	1.356(3)
C21-N4	1.370(3)	C21-C24	1.374(3)
C21-C2	1.467(3)	N4-C22	1.349(3)
C20-C19	1.395(3)	C24-C23	1.400(3)
C22-C23	1.357(3)	C1-N1-C16	119.33(16)
C9-C8-C13	119.53(18)	C9-C8-C7	120.42(17)
C13-C8-C7	120.04(16)	C12-C13-C8	119.35(18)
C12-C13-C14	118.80(16)	C8-C13-C14	121.82(16)
C6-C15-C16	118.10(16)	C6-C15-C14	119.72(16)
C16-C15-C14	122.17(15)	C18-N3-C17	110.76(17)
O2-C14-C13	119.12(17)	O2-C14-C15	123.02(17)
C13-C14-C15	117.84(15)	C15-C6-C5	120.86(17)
C15-C6-C7	121.66(17)	C5-C6-C7	117.45(16)
N1-C16-C3	119.60(17)	N1-C16-C15	120.75(16)
C3-C16-C15	119.65(16)	N1-C1-C2	120.56(16)
N1-C1-C17	113.36(16)	C2-C1-C17	126.07(16)
O1-C7-C8	121.18(17)	O1-C7-C6	120.20(17)
C8-C7-C6	118.61(16)	C2-N2-C3	118.68(16)
N2-C3-C4	118.92(17)	N2-C3-C16	120.73(17)
C4-C3-C16	120.21(18)	N3-C17-C20	105.76(18)
N3-C17-C1	117.66(16)	C20-C17-C1	136.48(19)
C4-C5-C6	121.22(17)	C10-C9-C8	120.19(19)
C11-C12-C13	120.72(18)	C5-C4-C3	119.79(18)
C9-C10-C11	120.6(2)	N3-C18-C19	107.55(19)
C12-C11-C10	119.6(2)	N4-C21-C24	106.55(18)

N4-C21-C2	118.95(19)	C24-C21-C2	133.78(19)
N2-C2-C1	119.97(17)	N2-C2-C21	114.80(17)
C1-C2-C21	125.19(18)	C22-N4-C21	110.0(2)
C17-C20-C19	108.19(19)	C18-C19-C20	107.71(19)
C21-C24-C23	107.8(2)	N4-C22-C23	108.2(2)
C22-C23-C24	107.5(2)		

Table 3. Bond lengths (Å) and angles (^{o}) for **dppp**.

N2-C5	1.316(3)	N2-C12	1.358(3)
N1-C6	1.325(3)	N1-C11	1.354(3)
C11-N3	1.358(3)	C11-C12	1.412(3)
N3-C15	1.325(3)	C6-C5	1.450(3)
C6-C7	1.461(3)	C13-C14	1.357(3)
C13-C12	1.400(3)	C5-C4	1.458(3)
C7-N4	1.371(3)	C7-C8	1.375(3)
N4-C10	1.344(3)	C15-C14	1.401(3)
N5-C1	1.352(3)	N5-C4	1.368(3)
C4-C3	1.379(3)	C3-C2	1.396(4)
C8-C9	1.401(4)	C2-C1	1.343(4)
C10-C9	1.354(4)	C5-N2-C12	118.57(17)
C6-N1-C11	118.43(16)	N1-C11-N3	117.23(17)
N1-C11-C12	120.51(18)	N3-C11-C12	122.22(18)
C15-N3-C11	117.45(19)	N1-C6-C5	120.66(17)
N1-C6-C7	115.43(17)	C5-C6-C7	123.87(18)
C14-C13-C12	118.2(2)	N2-C12-C13	120.44(18)
N2-C12-C11	120.77(18)	C13-C12-C11	118.74(19)
N2-C5-C6	120.45(17)	N2-C5-C4	115.55(18)
C6-C5-C4	123.88(18)	N4-C7-C8	107.08(19)
N4-C7-C6	119.69(19)	C8-C7-C6	132.3(2)
C10-N4-C7	109.3(2)	N3-C15-C14	123.3(2)
C1-N5-C4	109.2(2)	N5-C4-C3	106.5(2)
N5-C4-C5	118.40(19)	C3-C4-C5	134.0(2)
C13-C14-C15	120.1(2)	C4-C3-C2	107.9(2)
C7-C8-C9	107.3(2)	C1-C2-C3	107.2(2)
N4-C10-C9	108.9(2)	C2-C1-N5	109.2(2)
C10-C9-C8	107.3(2)		

Table 4. Bond lengths (Å) and angles (°) for **Ni(dppp)$_2$Cl$_2$**.

C1-N1	1.328(7)	C1-C2	1.379(8)
C2-C3	1.359(8)	C3-C4	1.417(8)
C4-N3	1.356(7)	C4-C5	1.383(7)
C5-N2	1.353(7)	C5-N1	1.362(6)
C6-N3	1.318(7)	C6-C8	1.446(8)
C6-C7	1.468(8)	C7-N2	1.332(7)
C7-C12	1.453(8)	C8-C9	1.358(9)
C8-N4	1.398(9)	C9-C10	1.328(9)
C10-C11	1.379(12)	C11-N4	1.389(10)
C12-C15	1.354(8)	C12-N5	1.399(9)
C13-C14	1.353(12)	C13-N5	1.404(11)
C14-C15	1.316(9)	C16-N6	1.309(7)
C16-C17	1.377(8)	C17-C18	1.369(9)
C18-C19	1.408(9)	C19-N8	1.340(8)
C19-C20	1.400(7)	C20-N6	1.347(7)
C20-N7	1.348(7)	C21-N8	1.314(8)
C21-C27	1.419(10)	C21-C22	1.478(8)
C22-N7	1.317(7)	C22-C23	1.436(9)
C23-C24	1.339(8)	C23-N10	1.388(13)
C24-C25	1.315(11)	C25-C26	1.305(12)
C26-N10	1.405(13)	C27-C30	1.335(9)
C27-N9	1.366(17)	C28-C29	1.264(19)
C28-N9	1.467(16)	C29-C30	1.234(12)
Cl1-Ni1	2.2773(17)	Cl2-Ni1	2.255(2)
N1-Ni1	2.004(4)	N6-Ni1	2.026(4)
N1-C1-C2	123.8(5)	C3-C2-C1	119.6(6)
C2-C3-C4	118.6(5)	N3-C4-C5	119.6(5)
N3-C4-C3	122.4(5)	C5-C4-C3	117.9(5)
N2-C5-N1	114.2(5)	N2-C5-C4	122.7(5)
N1-C5-C4	123.0(5)	N3-C6-C8	113.7(5)
N3-C6-C7	119.6(5)	C8-C6-C7	126.7(6)
N2-C7-C12	113.5(5)	N2-C7-C6	119.8(5)
C12-C7-C6	126.7(5)	C9-C8-N4	106.2(6)
C9-C8-C6	118.5(6)	N4-C8-C6	134.8(7)
C10-C9-C8	110.2(7)	C9-C10-C11	109.6(7)
C10-C11-N4	105.8(8)	C15-C12-N5	106.7(7)
C15-C12-C7	119.6(5)	N5-C12-C7	133.3(7)
C14-C13-N5	107.1(7)	C15-C14-C13	109.6(7)

C14-C15-C12	110.4(6)	N6-C16-C17	123.8(6)
C18-C17-C16	118.7(6)	C17-C18-C19	119.6(6)
N8-C19-C20	119.9(6)	N8-C19-C18	123.4(6)
C20-C19-C18	116.7(6)	N6-C20-N7	114.7(5)
N6-C20-C19	122.9(6)	N7-C20-C19	122.3(6)
N8-C21-C27	113.9(6)	N8-C21-C22	120.3(6)
C27-C21-C22	125.7(8)	N7-C22-C23	113.2(5)
N7-C22-C21	119.6(6)	C23-C22-C21	127.2(6)
C24-C23-N10	102.2(7)	C24-C23-C22	120.7(6)
N10-C23-C22	136.1(7)	C25-C24-C23	113.1(7)
C26-C25-C24	109.7(8)	C25-C26-N10	105.3(10)
C30-C27-N9	103.6(8)	C30-C27-C21	120.2(8)
N9-C27-C21	135.5(10)	C29-C28-N9	106.3(13)
C30-C29-C28	110.3(10)	C29-C30-C27	114.9(9)
C1-N1-C5	117.0(5)	C1-N1-Ni1	131.7(4)
C5-N1-Ni1	111.2(3)	C7-N2-C5	117.7(5)
C6-N3-C4	119.7(5)	C11-N4-C8	108.2(9)
C12-N5-C13	106.2(8)	C16-N6-C20	118.2(5)
C16-N6-Ni1	134.4(4)	C20-N6-Ni1	107.3(4)
C22-N7-C20	118.3(5)	C21-N8-C19	119.5(5)
C27-N9-C28	104.5(13)	C23-N10-C26	109.5(9)
N1-Ni1-N6	96.87(17)	N1-Ni1-Cl2	95.87(14)
N6-Ni1-Cl2	102.40(16)	N1-Ni1-Cl1	146.86(14)
N6-Ni1-Cl1	107.93(13)	Cl2-Ni1-Cl1	99.75(8)

List of Publications:

1) A Colorimetric Chemosensor for both Fluoride and Transitional Metal Ions Based on Dipyrrolyl Derivative. **Tamal Ghosh**, Bhaskar G. Maiya, Anunay Samanta. *Dalton Transactions*, **2006**, 795.

2) Mixed-Ligand Complexes of Ruthenium(II) Containing New Photo- or Electro-active Ligands: Synthesis, Spectral Characterization and DNA Interactions. **Tamal Ghosh**, Atindra D. Shukla, D. Amilan Jose, D. Krishna Kumar, Bhaskar G. Maiya, Anunay Samanta, Amitava Das. *Journal of Biological Inorganic Chemistry*, **2005**, *10*, 496.

3) Fluoride Ion Receptors Based on Dipyrrolyl Derivatives Bearing Electron-Withdrawing Groups: Synthesis, Optical and Electrochemical Sensing, and Computational Studies. **Tamal Ghosh**, Bhaskar G. Maiya, Ming Wah Wong. *Journal of Physical Chemistry A*, **2004**, *108*, 11249.

4) Structure-Property Correlations in DNA Binding and Photocleavage Characteristics of Metallointercallators. C. V. Sastri, M. Mariappan, **Tamal Ghosh**, Bhaskar G. Maiya. *Proceedings of Indian National Science Academy A*, **2004**, *70*, 355.

5) Visual Sensing of Fluoride Ions by Dipyrrolyl Derivatives Bearing Electron- Withdrawing Groups. **Tamal Ghosh**, Bhaskar G. Maiya. *Journal of Chemical Science*, **2004**, *116*, 17.

6) Dual Emission of Anthracene/Pyrene-(2,2′-bipyridine) Dyads and Fluorescence OFF/ON Signaling of Pyrene-(2,2′-bipyridine) Dyad with Post-Transition Metal Ions. **Tamal Ghosh**, Anunay Samanta, D. Amilan Jose, Atindra D. Shukla, Amitava Das (to be communicated).

7) Colorimetric Detection of Transition Metal Ions by Dipyridylquinoxalinazo Chemosensor. **Tamal Ghosh**, Anunay Samanta (to be communicated).